Mechanistic analysis of the pump cycle of the P-type ATPase KdpFABC

Dissertation

zur Erlangung des akademischen Grades
eines Doktors der Naturwissenschaften
(Dr. rer. nat)

an der

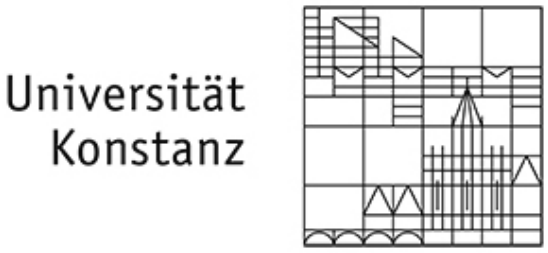

Mathematisch-Naturwissenschaftliche Sektion
Fachbereich Biologie

vorgelegt von

Bojana Damnjanović

1. Referent: Prof. Dr. Hans-Jürgen Apell
2. Referent: Prof. Dr. Wolfram Welte
3. Referent: Prof. Dr. Karin Hauser

Tag der mündlichen Prüfung: 17.12.2013

Table of Contents

Summary i

Zusammenfassung iii

1. INTRODUCTION 1

1.1. Membranes: structure, function and transport 1

1.2. Ion pumps *vs.* ion channels 4

1.3. ATPases: classification, function and structure 5

1.3.1. P-type ATPases 7

1.3.2. Structural properties of the P-type ATPases 10

1.3.3. Functional properties of the P-type ATPases 12

1.4. Potassium transport in E. *coli* 14

1.5. The KdpFABC complex, a member of the P-type ATPases 17

1.6. Structure-function relationship of the KdpFABC complex 26

1.7. Molecular mechanism of the KdpFABC 29

1.8. Electrogenic K^+ transport by the KdpFABC complex 30

1.9. Aim of the project 32

2. EXPERIMENTAL PROCEDURES 33

2.1. Bacterial strains and growth conditions 33

2.2. Purification of the KdpFABC complex 35

2.3. Biochemical assays 37

2.3.1. Protein determination 37

2.3.2. SDS-PAGE electrophoresis 38

2.3.3. Malachite green ATPase activity assay 38

2.4. Reconstitution of the KdpFABC complex 40

2.5. Voltage-sensitive dyes 42

2.5.1. Introduction into the principles of fluorescence 42

2.5.2. Use of RH421 dye for characterization of the detergent-solubilized KdpFABC 45
2.5.2a. Steady-State fluorescent measurements using RH421 dye 47
2.5.2b. Time-resolved measurements with caged ATP 49
2.5.3. The potential-sensitive fluorescent probe $DiSC_3(V)$ 52
2.5.3a. Investigation of the ion transport by KdpFABC reconstituted in lipid vesicles using $DiSC_3(V)$ 55

3. RESULTS **59**
3.1. Choice of detergent 59
3.2. Substrate dependence of the KdpFABC ATPase activity 61
3.3. RH421 steady-state experiments with the detergent-solubilized KdpFABC 64
3.3.1. Standard experiments 64
3.3.2. Ion-binding titrations 68
3.3.3. Effect of Mg^{2+} ions on K^+-binding affinity 74
3.4. $DiSC_3(V)$-fluorescence measurements with KdpFABC reconstituted in lipid vesicles 77
3.4.1. Calibration of the fluorescence signal of the $DiSC_3(V)$ dye 77
3.4.2. Electrogenicity of the K^+ transport by the KdpFABC 79
3.4.3. Role of H^+ in the transport process of KdpFABC 81
3.4.4. Effect of extravesicular K^+ and Mg^{2+} concentrations on the pumping activity of the KdpFABC complex 84
3.4.5. Effect of ADP and inorganic phosphate on the pumping activity of the KdpFABC complex 87
3.5. KdpFABC activity inhibition by *o*-vanadate 89
3.6. Temperature dependence of the KdpFABC activity 93
3.7. Time-resolved kinetics experiments with detergent-solubilized KdpFABC 96

4. DISCUSSION **101**

5. REFERENCES **119**

Summary

Due to the vital prerequisite for K^+ ions in bacterial cells, involved in important processes, such as maintenance of the turgor pressure, pH homeostasis, membrane voltage and enzyme activation, E. *coli* comprises a set of different specialized potassium transport systems. Under K^+-limiting conditions, the high affinity KdpFABC complex is expressed to sustain K^+ uptake. KdpFABC is a member of the P-type ATPase family with a unique subunit composition. It consists of four subunits, and the sites of ATP hydrolysis and ion transport are well-separated on two different subunits. Only the KdpB subunit exhibits an explicit homology to other P-type ATPases and represents the catalytic subunit performing ATP hydrolysis, whereas the KdpA subunit binds and transports K^+ ions and shows similarities to KcsA-like K^+-channel proteins. It was demonstrated that KdpFABC, like other P-type ATPases, undergoes a reaction cycle with large conformation changes, generally represented by a so-called Post-Albers cycle. A general feature is that the ion pump toggle between two main conformational states, E_1 and E_2, in which the ion-binding sites alternatingly face one of both membrane sides.

The aim of this work was to investigate the mechanistic aspect of the KdpFABC transport process, which would give more information about the coupling mechanism of energy-releasing ATP hydrolysis and the energy-consuming ion transport across membranes. For this purpose a fluorescence technique was employed that is based on the voltage-sensitive dye RH421, which enables a monitoring of ion movements in the membrane domain of ion-transport proteins. Based on this method, the electrogenicity of ion-binding partial reactions of the pump cycle of the detergent-solubilized KdpFABC was investigated. After finding the most appropriate detergent that preserves a functional complex, the apparent binding affinities for K^+ and H^+ were determined in both conformations, E_1 and E_2-P, and further analysis of mutual interference of K^+ and H^+ revealed a mixed inhibition. Binding of both K^+ and H^+ was found to be electrogenic. To compare transport and enzyme activity, the dependence of ATP hydrolysis on the proton concentration was measured. Furthermore, small ATPase activity was induced with Na^+ and H^+ in the absence of K^+, supporting previous conclusion that both ion species act as weak congeners of K^+. K^+-binding titrations were carried out under different conditions to examine the effect of Mg^{2+} concentration in the electrolyte. It was found that the amount of positive charge to be bound

to the membrane domain increases with the Mg^{2+} concentrations. This effect was assigned to the Gouy-Chapman effect.

The second set of experiments was performed with the reconstituted KdpFABC in E. *coli* lipid vesicles, using the membrane potential indicator $DiSC_3(V)$, that allows monitoring of the electrogenic pump activity. ATP-driven K^+ export across the vesicle membrane performed by the inside-out oriented KdpFABC pumps was electrogenic and confirmed that K^+ is transported out of the vesicles. The experiments performed in the absence of K^+ indicated an unexpected H^+ translocation opposite to the well-established K^+ transport, although to a significantly lower extent. The $DiSC_3(V)$ dye was used to investigate effects of different ions on the pump activity, such as H^+, Mg^{2+}, and K^+. The inhibition mechanism of ADP, inorganic phosphate and *o*-vanadate was studied, and compared to the results reported for the Na^+,K^+-ATPase. Experiments on the temperature-dependence of the ATPase and pump activities were used to determine the activation energies of the respective processes.

Time-resolved experiments with detergent-solubilized KdpFABC in Aminoxide WS-35 were used to analyze the kinetics of the involved processes, in the presence of different K^+, H^+ and ATP concentrations. These results are supportive of the proposal that the K^+-binding step occurs after the phosphorylation and conformation transition reaction steps, and therefore, it has to be assigned to the dephosphorylation partial reaction.

Three pump cycles derived from the general Post-Albers scheme of P-type ATPases have been introduced and discussed, with the ultimate goal to propose a possible molecular pump cycle, supported by the obtained experimental evidence. A more reliable assignment to the pump cycle of the KdpFABC requires more detailed investigation, and especially highly resolved structural information that will allow a definitive mapping of the ion-binding sites and their occupation.

Part of this work was published in:

- **Damnjanović, B.**, Weber, A., Potschies, M., Greie, J.C. and Apell, H.J. (2013) Mechanistic analysis of the pump cycle of the KdpFABC P-type ATPase, *Biochemistry 52*, 5563-5576.

Zusammenfassung

Kaliumionen sind für Bakterienzellen lebensnotwendig, da sie an wichtigen Prozessen wie dem Erhalt des Turgors, der pH-Homöostase, dem Membranpotential und der Enzymaktivierung beteiligt sind. *E. coli* besitzt mehrere verschiedene und spezialisierte Kalium-Transportsysteme. Unter der Bedingung von Kaliummangel wird der hochaffine KdpFABC Komplex exprimiert, mit dem die Kaliumaufnahme auch im mikromolaren Bereich aufrechterhalten werden kann. KdpFABC gehört zu der Familie der P-Typ ATPasen, weist jedoch eine einzigartige Zusammensetzung von verschiedenen Untereinheiten auf. Insgesamt besteht das Protein aus vier Untereinheiten, wobei die ATP-Hydrolyse und der Ionentransport auf zwei unterschiedlichen Untereinheiten stattfinden. Nur die KdpB-Untereinheit, welche für die katalytische ATP-Hydrolyse verantwortlich ist, weist eine signifikante Homologie zu anderen ATPasen des P-Typs auf. Die KdpA-Untereinheit, welche für die Bindung und den Transport der Kaliumionen zuständig ist, zeigt Ähnlichkeiten mit Proteinen der KcsA Kalium-Kanal Klasse auf. Es wurde gezeigt, dass der KdpFABC Komplex, analog zu anderen P-Typ ATPasen, einen Reaktionszyklus, den sogenannten Post-Albert Zyklus, hat, der mit großen Konformationsveränderungen verbunden ist. Das wichtigste Merkmal dabei ist, dass die Ionenpumpe zwischen zwei unterschiedlichen Konformationen E_1 und E_2 hin- und herwechselt, in denen die Ionenbindungsstellen alternierend den beiden Membranseiten zugewandt ist.

Ziel dieser Arbeit war es, die mechanistischen Aspekte des KdpFABC-vermittelten Ionentransports zu untersuchen, um mehr Informationen über den Mechanismus der Kopplung von energiefreisetzender ATP-Hydrolyse und energieverbrauchendem Ionentransport durch Membranen zu lernen. Um dies zu erreichen, wurde eine Fluoreszenzmethode verwendet, die auf dem potentialempfindlichen Fluoreszenzfarbstoff RH421 basiert. Diese ermöglicht den Nachweis von Ionenbewegungen in den Membrandomänen von ionentransportierenden Proteinen. Mit Hilfe dieser Methode wurde die Elektrogenizität der ionenbindenden Teilreaktionen des Pumpzyklus von detergenssolubilisierten KdpFABC-Präparationen untersucht. Nachdem ein für die Funktion des Proteins geeigneten Detergens gefunden worden war, wurden die Bindungsaffinitäten für Kaliumionen und Protonen in beiden Konformationen E_1 und E_2-P bestimmt. Weitere Untersuchungen zur Wechselwirkung von Kaliumionen und Protonen ergaben eine

wechselseitige Inhibition. Die Bindung von Kaliumionen und Protonen ist elektrogen. Um die Beziehung von Transport und Enzymaktivität zu bestimmen, wurde die Abhängigkeit der ATP-Hydrolyse von der Protonenkonzentration gemessen. Auch in der Abwesenheit von Kaliumionen konnte eine geringe ATPase-Aktivität in der Gegenwart von Natriumionen und Protonen beobachtet werden, was eine frühere Annahme stützt, dass Natriumionen und Protonen als Kongenere der Kaliumionen wirken. Weitere Kaliumtitrationen wurden durchgeführt, um den Einfluss der Magnesiumkonzentration im Elektrolyt zu untersuchen. Die Abnahme der positiven Nettoladung der Membrandomäne mit steigender Magnesiumkonzentration wurde dem Gouy-Chapman-Effekt zugewiesen.

Der zweite Satz von Experimenten wurde mit Präparationen durchgeführt, bei denen der KdpFABC-Komplex in Lipidvesikeln mit *E. coli*-Lipiden rekonstituiert wurde. Dabei wurde die Fluoreszenzfarbstoff $DiSC_3(V)$ verwendet, der als Indikator des Membranpotentials die Ermittlung der elektrogenen Pumpaktivität ermöglicht. Der ATP-getriebene Kaliumtransport durch die Vesikelmembran wurde mit inside-out orientierten KdpFABC-Pumpen durchgeführt und bewies die Elektrogenizität der Pumpfunktion. Es wurde bestätigt, dass Kaliumionen aus den Vesikeln heraustransportiert wurden. Experimente, die in Abwesenheit von Kaliumionen durchgeführt wurden, ergaben eine unerwartete Protonentranslokation, die in Gegenrichtung zu dem etablierten Kaliumtransport steht, jedoch mit einer signifikant geringeren Pumprate. Der $DiSC_3(V)$-Farbstoff wurde auch dazu verwendet, die Effekte verschiedener Ionen wie Protonen, Magnesium- und Kaliumionen auf die Pumpaktivität zu untersuchen. Hemmmechanismen von ADP, anorganischem Phosphat und *ortho*-Vanadat wurden untersucht und mit publizierten Ergebnissen der Na^+, K^+-ATPase verglichen. Experimente zur Temperaturabhängigkeit der ATPase- und Pumpaktivität wurden für die Ermittlung der jeweiligen Aktivierungsenergien verwendet.

Zeitaufgelöste Experimente mit dem Detergens-solubilisierten KdpFABC-Komplex wurden dazu verwendet, um die Kinetik der beteiligten Prozesse in Anwesenheit von verschiedenen Protonen-, ATP- und Kaliumionen-Konzentrationen zu analysieren. Die erhaltenen Ergebnisse stützen die Annahme, dass die Kaliumbindung erst nach der Phosphorylierung und dem Konformationsübergang in den $P\text{-}E_2$-Zustand geschieht. Daher ist der Kaliumtransport dem Halbzyklus mit der Dephosphorylierung zuzuordnen.

Drei mögliche Pump-Zyklen, die sich von dem allgemeinen Post-Albers Schema der P-Typ ATPasen ableiten lassen, wurden vorgeschlagen und diskutiert. Dies erlaubte, die

möglichen Pump-Zyklen mit Hilfe der vorgelegten experimentellen Daten einzuschränken. Um jedoch einen eindeutigen Pumpzyklus für den KdpFABC-Komplex zu erhalten, müssen noch weitere und detailliertere Untersuchungen durchgeführt werden. Insbesondere kann Information aus einer hochaufgelösten Struktur eine definitive Zuordnung der Ionenbindungsstellen und deren Besetzung ermöglichen.

Ein Teil der in dieser Arbeit vorgestellten Ergebnisse sind bereit publiziert worden in:

- **Damnjanović, B.**, Weber, A., Potschies, M., Greie, J.C. and Apell, H.J. (2013) Mechanistic analysis of the pump cycle of the KdpFABC P-type ATPase, *Biochemistry 52*, 5563-5576.

1. INTRODUCTION

1.1. Membranes: structure, function and transport

Membranes play an essential role in all living cells and their importance cannot be overstated. Both eukaryotic cells, including plant cells and animal cells, and prokaryotic cells, are enclosed by a cell membrane, providing cellular individuality (*1*). Membranes also form the interface of specialized intracellular compartments, like mitochondria, endoplasmic reticulum, Golgi complexes and the nucleus. Approximately half of their mass is lipid, which in aqueous environment spontaneously organizes itself forming a lipid bilayer. Due to their amphipathic character, under physiological conditions, membrane lipids assemble with their hydrophilic head oriented toward the aqueous medium, whereas the hydrophobic tail is buried in the interior of the membrane. Other major functional biomolecules of membranes are proteins, and they act as enzymes, pumps and channels, receptors, or they can have a structural role. Membranes are asymmetric structures, which can be attributed to the uneven distribution of lipids and proteins within membranes, but also due to the irregularly attached carbohydrates to the membrane proteins. The basic structure of cell membrane showing major constituents is given in *Figure 1*.

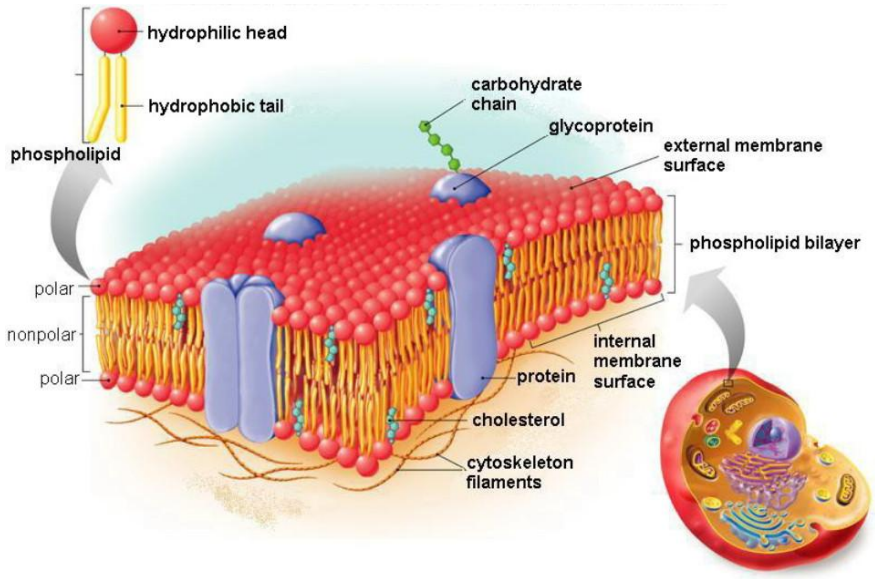

Figure 1. Illustrative model of membrane structure, showing major structural and functional components. Figure taken from (*2*).

According to the nature of their association to the membrane, proteins can be classified into groups of *i) peripheral membrane proteins,* not directly interacting with the lipid bilayer, but only weakly bound to the hydrophobic regions of integral proteins or electrostatically to charged lipid headgroups, and *ii) integral membrane proteins,* extensively interacting with lipids and generally spanning the bilayer. Due to the strong hydrophobic interaction of integral membrane proteins with lipids, these proteins require detergents or organic solvents for their solubilization. In contrast, peripheral proteins can be released by treatment with high ionic strength salt solutions, without altering the membrane integrity (*3*).

Beside the mechanical function of maintaining the physical integrity of the cell, the plasma membrane plays important roles in cell-cell interaction and movement of material and information. Integral membrane proteins are involved in the transport of various nutrients, crucial for cell growth and survival, employing different mechanisms. Certain molecules diffuse freely across the membranes, but the movement of others is restricted because of their charge, size and solubility. Various mechanisms are employed to maintain gradients of such molecules. Depending on the direction of the movement with respect to the existing electrochemical potential gradient of the transported species, transmembrane transport can be classified as *i) passive transport,* down the electrochemical potential gradient, thus dissipating energy, or as *ii) active transport,* when the solute is moved against its electrochemical potential gradient. For the active transport energy is required, and for primary active transport several different energy sources are utilized, *e.g.* sun light, various redox reactions or ATP hydrolysis. In case of secondary active transport, the energy stored in electrochemical gradients of one ion species is used by coupling their thermodynamically downhill movements to drive the uphill transport of another substrate. They are often referred to as co-transporters or exchangers. A graphic representation of different types of membrane transport is presented in *Figure 2A*. Transport systems can be functionally classified according to the number of molecules moved across the membrane and the direction of movement. If more than one species is moved across the membrane, it is possible to differentiate between *symport* and *antiport*, as shown in *Figure 2B*, whereas a *uniport* system moves one species bidirectionally. On other hand, active transport system can be characterized with regard to the net electric charge moved across the membranes as *electrogenic*, if it generates an electrochemical potential across the membrane by pumping one ion across the membrane without the compensating movement of another ion of the same charge in the opposite direction or *electroneutral*, if the same charge is moved in both

directions (*4;5*). The fact that almost 40 % of energy consumption is used for creation and maintenance of electrochemical potential gradient reflects its overall importance in all biological systems (*6*). Membrane proteins involved in regulation of the electrochemical gradient consist of *ion pumps*, utilizing primary source of energy, *ion exchangers*, members of secondary active transporters and *ion channels*, selective pore-like structures that transport ions *via* ligand- or voltage-controlled opening or closing followed by movements of ions down the electrochemical gradient (*7*). A widely used method to modify cellular membrane potential is the application of *ionophores.* They are lipid soluble macromolecules that are able to increase strongly, more or less selectively, the permeability of the membrane to specific ion species, when present in very low concentrations. It was shown that they act similarly when applied on biological and various artificial membranes, therefore, ionophores can be successfully employed for the investigation of different ion transport systems. One of the best characterized ionophore is valinomycin, a rheogenic ionophore, with the highest selectivity for potassium, as 1000 times higher than for sodium (*8*).

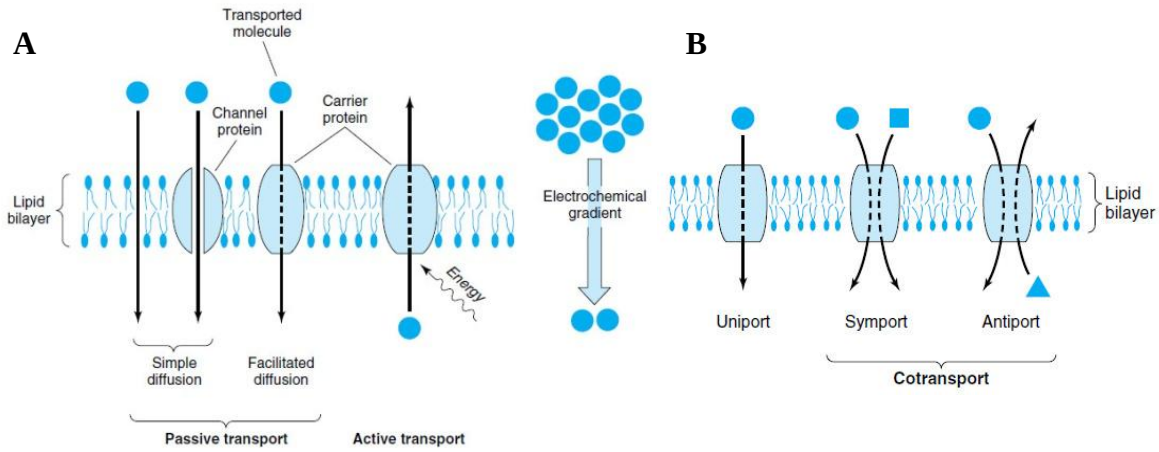

Figure 2. Schematic representation of different transport mechanisms (figure taken from (*6*)). **A**: Difference between passive and active transport **B**: Classification of transport systems regarding to the direction of movement and number of different transported species.

As already mentioned, cells expend metabolic energy to transport ions, accumulating one and removing others, creating the concentration difference between the inside and outside. The result of such a formation of an electrochemical potential gradient, especially for K^+ ions, generates a voltage difference called the membrane potential, which is essential for function of every living cell. The equilibrium potential for a particular ion species can be calculated using the Nernst equation, given in Eq. 1:

$$E = -\frac{RT}{zF}\ln\frac{Cout}{Cin} \qquad \text{(Eq. 1)}$$

R is the universal gas constant,

T is the absolute temperature,

z is the charge of the transported ion species,

F is the Faraday constant and,

c_{in} and c_{out} concentrations of transported ion species inside and outside of the cell, respectively.

Most animal cells maintain a membrane potential of about -70 mV, whereas in E. *coli* it was found to be -140 mV (*9*), where the negative sign indicates that the cytosol is more negative than the extracellular side.

1.2. Ion pumps *vs.* ion channels

The lipid bilayer of cell membranes, as previously discussed, is intrinsically impermeable to ions and polar molecules. However, inorganic ions play vital roles in processes such as nutrient uptake, energy transformation and storage, cell volume control *etc.* Membrane permeability is controlled preferentially by two classes of membrane proteins, *pumps* and *channels*. Ion channels let selected ions to diffuse rapidly down electrical and concentration gradients, whereas ion pumps consume energy to slowly move ions thermodynamically uphill. Passage of ions through the channel is regulated by a gate, whose opening and closing is controlled by appropriate signals. Through a single open ion channel 10^7 ions/s can pass, creating an electric current. Starting and stopping of that current corresponds to opening and closing events, occurring in the order of up to a hundred times per second. Ion pumps can be described in similar manner, but with two gates, opening and closing strictly alternatively (*10;11*). Ion movements performed by pumps are limited by the rate of the conformational transitions that alter access to the ion translocation pathway. Consequently, ion transport through ion channels is several orders of magnitude faster than through pumps. Due to the significantly different speeds of performing their tasks, pumps and channels have been investigated as unrelated groups. However, new functional and structural information about both of the groups suggest reevaluation, emphasizing similarities between these transporters. The recently demonstrated close genetic relationship

between pumps and channels suggested that the channels may have derived from pumps upon evolutionary degradation of a gate (*12;13*).

Although the general functional distinction between pumps and channels is the capability of the certain membrane protein for thermodynamically uphill transport, there are cases of proteins simultaneously expressing both channel and pump functions, or even chemically-induced loss of tight coupling between pump's two gates. An example of such a transformation of a pump into a channel is the effect of marine toxin, palytoxin, on the Na^+,K^+-ATPase (*14;15*). Palytoxin binds specifically to the extracellular side of the pump, disrupting the communication between the two gates, allowing both to be open at the same time. In this mode, the Na^+,K^+-ATPase works as a channel, with both gates still functional and responding to their ions, but uncoupled.

Although it is reasonable to assume that a pump loses function of a gate during evolution becoming a channel, it might be possible that an ion pump evolved from a channel by gaining a second gate (*10;16*). Some of the examples of ion-channel chimeras are the CFTR (cystic fibrosis transmembrane conductance regulator) Cl-channel, only one of a thousand ABC proteins known to function as an ion channel (*17;18*), and the KdpFABC complex in which a KcsA K^+-channel-like subunit and a P-type ATPase component are assembled (*19*). The later example, however, supports the conceptually less likable process, in which the ion channel evolved to the ion pump by forming an additional gate.

1.3. ATPases: classification, function and structure

ATP is used as an energy source, directly or indirectly, in virtually all biological systems. Therefore, ATP synthesis and ATP hydrolysis must be tightly coupled so that this cycle is able to satisfy the energy needs of the cells. ATP consumption is accomplished by a diverse group of transport systems, called *ATPases*, present in entire biological world, from bacteria to eukaryotes. These biological nanomachines utilize the Gibbs free energy of ATP hydrolysis to create electrochemical potential gradients for the transported ion across the membrane. Today, four structurally different groups of ATPases are known, with a general role of translocating numerous different ion species and/or molecules across biological membranes. ATPases are involved in many different physiological processes and different mutations of these proteins have been identified to cause a number of diseases (*20*).

Members of the first group, *V-type ATPases*, with a nomenclature derived from their principal localization, are found in intracellular vacuoles in both eukaryotic and prokaryotic cells. They represent key enzymes involved in many different intra- and inter-cellular processes (*21*). They are proton pumps and one of their roles is to regulate the acidification of intracellular compartments. They have a complex structure, and in some animal cell types are constituted of more than 20 subunits (*22*). For the overall mechanism of V-ATPases in catalyzing ATP hydrolysis and proton movement, a rotation of specific subunits is suggested (*23*).

In the second group, the *F-type ATPases*, two modes of operation have been found. Accordingly they are called F_0F_1 *ATPases* or *ATP synthases*. In the latter mode they work in the reverse mode compared to other members of ATPases (*24;25*). They synthesize ATP from ADP and inorganic phosphate in the presence of Mg^{2+} ions, in response to an electrochemical gradient of protons generated by an electron transport chain. These enzymes can work also in the "normal" mode, with an ATP-driven proton (or sodium) pumping across the membrane.

Members of the third group, *P-type ATPases*, are involved in transport of various cations - proton, potassium, sodium, calcium, as well as other metal ions across membranes of prokaryotic and eukaryotic cells (*26*). After the discovery of the first member of this group (the Na^+,K^+-ATPase, Jens Skou, 1957, (*27*)), investigation of these membrane proteins attracted substantial research efforts, leading to significant insight into the underlying ion transport mechanisms. The name is based on its covalently phosphorylated intermediate that is characteristic for the pump catalytic cycle, first introduced by Ernesto Carafoli (*28;29*). Since the KdpFABC complex of E. *coli* is a member of the P-type ATPases, this group will be presented into more details in the following paragraph.

The fourth group, named *ATP-binding cassette* transporters or *ABC-type* transporters (*30;31*), represents by far the largest group involved in the active transport of ions, but also of a variety of substrates including amino acids, sugars, lipids, toxins *etc*. Although it has been demonstrated that these transporters indeed hydrolyze ATP for substrate transport, the exact molecular mechanism of coupling of ATP hydrolysis and transport process remains unclear up to now.

In structural terms the F- and V-ATPase are much more complex than the pumps belonging to the P- or ABC-type ATPases. Therefore, one might expect that the P- and ABC-type ATPases would have been the first to be crystallized and solved structurally. The

first highly resolved structure, however, was the catalytic subunit F_1 of the more complex F-type ATPase, while so far the structure of Ca^{2+}-ATPase is the best described P-type ATPase. A graphic representation of the four different groups of ATPases is shown in *Figure 3*.

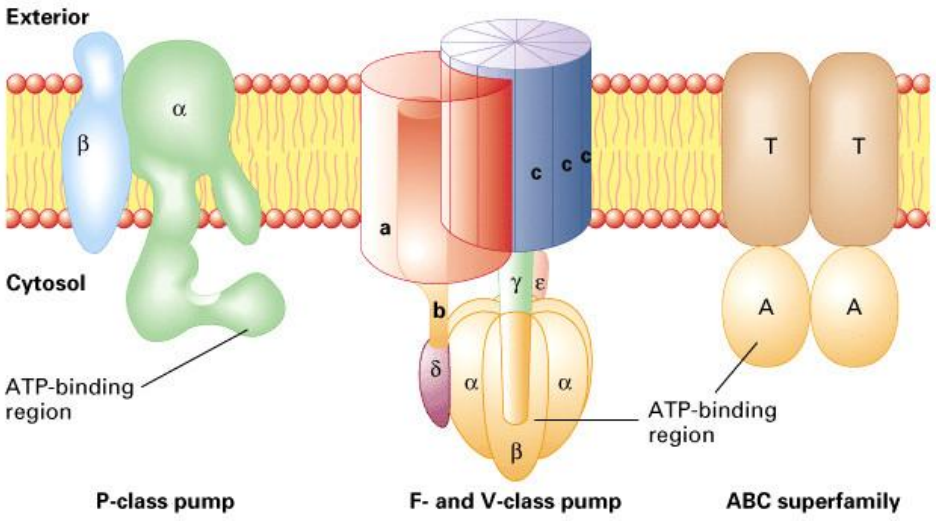

Figure 3. The illustrative representation of the four classes of ATP-driven transport proteins (*32*).

1.3.1. P-type ATPases

P-type ATPases are a large family of ubiquitous and diverse ion pumps, present in all living organisms, and key players in many different physiological processes, ranging from the generation of membrane potential to muscle contraction and toxic ions removal. Over the last five decades these membrane proteins are the most investigated and described transport systems (*33-35*). Based on the sequence homology the P-type ATPases are generally divided into five subfamilies, with respect to transported substrates and the regulation process. The overview of the P-type ATPases classification is given in *Figure 4.*

Type I ATPase contains the most ancient ion pumps. KdpFABC of E. *coli* is a prototype of type IA, transporting K^+ into the cell as an emergency system. Members of type IB ATPases, like bacterial metal-resistance proteins, remove toxic transition metal ions such as Zn^{2+}, Pb^{2+}, Cu^+ or Cd^{2+} from the cell. The homeostasis of trace elements Cu^+ and Zn^{2+} is accomplished by balancing the activity of these pumps and ABC-type metal-uptake proteins. Mutations in human Cu^+-pumps cause the lethal, hereditary Menkes and Wilson disease, raising even more interest in detailed investigation of these pumps.

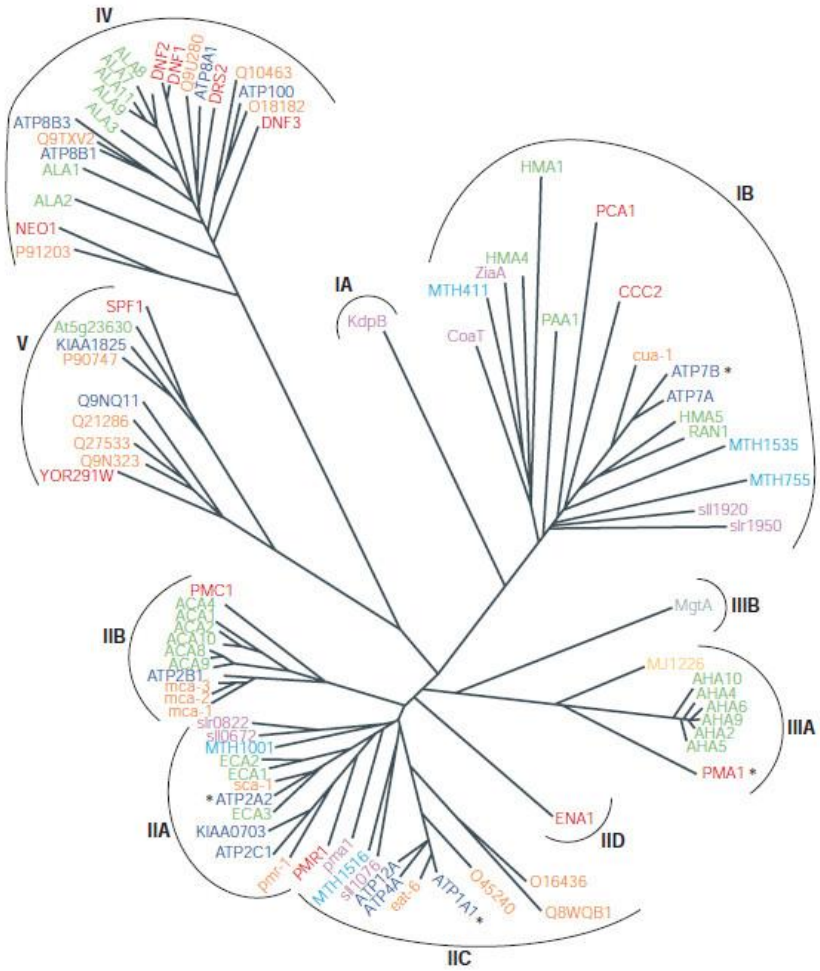

Figure 4. Phylogenetic tree of the P-type ATPase family. Classification is based on the transported substrates and the regulation processes (*33*).

Types II and III ATPases are so far the most diverse and most investigated members of this superfamily, responsible for creating and maintaining membrane potentials in various animal and plant cells. Representative of type IIA is the SR Ca^{2+}-ATPase, the first one with a resolved atomic structure (*36*). It pumps two Ca^{2+} per one ATP molecule, in exchange for two or three protons (*37*). The activity of type IIA pumps in animal cells is regulated by phospholamban (*38*), whereas those in type IIB, like the plasma-membrane Ca^{2+}-ATPase, have calmodulin-binding regulatory domains (*39*). The Na^+,K^+-ATPase and gastric H^+,K^+-ATPase are members of type IIC subgroup. The Na^+,K^+-ATPase removes three Na^+ in exchange for the import of two K^+ per one cycle. In transport-active tissue such as kidney, it was reported to consume up to 30 % of the cellular ATP. It is an electrogenic pump and generates an electrochemical gradient across the membrane, which is essential for a number of different vital processes in animal cells, such as secondary transport across membranes,

signaling, membrane potential and volume regulation (*40*). The Na^+,K^+-ATPases have an additional regulatory subunit in various tissues, which are members of the FXYD protein family, a family of small hydrophobic polypeptides with a single transmembrane span (*41*). The gastric H^+,K^+-ATPase is closely related to the Na^+,K^+-ATPase. It is an electroneutral pump, secreting hydrochloric acid into the stomach. Type IIC ATPases are hetero-oligomers, with heavily glycosylated, single membrane-spanning β-subunit that is essential for assembly of the complex, and a catalytic α- subunit, showing all the characteristics of the P-type ATPases. Type IID contains the eukaryotic Na^+-ATPases.

Type IIIA ATPases are proton pumps found in the plasma membranes of plants and fungi, involved in maintenance of the intracellular pH ≈ 6 with respect to the extracellular pH of 3.5 (*42*). The membrane potential in plants and fungi is a proton potential, since no Na^+,K^+-ATPase is present in these systems. The proton pump is a powerful electrogenic pump, transporting one H^+ per ATP molecule without counter transport of any other ion. Unlike other P-type ATPases, the H^+-ATPases have an autoinhibitory, carboxy-terminal extension. A small class of scarcely known bacterial Mg^{2+}-ATPase is grouped as type IIIB ATPases.

Type IV ATPases are found in eukaryotic cells, and are close relatives to the members of type I ATPases. They are also known as lipid flippases, since they are involved in lipid transport from the inner to the outer leaflet, thus sustaining lipid bilayer asymmetry. Intriguing is the proposed possibility of these flippases to bind and transport both ions and lipids, since the sequence comparison revealed that they have the general features of the P-type ATPases, including the ion-binding site located in the membrane. Although the possibility that the binding site can translocate both ions and lipids is not yet clarified, one hypothesis is that flippases work as ion pumps associated with lipid-transport proteins such as the ABC lipid-transporters (*43*).

The most recently defined class of P-type ATPases, with so far unclear biological functions are type V ATPases (*44*). Presumably they work as ion pumps, but their substrate specificities are still unknown.

1.3.2. Structural properties of the P-type ATPases

All members of the P-type ATPases are multi-domain membrane proteins with molecular masses of 70–150 kDa. They have an elongated form, with one domain embedded in the membrane, consisting of even number of transmembrane-spanning segments, and only a small fraction exposed to the extracellular side. The other part represents a large cytoplasmic headpiece. Both N- and C-terminal ends are facing the cytoplasmic side. The sequence comparison revealed that all members consist of four well-defined and highly-conserved domains, and according to their function or position they are named phosphorylation (P) domain, nucleotide binding (N) domain, actuator (A) domain and membrane (M) domain.

The P domain is the catalytic core of the enzyme, and it contains conserved sequence DKTGT with the aspartate residue that is reversibly phosphorylated during the reaction cycle. It exhibits a Rossmann fold, and it is the most highly conserved of the four main domains, with no large insertions or deletions. Two more important sequences located in the P domain are TGDN and GDGXND. They are involved in Mg^{2+} coordination coupled with ATP binding at the phosphorylation site.

The N domain is linked by a highly conserved narrow hinge of two antiparallel peptide strands to the P domain. It performs ATP binding and enables phosphorylation of the P domain. Apart from a conserved sequence motif that defines the nucleotide binding site, the size and sequence of the N domain is the most variable among the three cytoplasmic domains.

The A domain is almost as highly conserved as the P domain, including a loop that contains the TGE sequence motif. It is connected to the transmembrane region by two or three long and flexible linker sequences, allowing the rotation of the domain around its axis. Although the A domain contains no specific substrate-binding site, it plays an important role in the molecular mechanism of the ion transport. It was shown that it rotates around an axis almost perpendicular to the membrane, so that the TGE loop approaches closely the phosphorylation site during the ion-pumping cycle (*45;46*). Some P-type ATPases have different amino-terminal extensions fused to the A domain, like fungal H^+-ATPases, but the role of these extensions has yet to be determined.

The M domains have a low degree of sequence homology (~18 %), but their overall structures are very similar. Like the N domain, the transmembrane domain is connected to

the catalytic core of the P domain with long M4 and M5 helices. The M domain consists of 10 segments, first six form the T domain and last four segments form S domain. The ion-binding site(s) are located within the T domain, which is flexible and moves during the catalytic cycle during the association/dissociation of ion(s). The number of ion-binding sites differs: one (type III and type IIB), two (type IIA) or three (type IIC). The third ion binding site is formed by the S domain, which provides structural support to the T domain. During the catalytic cycle the S domain remains more rigid than the T domain. Among the members of the type IA ATPases, the S domain consists of a single helix at the C-terminal end. A schematic overview of the main structural domains is given in *Figure 5*.

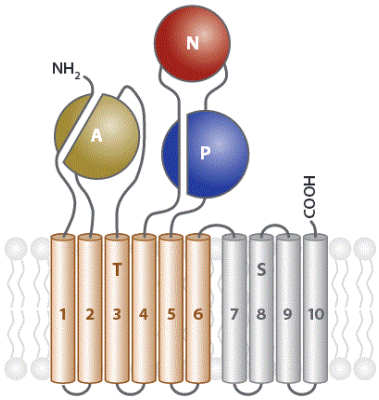

Figure 5. A schematic overview of the structural organization of the P-type ATPases, with the main domains, P, N, A, T and S labeled with capital letters (*35*).

According to the available structural information about different members of the P-type ATPases, it seems that the overall structure of these ATPases is more highly conserved than their sequences, implying that preservation of functionally unimportant residues is unnecessary. X-ray structures of the SR Ca^{2+}-ATPase show significant differences in the arrangement of helices in the M domain, and that M 4-6 are essentially responsible for the mechanical coupling of phosphorylation and ion-binding processes, whereas the P, N, and A domains move as rigid bodies (*36;45*). Even though different domains have different roles in the molecular mechanism of ion translocations, reaction steps of ATP binding/hydrolysis, enzyme phosphorylation/dephosphorylation and ion binding/release are essentially the same for all P-type ATPases. Therefore, the functional sites in the cytoplasmic domains involved in these reaction steps are unaltered, and ion-binding sites in the membrane domain are correspondingly modified to fit to different ions with different charges and radii.

1.3.3. Functional properties of the P-type ATPases

It is well known that the P-type ATPases undergo large conformational changes in order to transport ions, followed with several intermediate states (*47*). Enzymes exist in two distinct principal conformations, E_1 and E_2, with different orientation of the binding sites and correspondingly different affinities for the ATP and the transported ion species. The overall transport cycle is summarized with a so-called Post-Albers cycle, universally accepted for all members of the P-type ATPases (*48;49*). The general scheme is given in *Figure 6.*

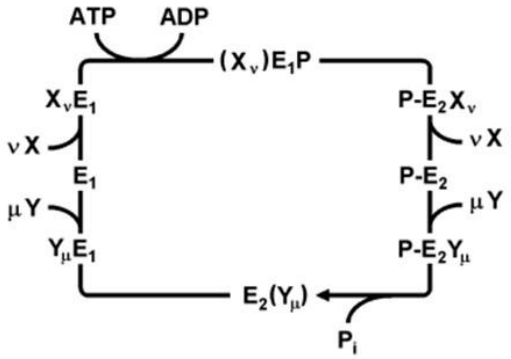

Figure 6. General model of ion-transport cycle accepted for all members of the P-type ATPase, known as a Post-Albers scheme.

The Post-Albers cycle describes the transport process as a Ping-Pong mechanism, implying that both ion species are transferred successively across the membrane and in the opposite directions (*50*). Although the term electrogenicity was originally introduced for the complete ion pumping cycle, it is possible to distinguish two half cycles in which only one ion species is transported, and further define them as electrogenic or not. According to the classical theory, the pumping process consists of a set of consecutive reactions:

i) Ion binding – the enzyme in the E_1 state has high-affinity binding site(s) accessible from the cytoplasm, and ν ions of species X are able to bind. Binding of ion(s) induces a helix rearrangement that generates a Mg^{2+} binding site close to the Asp residue.

ii) Ion occlusion followed by enzyme phosphorylation – in this intermediate state, noted as $(X_v)E_1P$, bound ion(s) are unable to exchange with either aqueous phase. Phosphorylation occurs at the P domain of the protein. Because of the electrostatic repulsion from the negatively charged γ-phosphate of ATP, the highly conserved Asp can be phosphorylated

only if Mg^{2+} is bound at the generated Mg^{2+}-binding sites, which is possible only if the ion binding site(s) are occupied (*40*). In this manner ion binding and phosphorylation are tightly coupled. Upon phosphorylation of the P domain, the ATP-mediated linkage to the N domain breaks, creating a stretch of the linker sequence between the M3 and A domain.

iii) Conformational transition – the stretching creates tension that is the driving force for the further step of dephosphorylation. Consequently, the A domain performs a 90° rotation, moving on the top of the bended P domain, with an associated conformational change from E_1-P to P-E_2. This is the slowest and rate-limiting step of the catalytic cycle.

iv) Ion deocclusion and release to the other side of the membrane – as a consequence of the A domain rotation, the high-affinity binding sites are abolished, followed by opening of ion exit channel to the other side of the membrane and ion release. Finally, the TGE motif is moved closely to the phosphorylated Asp residue.

v) Binding of counterion to the P-E_2 conformation – this causes closing of ion exit channel in the T domain and further shifting the TGE motif closer to the phosphorylated Asp residue. This allows a water molecule to be positioned between the Glu residue of the TGE and the phosphorylated Asp, carrying out the nucleophilic attack on the phosphate bond. Binding of μ counterions of species Y initiates dephosphorylation and the intermediate state of ion occlusion, $E_2(Y_\mu)$. As a result of inorganic phosphate release, the A domain moves away from the P domain, taking back the enzyme to the E_1 state. This is accompanied with helical movement in the M domain, modifying the high-affinity binding site for Y ions, and opening of the exit channel for these ions to the cytoplasmic side of the membrane, and another cycle can start.

According to this model, ions are not pushed through the membrane, but at a fixed position alternate by being present at either side of the membrane (*35*). Until now, high-resolution 3D structures of the Ca^{2+}-ATPase have been solved both in its E_1 conformation with two Ca^{2+} ions bound and E_2 conformation stabilized by the specific inhibitor tharpsigargin (*36;45*). It was demonstrated that during the transition from E_1 to E_2 state, significant rearrangements of the membrane helices occur, followed by the disruption of the coordination of the two Ca^{2+} ions, resulting in lower binding affinity. However, so far no information is available, regarding the coupling mechanism of enzymatic and transport functions.

1.4. Potassium transport in E. *coli*

Na^+ and H^+ gradients in bacteria are generally used as a convertible energy sources, playing a major role in the energetics of the cell. However, only K^+ ions are used to establish the turgor pressure, which is a vital prerequisite for prokaryotic cells (*51*). Furthermore, cytoplasmic potassium ions are involved in other important processes such as activation of the enzymes (*52*) and cell pH homeostasis, whereby the regulation of cytoplasmic pH is a contribution of both K^+,H^+ and Na^+,H^+ antiporters (*53*). A variety of membrane-bound proteins, acting as ion channels or transporters, is involved in the establishment and regulation of these ion fluxes. Since one of the most important stress factors is related to the osmolality of the surrounding medium, prokaryotic cells require fast response systems for osmoregulation. As a first response to an osmotic upshock, an increase in the cellular K^+ concentration is observed, in order to avoid extreme water efflux. This K^+ accumulation in the cytoplasm can increase in a short time the K^+ concentration from 200-500 mM under normal conditions up to molar range, and it is mainly achieved by the Trk potassium uptake system (*54*). Because of the presence of negatively charged molecules, not all cytoplasmic K^+ ions are osmolyticaly active. However, around 44 % of the total K^+ is free, even at low external osmolality (*55*). As a counterbalance of the influx of positively charged K^+ ions, the bacteria start synthesis of organic anions, like glutamate. At the point when the K^+ concentration reaches a critical point, a secondary response starts, comprised of uptake or synthesis of neutral organic solvents, like proline, glycine betaine or ectoine, or uncharged carbohydrates, like trehalose (*56;57*). These compounds do not contribute to the electrochemical gradients of the cell. In case of an osmotic downshock, cells react with a complete loss of potassium glutamate and trehalose (*58*). Due to different response mechanism to environmental conditions involving K^+, the E. *coli* cell developed a set of well-defined and specialized K^+ transport systems. An overview of the systems involved in K^+ transport in E. *coli* known so far is shown in *Figure 7*.

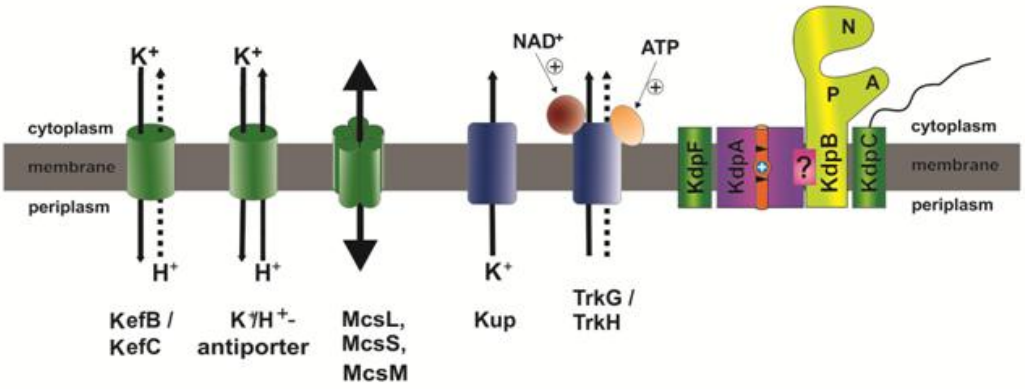

Figure 7. An overview of different K^+ transport systems found in E. *coli*, according to (*59*).

The homologous Kef potassium channels, KefB and KefC, are involved in fast K^+ efflux, and play an essential role in the removal of toxic regents, such as methylglyoxal, chlorodinitribenzole and N-ethylmaleimide (*60*). Activation of Kef channels results in fast efflux of K^+ ions followed by Na^+ influx and acidification of the cytoplasm. A so far biochemically uncharacterized K^+/H^+ antiporter is also involved in K^+ efflux (*61*). Another response to an extreme decrease in the external osmolality is K^+ efflux performed by mechanosensitive channels. Based on the electrophysiological data known so far, there are three different types of mechanosensitive channels, with different response mechanism to a membrane pressure gradient (*62*). At external K^+ concentrations above 200 µM, K^+ influx is mediated by the TrkG/TrkH and Kup uptake systems. The TrkG/TrkH system exhibits high uptake rates (v_{max}: 240 µmol g^{-1} min^{-1} and 310-450 µmol g^{-1} min^{-1}, respectively), but only moderate affinities for K^+ (K_M: 0.3–1.0 mM and 2.2–3.0 mM, respectively) (*63*). The K^+ uptake process by the Trk system requires a proton motive force and ATP that is coupled to a H^+ symport but not hydrolyzed. On the other hand, the Kup system transports K^+ with rather low affinity and low uptake rates, with K_M of 0.3 mM and v_{max} of 30 µmol g^{-1} min^{-1} (*64*). Similar to the Trk system, Kup acts as a K^+,H^+ symporter, and beside K^+ it can transport also Cs^+ and Rb^+ ions. The low affinity K^+ uptake systems TrkG/TrkH, Kup and KtrAB are not able to meet the cell's need for potassium at low external K^+ concentrations ($[K^+]_{cyt}$ < 100 µM), required for proper ion homeostasis. Under these K^+-limiting conditions, many prokaryotes can express a high affinity K^+ transport system, the membrane-bound KdpFABC complex (*65;66*). In this ion pump, coupling of ATP hydrolysis to ion transport

leads to a high affinity uptake of potassium ($K_M \leq 2$ µM), but only at moderate transport rates (v_{max} = 150 µmol g^{-1} min^{-1}) at 37 °C (*67*).

Regulation of Kdp expression and Kdp distribution

The Kdp system is genetically organized in a regulon, consisting of two operons (*Figure 8*). The first one is built up of four structural genes, *kdpFABC*, coding for the membrane-bound proteins of the KdpFABC transport complex (*65;68;69*). The adjacent operon *kdpDE* codes for the polypeptides regulating the first operon (*70;71*). KdpD, the membrane-bound sensor kinase, and KdpE, the cytoplasmic response regulator, are parts of the two component sensor kinase/response regulator system. The KdpD is inserted into the membrane and composed of four transmembrane helices, with both N- and C-terminal facing the cytoplasm (*72;73*). Upon a stimulus, that is so far an object of debate, dimerized KdpD undergoes ATP-mediated phosphorylation at the C-terminal. The phosphoryl group is further transferred to KdpE, which becomes also a dimer. Dimeric KdpE-P binds to the promoter region of the *kdpFABC* operon, thus inducing its transcription as a classical helix-turn-helix transcription factor. Without stimulus, the KdpD is able to dephosphorylate KdpE-P, leading to a termination of the KdpFABC synthesis (*74-76*). Even though the turgor model is still controversially discussed after it was proposed that changes in turgor pressure are sensed by KdpD, *kdp* expression is only observed under emergency conditions of either low external K^+ concentration or high osmolality.

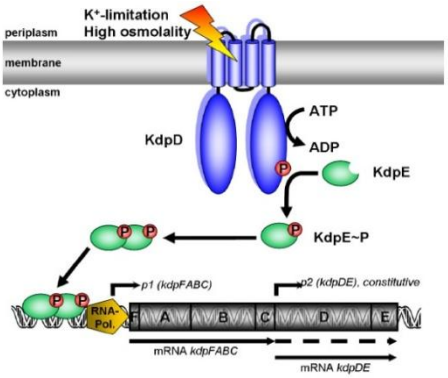

Figure 8. Schematic representation of organization and regulation of the *kdpFABCDE* regulon (*59*).

The *kdp* operon has been found in a variety of prokaryotes. Osmotic stress is one of the most vulnerable issues in prokaryotes, which is why the presence of fast and effective response

mechanisms is required. Even though more than 30 different organisms, both bacteria and archaea, are known to contain the *kdp* operon, not all of them contain the additional *kdpDE* operon as regulatory two component system. Recently, the *kdpFABC* was also found in archaea, *Halobacterium* species NRC-1 and *Thermoplasma acidophilum*, but both lack the regulatory *kdpDE* operon. The Kdp-ATPase systems can be observed as bacterial inventions as a K^+-scavenging system, since their role in archaea is still unknown.

1.5. The KdpFABC complex, a member of the P-type ATPases

As already mentioned, KdpFABC is an emergency potassium uptake system, expressed only under the K^+-limiting conditions. Biochemical properties, *e.g.* the potassium transport energized by ATP hydrolysis (*77*), inhibition of activity by micromolar concentrations of *o*-vanadate (*78;79*), and the presence of a phosphorylated intermediate during the pumping cycle (*79*), led to the conclusion that the KdpFABC belongs to P-type ATPase superfamily. The KdpFABC complex of E. *coli* was the first P-type ATPase discovered in bacteria. It has a high affinity for potassium, unique structure and subunit composition. All other P-type ATPases known so far contain in general a central catalytic subunit, including both ion transport and ATP hydrolysis, according to the Post-Albers cycle. In contrast, the KdpFABC complex consists of four subunits (*19*), and the sites of ATP hydrolysis (and hence phosphorylation) and ion binding are well separated on two different subunits. Only the KdpB subunit of KdpFABC complex exhibits explicit homology to other P-type ATPases and represents the catalytic subunit performing ATP hydrolysis. The three additional subunits have no similarities to the P-type ATPases: KdpA, structurally similar to KcsA-like K^+ channels, binds and transports K^+, KdpC acts as a molecular chaperone, and KdpF has a role of molecular glue (*80*). Møller *et al*. suggested that the unusual composition of the KdpFABC complex could represent a "missing link" between prokaryotic heavy-metal transporters (type IB) and the mostly investigated eukaryotic type IIA P-type ATPases (*81*).

A more detailed overview of KdpFABC subunits' characteristics known so far will be given, followed by a presentation of the structure-function relationship of subunits, which leads to a high affinity K^+ ion pump with unique composition and a so called "division of labor" between subunits.

The KdpA subunit

The binding and translocation of K^+ ions is mediated by a 52 kDa hydrophobic membrane-bound protein, KdpA, which exhibits no homology to other members of the P-type ATPase family. This lack of ion-binding sites in the catalytical subunit singles out the KdpFABC complex from the rest of the family. Sequence alignment (*82;83*) and mutagenesis studies (*84-86*) gave first indication that the KdpA is the K^+ binding and translocating subunit of the KdpFABC complex. The KdpA subunit shows similarities to potassium channels from KcsA-type, which was confirmed both theoretically and experimentally (*86;87*). It was hypothesized that KdpA and KtrAB/Trk families of active transport proteins evolved in prokaryotes from the family of potassium channel proteins, and that the same structural molecular mechanism controlling the pore and selectivity for K^+ is present also in more complex and recent transporters (*88*). The postulate that the KdpA is related to the K^+ channels is based on the existence of a similar pattern of residue conservation over the proposed structure, with notion that the KdpA family is overall better conserved than both Trk and KtrAB families. Even though there is a general agreement that KdpA has selectivity filter sequences similar to those found in KcsA-type channels, the number and localization of these regions are still unknown. On one hand, the authors have concluded that KdpA has two KcsA-like selectivity filter sequences at the periplasmic side, and one cytoplasmic K^+ binding site where the ion becomes occluded (*84;85*). Buurman *et al*. built a first model of KdpA with 10 transmembrane helices, instead of previously predicted 12, and they demonstrated that KdpA is able to insert the membrane in the absence of either of the other subunits. On the other hand, it was demonstrated that KcsA from *Streptococcus lividans* is built up of four single MPM motifs (membrane/P-loop/membrane), whereas the KdpA consists of a single subunit with four MPM motifs arranged in the same configuration (*82;83*). Additionally, this alternative model has been successfully used as a template for the identification and characterization of the selectivity filter regions within KdpA subunit (*86;89-91*). These results showed that three conserved glycine residues in KdpA, G232, G233 and G234, form a selectivity filter-like sequence, similar to that found in the KcsA K^+ channel. In particular, G232 appeared to be of crucial importance for K^+ affinity and selectivity, while a variety of amino-acid substitution is tolerated at positions 233 and 234. Analysis of transport properties of the purified and reconstituted A:G232D KdpFABC complex demonstrated that the replacement of Gly^{232}

with aspartate, the first residue within highly conserved GGG motif, not only changed the K_M from 2 µM to 1.2 mM, but also strongly affected the ion selectivity. The topological arrangement of KdpA based on existing models is illustrated in *Figure 9.*

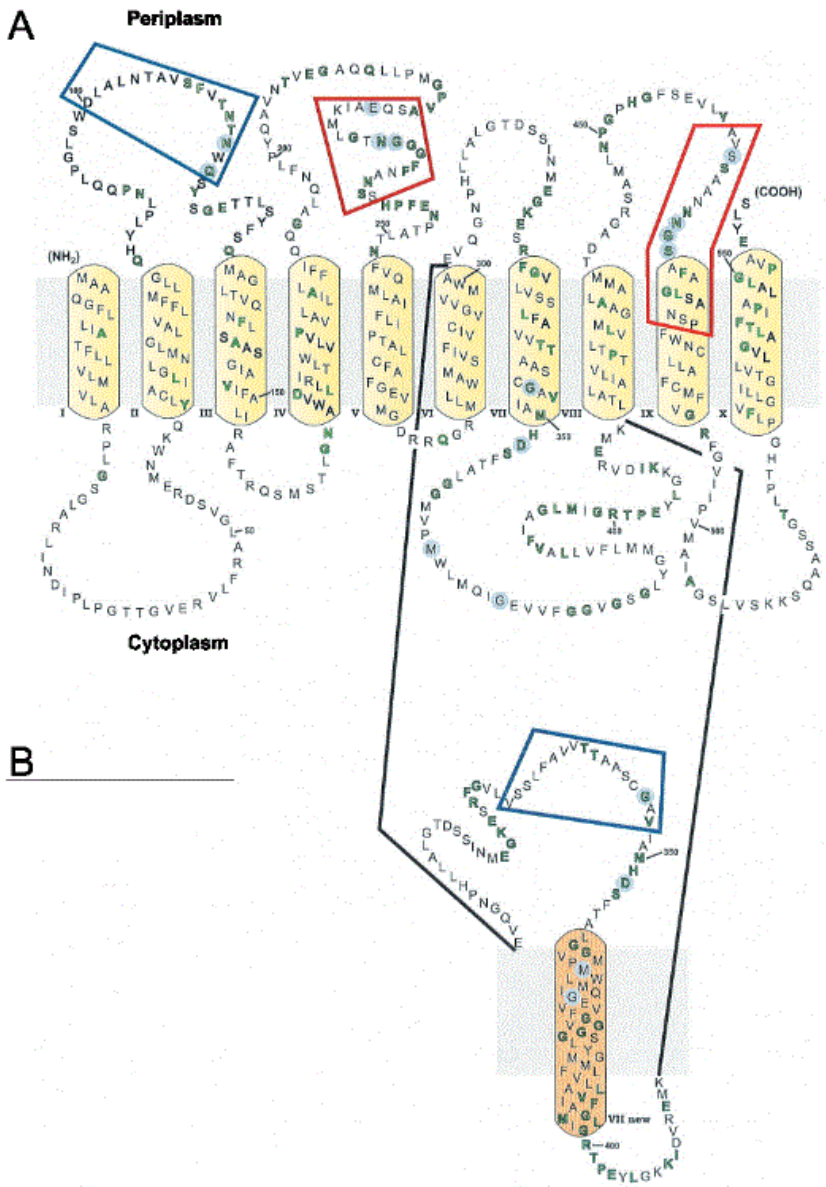

Figure 9. A: Topological model of the KdpA according to reference (*84*) **B:** Topological model of the KdpA according to reference (*82*), showing only the part that differs significantly from the model proposed by Buurman et al.

The KdpB subunit

The investigation and understanding of the structure and function of the KdpFABC complex has developed rapidly in recent years. Previous studies were focused on KdpA, KdpC and KdpF subunits, without counterparts in the P-type ATPase family, whereas the central subunit KdpB came into focus in more recent research. The KdpB is a 72 kDa polypeptide that exhibits catalytic properties detectable during the reaction cycle of the KdpFABC complex (*92;93*). As mentioned above, it is the only subunit comprising the typical four functional and structural domains, M, P, A, and N, present also in the other members of the P-type ATPase family. Reported homology to other P-type ATPases, due to the highly conserved regions, first summarized by Serrano (*94*), allows a facilitated investigation of the KdpB subunit. Ongoing discussion that the KdpFABC may represent an ancestor for the P-type ATPases (*44;95*) is based on a proposed topology for KdpB serving as a core motif for other members, comprising similar architecture with additional N- and/or C-terminal spans (*Figure 10*).

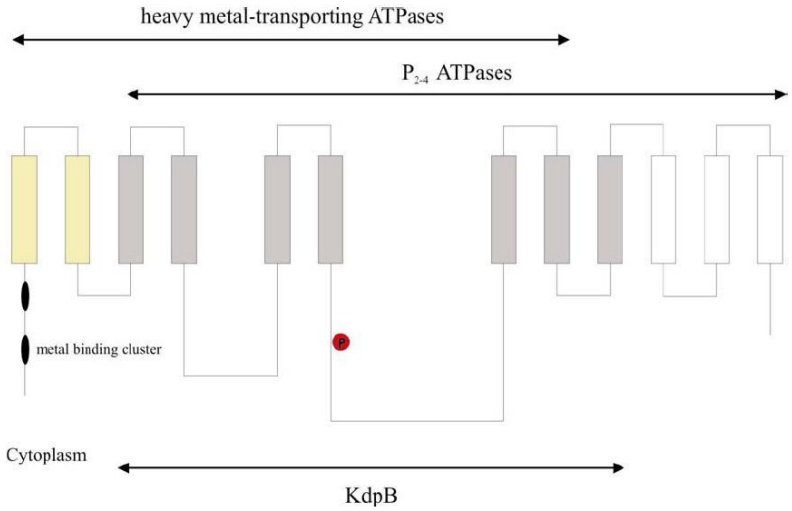

Figure 10. Schematic topology of the catalytic subunits of P-type ATPases, according to references (*44*) and (*95*).

Depending on the transport specificity and the source of the particular P-type ATPase, these proteins span the membrane seven to ten times. The proposed topology for the KdpB (type IA) suggests seven transmembrane helices (*Figure 10*, shown in gray). Heavy-metal transporters (type IB) have two additional helices at the N-terminus along the six in common with other members. Members of the types II - IV have ten transmembrane spans,

with additional three helices extending the C-terminus. The type V ATPases, with still unknown substrate specificity, might have twelve transmembrane spans. Although, the Kdp-ATPase was grouped close to the heavy-metal transporters according to the P-type ATPases classification, the KdpB subunit shows differences in comparison to this subgroup. Experimental studies proved that the ATPase activity of the KdpFABC complex can be inhibited by FITC, with FITC-binding site located within ^{395}KGSVD motif. The existence of a FITC-binding motif within the KdpB, a feature common to types II-V P-type ATPases, is a major difference between KdpFABC and heavy-metal transporters (*96*).

All P-type ATPases have large cytoplasmic loops connecting transmembrane helices TM2 and TM3, and TM4 and TM5. The first one represents the actuator domain, and the second loop is composed of two separated domains, the phosphorylation (P) and the nucleotide-binding (N) domain. These two domains are connected by a rather flexible hinge, involved in the delivery of the γ-phosphate group to the P domain. It was demonstrated that KdpB contains two charged amino acids, Asp583 and Lys586, located in the center of the TM5, and that both amino acids are conserved throughout all KdpB polypeptides, but with no counterpart in the other P-type ATPases (*97;98*). Furthermore, it was shown that the residue Asp583 plays a dominant role in the function of KdpB subunit, and that a removal of the negative charge at this position leads to loss of ATPase activity and a reduced sensitivity to *o*-vanadate. Electrophysiological measurements of KdpFABC-containing proteoliposomes adsorbed to black lipid membranes suggested that a protein-bound negative charge might move relative to the membrane during the reaction cycle, and the Asp583 might be a good candidate for this role (*99;100*). These results led to the conclusion that the Asp583 plays a role in coupling of ATP hydrolysis and ion transport, directly or indirectly, by being involved in the intra-subunit communication of the KdpB.

The A domain is connected to the transmembrane domain with short linker sequences. The conserved TGE motif is found in the A domain of almost all P-type ATPases (*81;101*), most likely involved in the process of dephosphorylation of the P-E_2 state. Results obtained so far suggest that the TGE motif approaches the phosphorylation site in the P-E_2 and E_2 states of the enzyme.

As already mentioned, the H4H5 loop consists of the P and N domain. The P domain shows similarities to the HAD superfamily (*102*), named after the L-2-haloacid dehalogenase, based on the core structure comprising a classical Rossmann fold (*36;103*). It carries the highly conserved DKTGT motif, which can be described as a key motif whose

presence classifies the enzyme as a member of the P-type ATPase family. This motif contains the aspartate residue, Asp307, which is reversibly phosphorylated by the γ-phosphoryl group of ATP during the catalytic cycle, whereas the other conserved residues are involved in the coordination of Mg^{2+} ions.

An important question arising from the catalytic cycle of the P-type ATPases has always been how nucleotide binding is performed by the clearly distinguished N domain. Due to its solubility and folding properties, the structure of the N domain of KdpB subunit, but also of other P-type ATPases, has been solved with X-ray crystallography or NMR spectroscopy (*45;104-107*). The available structural information enable the comparison of the nucleotide binding mechanisms of different of P-type ATPases. The three-dimensional structure of the KdpBN solved by NMR provides another approach to elucidate if KdpB is closer related to the type I or types II / III P-type ATPases (*92;108*). The KdpBN forms a curved, six-stranded, antiparallel β-sheet domain flanked by two pairs of α-helices (*Figure 11*). One is tightly packed to form the hydrophobic core of the domain (α1 and α2), and the other helix is more solvent (α3 and α4). In other P-type ATPases the loop between helix α2 and strand β2 contains an additional helix, whereas in the KdpBN this is replaced by a short 3_{10}-helix. Both N- and C-terminus are highly flexible. Although N domains among the eukaryotic P-type ATPases exhibit rather large insertions, their core structure is similar and it is resembled in the KdpBN. Nevertheless, the particular mechanism of the nucleotide binding is different among the P-type ATPases. In order to analyze the nucleotide-binding mechanism of KdpBN into more details, structures of both apo- and holo-form of KdpBN were solved (*95;108;109*).

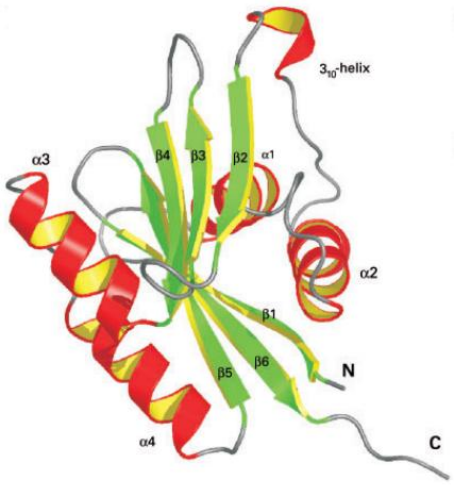

Figure 11. The structure of KdpBN (according to reference (*109*)).

As in other P-type ATPases, a conserved phenylalanine residue, Phe377 in the KdpB, interacts with the aromatic ring of the bound ATP, with a π-π stacking interactions, whereas the Lys395 stabilizes the complex from the other side by means of cation-π interactions with the aromatic part of the nucleotide (*110*). The shape of the nucleotide binding pocket of KdpBN (*Figure 12*), determined by the curved β-sheet and helices α1 and α2, allows a rapid exchange of the nucleotide, which is a prerequisite for the reaction cycle (*95;108*). The NMR-spectroscopy derived structures of the KdpBN showed that the nucleotide binding domain cannot discriminate between ATP, ADP, AMP and AMP-PNP, and that only the aromatic head group is positioned within the binding site, while the triphosphate group is not in close contact with the N domain. This means that the nucleotide itself is forced to adopt almost a linear form, as shown in *Figure 12*. This binding mode facilitates the release of the γ-phosphate group to the neighboring P domain, and it is controlled by Phe377, Lys395 and Asp344 in the core, and additionally stabilized by Arg317 and Arg382 on the surface. Furthermore, binding and release of the ligand does not require energy-consuming conformational changes, consistent with a low binding affinity of 1.4 mM. This value is in strong contrast to other P-type ATPases, *e.g.* reported values in case of the N domain of SERCA and Wilson disease protein are 10-100 µM and 70 µM, respectively (*111;112*). This discrepancy may be due to the different structures of the enzymes and the fact that KdpBN comprises no interaction with the ribose moiety of the bound ATP molecule, like it was found for the Wilson disease protein N domain.

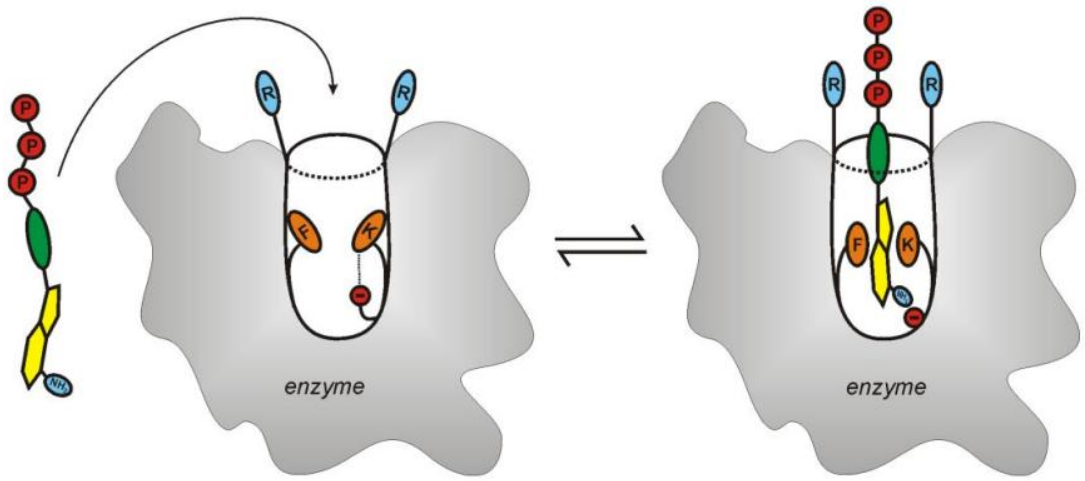

Figure 12. The schematic drawing of the nucleotide binding pocket of the soluble N domain of KdpB subunit (*108*).

Comparison of KdpBN to the other know N domain structures, implies that KdpBN represents a minimal-scheme for the nucleotide-binding domain, but also the basic ATP-binding motif comprised of Phe377, Lys395 and Gly396, conserved among the type II - IV P-type ATPases. The noteworthy observation is that neither the KGXXE/D motif nor an equivalent for Phe377 was found in the group of heavy-metal transporters. This leads to the conclusion that the Kdp-ATPase system is more closely related to alkali- and earth-alkali-transporting P-type ATPases, since it shares more similarities with the proton pump (type III), than with previously suggested concurrence with the type IB ATPases. Therefore, the classification of the P-type ATPases family should be revised.

The KdpC subunit

The KdpC subunit is a peptide of 21 kDa, containing one transmembrane helix and large extension facing the cytoplasm (*113*), while the N-terminus is oriented towards the periplasm. It comprises no homologies to any other known protein so far, and its function is still not fully understood. Based on the secondary structure prediction, hydropathy plot and sequence alignment, the KdpC seems to be composed of four parts, two of which are highly conserved among different organisms and located within the hydrophilic portion of KdpC (*113*). Earlier experiments of mutational analysis demonstrated that KdpC subunit is essential for the KdpFABC complex (*114*). Investigation of the assembly of the three subunits KdpA, KdpB, and KdpC revealed a strong interaction between KdpA and KdpC, and only a weak interaction between KdpB and KdpC subunits. In addition, when the KdpC subunit is not present, the other two subunits are unable to form a partial complex, suggesting that KdpC acts as a structural mediator between KdpB and KdpA (*115*). Its functional role was first indicated by significant interaction with radioactive probe [^{32}P]-2-azido-ATP, and confirmed by results showing that the KdpC subunit selectively binds one ATP molecule within its hydrophilic portion, $KdpC_{sol}$ (*116*). The binding constant was found to be in milimolar range, and this low binding affinity was explained by the fact that only the ribose moiety of ATP is supposed to interact with $KdpC_{sol}$. Recent experiments showed that the interaction between ATP and KdpC is dependent on the presence of a conserved glutamine residue, also present in ABC transporters (*117*). The mechanistic function of this glutamine side chain in the nucleotide-binding mechanism of ABC transporters is the formation of two hydrogen bonds with the two hydroxyl groups of the

ribose moiety of the nucleotide (*118*). Furthermore, the $KdpC_{sol}$ domain interacts with the N domain of the KdpB subunit in the proximity of the ATP-binding pocket, forming a KdpBN/$KdpC_{sol}$/ATP ternary complex, resulting in significant increase of the ATP binding affinity of the KdpB subunit. This model of cooperative ATP binding by KdpB and KdpC leads to the conclusion that KdpC acts as a catalytical chaperone, by binding an ATP molecule and/or guiding it into the nucleotide-binding pocket of KdpB.

There are several examples of additional regulatory subunits affecting protein activity, like γ-subunit of the Na^+,K^+-ATPase, or phospholamban and calmodulin in the case of Ca^{2+}-ATPase. Such a regulation is a result of the interaction with dynamically moving catalytic domains, or direct modulation of the affinity of the ATP binding site. All regulatory subunits are small integral membrane subunit with cytoplasmic extension carrying the regulatory function. Based on these features, it was considered that the KdpC resembles these regulatory proteins, but none of these enzymes proved to be essential for protein activity, whereas KdpC exhibits a unique function within the KdpFABC complex.

The KdpF subunit

The KdpF subunit is one of the smallest hydrophobic protein of only 3 kDa known so far, consisting of only one transmembrane helix without any extensions. Sequence analysis demonstrated that it is an integral part of the KdpFABC complex, and high resolution SDS-PAGE revealed a corresponding protein band (*119*). Although deletion of the *kdpF* gene did not affect the growth of the cells under K^+-limiting concentration, purification of resulting KdpABC complexes showed a complete loss in ATPase activity. Furthermore, in the absence of the KdpF subunit, a clear tendency of the complex to disintegrate was observed. Interestingly, the addition of the separately purified KdpF, or addition of a high amount of E. *coli* lipids to the detergent-solubilized KdpABC complex, was able to completely restore ATPase activity. These findings suggest that the KdpF stabilizes complex *in vitro*, most probably acting as a lipid-like peptide.

1.6. Structure-function relationship of the KdpFABC complex

The stability of the KdpFABC complex upon solubilization with non-ionic detergents indicates the existence of strong subunit interactions (*115*). As already mentioned, both KdpA and KdpC subunits are necessary to assemble a stable complex containing the catalytic KdpB subunit. Investigation of the assembly of the KdpFABC complex revealed a strong interaction between KdpA and KdpC, but only a weak interaction between KdpB and KdpA, whilst KdpF stabilizes the complex *in vitro*. The functional unit of the KdpFABC complex is a homodimer, in which two adjacent KdpFABC monomers interact *via* their neighboring KdpB subunits (*120;121*). However, at concentrations lower than 30 nM the complex exists as a functional monomer. Therefore, the dimerization does not seem to be essential *in vivo*, and although oligomerization is found within other P-type ATPases, the physiological role of an oligomer formation is still not fully understood (*122;123*).

The already mentioned significant difference of the ATP-binding affinity for KdpBN and other P-type ATPases, can be explained by the fact that KdpBN comprises no interaction with the ribose moiety of the bound ATP, in contrast to the extensive nucleotide/protein interaction *via* the ribose moiety in case of other P-type ATPases. Consequently, there has to be an additional mechanism, maintaining the ATP molecule bound inside the nucleotide-binding pocket despite the low binding energies provided by the side-chain interactions. It has been shown that the nucleotide-binding site is neither selective for the phosphate moiety nor for the base moiety, thus leaving the nucleotide's ribose moiety open for specific binding to the KdpC. This proposal is in agreement with previous findings that the hydrophilic portion of KdpC selectively binds one ATP molecule (*116*). The hypothesis that KdpB and soluble portion of KdpC directly interact during nucleotide binding was analyzed by isothermal titration calorimetry (ITC). No interaction between $KdpC_{sol}$ and KdpB was found in the absence of ATP, while the K_d of (1.0 ± 0.2) mM was calculated from the ATP titration of KdpB experiments. However, a K_d of 3.4 µM was calculated from (KdpBN+ATP) titration with ($KdpC_{sol}$+ATP) experiments, indicating the formation of a ternary complex KdpBN/$KdpC_{sol}$/ATP at a stoichiometry 1:1:1. This resulted in a considerably high affinity, comparable to that of ATP binding to other P-type ATPases. The formation of this ternary complex is most likely not affected by the γ-phosphate group, since it protrudes far away from the binding pocket facing the phosphorylation site within the P domain. Results of 2D [^{1}H - ^{15}N] HSQC spectra of ^{15}N-labeled KdpBN with bound

AMP-PNP recorded in the absence and presence of equimolar amount of unlabeled $KdpC_{sol}$, confirmed the notion that with the ATP bound to the KdpBN, KdpC closes the binding pocket by interactions at the outer rim of the nucleotide binding pocket, thus preventing an exchange of the ATP molecule (*117*). The ATP binding motif within KdpC, the 140-QIPRVAKARNL-150 motif, and especially the conserved Gln140 proved to be essential for efficient ATP binding. The fact that no large-scale conformational changes occur upon nucleotide binding, indicates that ATP-induced domain rearrangements are not obligatory for the reaction cycle of the KdpFABC, in contrast to results published in case of the Na^+,K^+-ATPase N domain (*124*).

The nucleotide-binding mechanism can be summarized as follows: the ATP molecule enters the KdpBN domain, where Asp344 forms a hydrogen bond with the amino group of the purine ring, while Lys395 is involved in cation-π stacking. At the rim of the nucleotide binding pocket the positively-charged Arg317 and Arg382 residues orient the triphosphate group by hydrogen bonds formation towards the P domain, whereas Glu348 and Asp399 produce the same effect by electrostatic repulsion of the phosphates. Upon ATP binding, the KdpC/KdpBN interaction is triggered, and following the formation of the hydrogen bond between the hydroxyl groups of the ribose and the Gln140 of KdpC, KdpC finally closes the binding pocket, thus entrapping the ATP molecule. Although the nucleotide binding pocket is blocked, the triphosphate group is able to protrude toward Asp307 in the P domain of the KdpB subunit. Upon the subsequent dephosphorylation step followed by large conformational rearrangements, the opening of the nucleotide binding pocket occurs (*19;92*). The KdpC subunit is displaced from the nucleotide-binding pocket of the KdpB, most likely upon movement of the A domain towards the P domain in the E_2 state of the enzyme.

In contrast to other P-type ATPases, the KdpFABC complex has to couple energy and transport between two different subunits. Although the energy-generation process is the same for all members of this family, the mechanism of substrate translocation has to differ. Therefore, an important question is the mechanism by which the energy obtained by the KdpB is efficiently transmitted to the ion-transporting KdpA subunit of the KdpFABC complex. Computational sequence comparison of KdpB with other P-type ATPases identified two conserved residues, Asp583 and Lys586 located in TM5, that are most likely forming a dipole in the membrane, but that do not have any homologous counterpart in other P-type ATPases. This conserved dipole is considered to be involved in charge displacement

during the K^+-independent electrogenic partial reaction step of the catalytic cycle (*100*). Mutational studies in case of Asp583 showed that in isolated KdpFABC mutants, K^+-stimulated ATPase activity and ion transport rates were significantly reduced when the negative charge was eliminated (*97*). Furthermore, the presence and the correct positioning of these residues are essential for the energy coupling between the KdpB and KdpA subunit. Mutational studies confirmed that a regulatory K^+-binding site is located in the KdpA subunit and is most probably identical with the K^+-binding site responsible for substrate translocation. The hypothesis is that existence of functional dipole Asp583/Lys586 is involved in both the energy transmission from KdpB to KdpA, and the K^+ stimulus from KdpA to KdpB subunit. However, the findings showing that alterations of the dipole charges affect the transport rates, but do not affect the K^+ binding affinity, indicate that both Asp583 and Lys586 are not directly involved in the establishment of the K^+-binding site, but rather have a role in the enzymatic/transport coupling mechanism. All tested mutants showed higher resistance towards the specific P-type ATPases inhibitor, *o*-vanadate, which is known to inhibit the enzymes in its E_2 conformation. These results suggest that alterations of the dipole affect the E_1-P → P-E_2 conformational transition by stabilizing the E_1-P state, thus shifting the equilibrium away from the E_2 conformation. Results based on the electrostatic interaction model indicate that the conserved Arg493 residue in KdpA is another possible charged residue that is involved in the coupling mechanism. According to the current model of KdpA, Arg493 is located in one of the helices which is not part of the putative K^+ channel (*82*). The subunit organization within the KdpFABC complex is shown in *Figure 13*, with marked essential residues that are involved in ATP hydrolysis and ion transport.

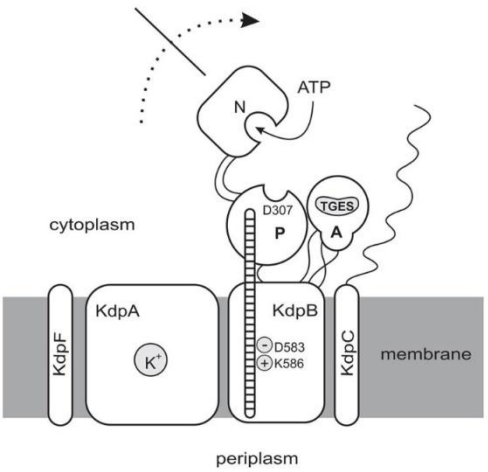

Figure 13. Assembly of the KdpFABC complex with marked residues involved in the ATP hydrolysis and ion transport.

1.7. Molecular mechanism of the KdpFABC

When discussing the reaction cycle of the KdpFABC, both the concepts and structures of ion channels and ion pumps should be taken into account. However, a recently presented study indicates that the nucleotide-binding mechanism of KdpFABC resembles that found in ABC transporters (*117*), extending the level of concept mixture from ion channels and ion pumps, to a third major group of transmembrane transport system, the ABC systems.

So far, the only proposed reaction cycle for KdpFABC complex was suggested by Haupt *et al.* (*Figure 14*). Their model includes the concept of a flexible N domain, engaging and disengaging the P domain merely by the Brownian fluctuations (*36;104*), and that binding of the transported ion is a key step leading to a formation of a high-ATP affinity conformation. The flexibly linked N domain indicates that the increase in ATP affinity is a direct result of an activation of the phosphorylation site. In case of the reaction cycle, this could mean that in the absence of transported substrate, the N domain swings back and forth towards the P domain, with ATP being bound and released, with a binding affinity similar to that of the isolated KdpBN. Since this scenario is not likely to happen under physiological conditions, activation of the ATPases occurs by reversible phosphorylation of a regulatory subunit (type II - IV) or by their synthesis only when needed, like in case of the KdpFABC complex (*95*).

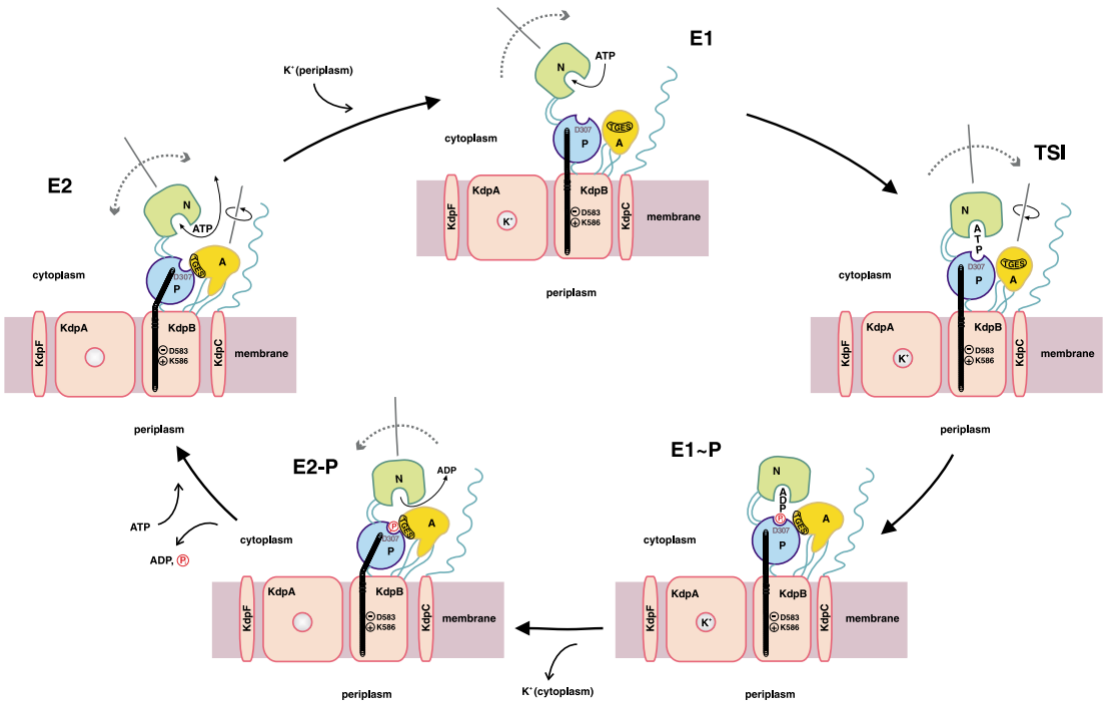

Figure 14. The proposed reaction cycle for the KdpFABC complex (according to the reference (*109*)).

As mentioned above, the general Post-Albers scheme (*Figure 6*) includes two conformational states of the enzyme, the unphosphorylated E_1 with high-affinity ion-binding site(s) on the extracellular/periplasmic side of the membrane, and the phosphorylated P-E_2 state with low-affinity binding site(s) facing the cytoplasm. Upon binding of K^+, a rearrangement of the transmembrane helices occurs *via* stretching of TM5, leading to the E_1 state. Binding of the transported ion at the same time activates the phosphorylation site, Asp307, within KdpB domain. Enzyme in the E_1 conformation has high affinity for ATP, as a result of the cooperative ATP binding by KdpBN and $KdpC_{sol}$. At this point the N domain is still supposed to remain flexible in case that no cytoplasmic ATP is present. With binding of ATP the N domain approaches the P domain, trapping the nucleotide, which is presented by the short-lived transition state (TSI), subsequently leading to the high energy E_1~P state. Upon phosphorylation, the A domain rotates along its axis and moves the TGE motif toward the P domain. Subsequently, the formation of the phosphoenzyme causes the conformational change, within the transmembrane domain, resulting in formation of the P-E_2 state with altered orientation of the dipole between the Asp583 and Lys586 residues located in TM5 of the KdpB. This state of the enzyme has a significantly lower ion-binding affinity, thus K^+ is released to the cytoplasmic side of the membrane. The link between the N and P domain is disrupted, the N domain swings back further and causes the Asp307 to be freely accessible and dephosphorylated by the A domain, finally converting the enzyme to the E_2 state. This is readily followed by K^+ binding, the enzyme returns to the E_1 state and reactivates the phosphorylation site, thus the reaction cycle can start again.

1.8. Electrogenic K^+ transport by the KdpFABC complex

As mentioned above, ion transport performed by a membrane protein is called electrogenic when net charge is moved across the membrane, therefore, affecting the existing membrane potential. In case of the Na^+,K^+-ATPase and Ca^{2+}-ATPase, the overall transport is electrogenic, transferring one or two net charges across the membrane, respectively. Although overall transport of the H^+,K^+-ATPase is electroneutral, it was demonstrated that partial reactions are electrogenic, since the net charge is translocated in each half cycle. The corresponding transport stoichiometries of these prominent members of P-type ATPases are: $3Na^+/2K^+$, $2Ca^{2+}/2H^+$ and $2H^+/2K^+$. Investigation of the electrogenicity

of the ion transport, in both overall process and partial reactions, provides important information about the transport mechanism, specifically the number of charges cotransported during the reaction cycle.

Although the KdpFABC complex has been investigated intensively performing genetic, physiological and various biochemical studies, knowledge about the mechanism of ion transport of this unique system is still limited. First experiments aiming for the K^+ transport performed by the Kdp system were done in intact cells. The results showed that net K^+ uptake by KdpFABC leads to the depolarization of the cell membrane, suggesting that the K^+ transport process is electrogenic (*67;125*). However, the electrogenicity of a single component was difficult to determine in native membranes. Next step was using right-side-out vesicles and an ATP-generating system, which maintained ATP to be the driving force for electrogenic K^+ uptake by the Kdp system. Furthermore, no movement of H^+, in symport or antiport with K^+, was detected utilizing this technique (*126*). Studies of the electrical properties of KdpFABC using a black lipid membrane (BLM) technique demonstrated that a stationary electrical current is generated upon activation of the pump reconstituted in liposomes by photochemically released ATP in the presence of K^+, and confirmed that extracellular K^+ activates the KdpFABC complex *in vivo (99).* In the same study, experiments with different ionophores, used to modify the conductance of the lipid membrane, showed that transport activity of the KdpFABC is the same whether the membranes are conductive only for K^+, achieved by the K^+ ionophore valinomycin, or both K^+ and H^+, achieved by protonophore 1799 together with the K^+/H^+ exchanger monensin. Another approach that also confirmed electrogenic nature of ion transport by the KdpFABC consisted of fluorescence measurements with vesicles containing reconstituted KdpFABC. Using the potential sensitive dye $DiSC_3(V)$ it was demonstrated that the inside-out reconstituted enzyme generates an inside negative potential upon ATP activation, as result of the transport of positive charge out of the proteoliposomes.

Many P-type ATPases perform transport of two different ion species, sequentially and in opposite direction. Starting point in gathering more information about the reaction cycle of the KdpFABC is the comparison with well-described members of the P-type ATPase family, *e.g.* the Na^+,K^+-ATPase. The Na^+,K^+-ATPase exports three Na^+ to the extracellular side and imports two K^+ into the cell per one hydrolyzed ATP molecule. KdpFABC transports K^+ ions into the cell, and it is reasonable to assume that the K^+ transport occurs – similar to the Na^+,K^+-ATPase – in the second half cycle, related to the $E_2 \rightarrow E_1$ transition. In case that

KdpFABC indeed transports another ion in opposite direction to the K^+ transport, proton is most likely to be the counterion. Since it was confirmed by different techniques that the net positive charge is translocated to the intracellular side of the KdpFABC complex, two scenarios are suggested – transport of only K^+ ions, or transport of one H^+ and two K^+ in the opposite directions. Experimental results available so far do not distinguish between both possibilities. Investigation of a possible proton counter transport can be difficult, usually due to rather high proton permeability of the proteoliposomes. Another approach consisted of measuring transient currents using planar lipid membranes to which liposomes reconstituted with the KdpFABC were adsorbed, generated by photolytic ATP release from caged ATP, at different pH (*100*). Results obtained in the absence of K^+ suggested that protons do not play a significant role in the electrical signal generated by KdpFABC, but still it could not be completely excluded. According to the data acquired in the absence of K^+, an electrical signal upon activation was found, and it was assigned to the KdpFABC, since it was inhibited after addition of 1mM *o*-vanadate. The sign of the signal corresponded to a translocation of positive charges to the intracellular side or that of negative charges to the extracellular side of the protein. The proposed kinetic model for the KdpFABC that includes both transient current in the absence of K^+ and a stationary current in the presence of K^+, suggests an electrogenic conformational transition in the absence of K^+ followed by K^+ transport in its presence. However, the approved explanation for this observation is still lacking.

1.9. Aim of the project

In this work, the nature of the pumping process of KdpFABC will be investigated. The electrogenicity and binding affinities of the ion pump for both K^+ and H^+ will be determined in detergent-solubilized complexes, in both conformations, by use of the RH421. $DiSC_3(V)$-fluorescence measurements with KdpFABC-containing proteoliposomes will be employed in the study of a possible H^+ translocation, and effect of various ions and substrates on the pump activity. Time-resolved fluorescence measurements with caged ATP will provide additional kinetic information regarding the reaction cycle. Finally, Post-Albers schemes, derived from a general model accepted for the P-type ATPases, will be introduced to describe a possible molecular pump cycle, supported by the gathered experimental results.

2. EXPERIMENTAL PROCEDURES

2.1. Bacterial strains and growth conditions

KdpFABC complex with a C-terminal His_{14}-tag at the KdpA subunit cloned in a plasmid pGS4 was expressed in E. *coli* strain TKW3205 (*ΔkdpABC'05 nagA-trkA405 trkD1 Datp706*), with ampicillin as the selection marker, and under the control of the wild-type promoter (*78;120*). To express KdpFABC protein, E. *coli* cells were adapted to low potassium concentrations in a pre-culture over a period of three days, successively decreasing the potassium concentration in the medium. Finally, potassium-free minimal medium was inoculated with the preceding overnight culture, and protein expression was induced by subsequent additions of 45µM KCl at the time points when cell growth reached a plateau (*Figure 15*). Cells were harvested by centrifugation at optical density of ~1 at 600 nm, and cell pellets were flash frozen in liquid nitrogen and stored at -80 °C.

List of prepared solutions

20 % D-Glucose

6 mM $FeSO_4$

1 mg/mL Thiamin

1 M KCl

Ampicillin 50 mg/mL, kept at -20°C

KML (modified LB) medium (*127*)

10 g trypton

5 g yeast

10 g KCl

K0 (minimal) medium (*92*)

23 mM NaH_2PO_4

46 mM Na_2HPO_4

8 mM $(NH_4)_2SO_4$

1 mM Tri-Na-Citrat

0.4 mM $MgSO_4$

$K0^+$ medium (1L)	**K_{50} medium (5 mL)**	**K_{10} medium (5 mL)**
K0 medium supplemented with 0.006 mM $FeSO_4$ 0.4 % D-Glucose 1 µg/mL thiamin 50 µg/mL ampicillin	4.65 mL $K0^+$ 250 µL 1 M KCl 100 µL 20 % D-Glucose	4.75 mL $K0^+$ 50 µL 1 M KCl 100 µL 20 % D-glucose
K_5 medium (50 mL)	**K_1 medium (200 mL)**	**$K_{0.05}$ medium (1L)**
45 ml $K0^+$ 500 µL 1 M KCl 1 mL 20 % D-glucose	200 µL 1M KCl 4 mL 20 % D-glucose ad 200 mL $K0^+$ medium	50 µL 1 M KCl 20 mL 20 % D-glucose ad 1 L $K0^+$ medium

Protocol

1. day Cells were plated from a glycerol stock on LB agar plates with 50 µg/mL ampicillin. Cells were grown overnight at 37 °C.

2. day A single colony was picked from the plate with a pipette tip and inoculated in 5 mL KML culture containing 50 µg/mL ampicillin. Culture was grown with shaking (200 rpm) at 37°C. After 8h 100 µL of the culture was transferred to 5 mL K_{50} culture, and left overnight shaking at 37 °C.

3. day 100 µL of the culture was transferred to 5 mL K_{10} culture. Culture was grown for 8h at 37 °C. The whole volume of K_{10} cell culture was transferred to 50 mL of K_5 medium, and left overnight on 37 °C while shaking.

4. day The appropriate amount of K_5 culture was transferred into 200 mL K_1 culture, so that the final OD_{600} was 0.1. After incubating for 8h at 37 °C, the OD_{600} was measured and the appropriate volume was transferred to 1 L of $K_{0.05}$ culture, with the final OD_{600} of 0.1.

5. day The OD_{600} was measured and the appropriate volume of $K_{0.05}$ culture was transferred to 20 flasks filled with 1 L $K0^+$ medium, with the final OD_{600} of 0.05. The main culture was grown at 37°C, while the OD_{600} was measured every 30 minutes, and the growth curve was followed. When cell growth reached stationary phase, 1 mL 45 mM KCl was added to each flask. The induction steps were repeated until the final measured OD_{600} was approximately 1. Finally, the cells were immediately harvested by centrifugation at 5 000 g for 5 minutes at 4 °C. The cell pellet was collected, flash frozen in liquid nitrogen and stored at -80 °C. The characteristic bacterial growth curve is shown in *Figure 15.*

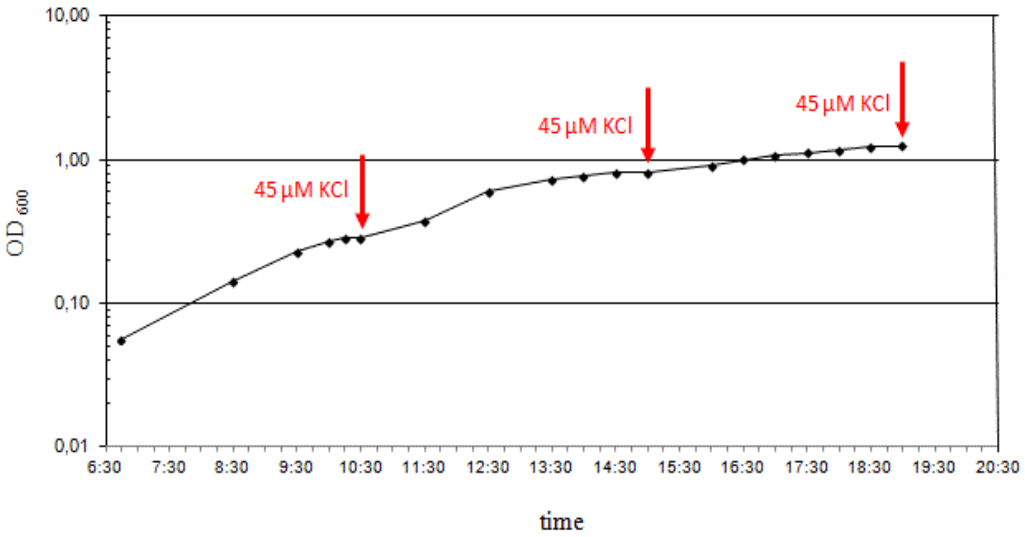

Figure 15. Characteristic bacterial growth curve, with indicated three induction steps of 45 µM KCl additions at time points when cells growth reached a stationary phase.

2.2. Purification of the KdpFABC complex

All steps were performed on ice, unless stated otherwise. 30 g of E. *coli* cell pellets were thawed and dissolved in approximately 40 mL buffer of 50 mM Tris-HCl at pH 7.5, 20 mM $MgCl_2$, 10 % (*v/v*) glycerol, supplemented with a protease inhibitor cocktail tablet (EDTA free), 5 mM DNase I and 0.5 mM PMSF. Cells were then lysed with 2-3 cycles of French press, using a pressure of 10 000 psi. Unbroken cells were removed by centrifugation at 10000 g for 15 minutes at 4 °C. Subsequently, the cell membranes were collected by ultracentrifugation at 200 000 g, at 4 °C for 1h, and further resuspended in 50 mM Tris-HCl at pH 7.5, 20 mM $MgCl_2$, 20 % (*v/v*) glycerol and 0.5 mM PMSF. Membranes were homogenized, and the concentration of the membrane protein was determined with BCA assay. Finally, the membranes were shock frozen in liquid nitrogen and stored at -80 °C.

Purification of the KdpFABC complex was carried out according to the previously published protocol (*120*). His_{14}-tagged KdpFABC complex was purified *via* metal-chelate affinity immobilization, followed by size exclusion chromatography. Cell membranes were dissolved in 50 mM Tris-HCl at pH 7.5, 10 mM $MgCl_2$, 10 % (*v/v*) glycerol, 1 mM DTT and 0.5 mM PMSF at a final protein concentration of 5 mg/mL. The KdpFABC complexes were solubilized with 1 % (*w/v*) Aminoxide WS-35 for 1h by gentle stirring at 5 rpm on a rotator at 4 °C. The solubilized protein was collected by centrifugation at 200 000 g for 1h at 4°C,

and the supernatant was applied to a 5mL HisTrap column (GE Healthcare), pre-equilibrated with 5-10 column volumes of buffer containing 50 mM Tris-HCl at pH 7.5, 20 mM $MgCl_2$, 10 % (*v/v*) glycerol, 150 mM NaCl, 10 mM imidazole, 0.5 mM PMSF and 0.2 % (*w/v*) Aminoxide WS-35. After three binding cycles, HisTrap column was connected to a FPLC system (Amersham, Biotech), previously washed with distilled water and equilibrated with the washing buffer, containing 50 mM Tris-HCl at pH 7.5, 20 mM $MgCl_2$, 10 % (*v/v*) glycerol, 150 mM NaCl, 20 mM imidazole, 0.5 mM PMSF and 0.2 % (*w/v*) Aminoxide WS-35. The HisTrap column was washed with 30-50 mL of washing buffer at a flow rate of 0.5 mL/min. Thereafter, the KdpFABC was eluted with the same elution buffer containing 130 mM imidazole, at the flow rate of 0.5 mL/min. From the elution protein profile, protein-containing fractions were collected and checked on a 12.5 % SDS-PAGE gel. The KdpF subunit, the smallest subunit of only 3 kDa, is not visible on this type of SDS-PAGE gel, since its working range is between 10- 250 kDa.

Afterwards, the fractions containing KdpFABC subunits in stoichiometric amounts were collected and concentrated at 10 000 g (Vivaspin 6, molecular weight cut off 50 000 Da, Sartorius) to a final volume of approximately 500 µL. The sample was then loaded on a Superdex 200 HR 10/30 column (GE Healthcare), previously equilibrated overnight with gel filtration buffer containing 50 mM Tris-HCl at pH 7.5, 150 mM NaCl, 0.5 mM PMSF, and 0.2 % (*w/v*) Aminoxide WS-35, and eluted at the flow rate of 0.5 mL/min. Corresponding fractions were again loaded on a 12.5 % SDS-PAGE gel, and further concentrated as described above. Examples of the KdpFABC elution profile after gel filtration and corresponding SDS-PAGE gel are given in *Figure 16.*

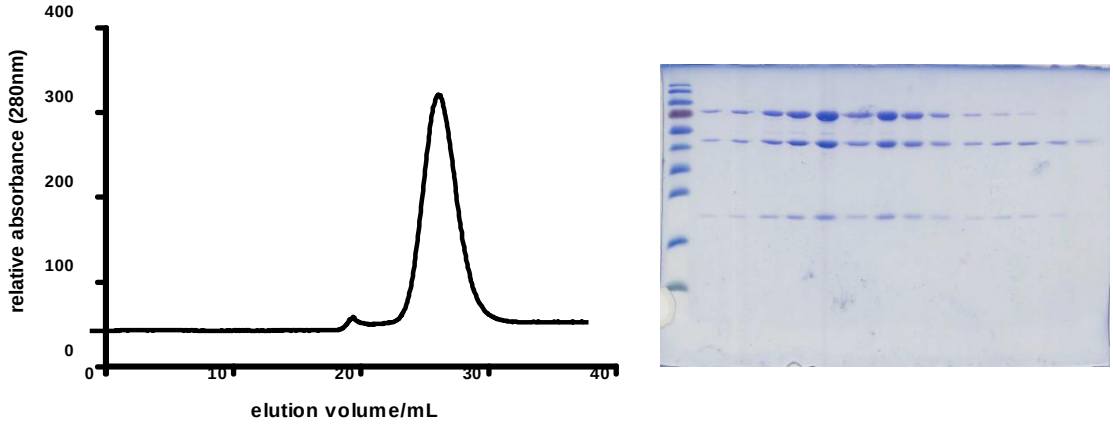

Figure 16. KdpFABC elution profile (left) after gel-filtration and corresponding SDS-PAGE gel (right).

Alternatively, different detergents were used for purification of the KdpFABC complexes. In these analogous procedures, the concentration of the detergent chosen for the enzyme solubilization was also 1 % (*w/v*) and 0.2 % (*w/v*) for further purification.

2.3. Biochemical assays

2.3.1. Protein determination

The concentration of membrane protein was determined with bicinchoninic acid assay (*128*), according to the manufacturer's protocol (*Pierce*). The assay was carried out in disposable semi-micro plastic cuvettes. In order to obtain a calibration curve, five 50 µL samples with different amount of BSA, ranging between 0 and 30 µg, were prepared. Sample of the membrane protein with an unknown concentration contained 1 µL of the membranes and 49 µL of distilled water. The same volume of the sample buffer alone was used for background determination. All samples were filled up to 1 mL total volume with the working reagent, prepared by mixing buffers A and B in a ratio of 50:1. After 30 minutes incubation at 37 °C, absorption was measured at 562 nm. The sample concentration was obtained by interpolation on the calibration curve of the sample absorbance corrected for the background absorbance.

The protein concentration of the detergent-solubilized KdpFABC complex has been determined with the Lowry assay (*129*). The assay was carried out in disposable glass vials. To obtain the calibration curve, five 10 µL samples were prepared containing known amounts of BSA between 0 and 30 µg. For the measurement of the KdpFABC concentration, 1 µL of the sample was used, and filled up to 10 µL with distilled water. Equal volume of the corresponding buffer was used for background determination. To each vial 400 µL of 0.5 M NaOH was added and incubated at 37 °C for 30 min. Meanwhile, an appropriate volume of reagent D was prepared by mixing 1 % $CuSO_4$, 2 % disodium tartrate and 4 % Na_2CO_3 in ratio 1:1:98. After incubation, 1 mL of reagent D was added to each vial and incubated at room temperature for 15 min. Finally, 1 mL of 1:10 Folin-Ciocalteu Phenol reagent was added to each sample and incubated at room temperature for 30 min. The absorbance of each sample was measured at 700 nm with a Perkin-Elmer Lambda 40

UV/VIS Spectrometer using a cuvette made of special glass (Hellma, type 100-OS), using distilled water as reference.

2.3.2. SDS-PAGE electrophoresis

The presence of all subunits in stoichiometric amounts and purity of the eluted KdpFABC complexes have been estimated by SDS polyacrylamide gel electrophoresis, prepared according to Laemmli (*130*). The acrylamide concentration was 12.5 %, and the separated proteins were stained with Coomassie blue G250. The gels were run at the constant voltage of 160 V in the stacking gel and 250 V in the separation gel, with a BioRAD 3000Vi electrophoresis power supply.

2.3.3. Malachite green ATPase activity assay

The specific ATPase activity of the detergent-solubilized KdpFABC complex, as well as of the protein reconstituted in lipid vesicles has been determined with malachite green activity assay, according to the previously described protocol (*131*). The assay is based on the complex formed between malachite green molybdate and free orthophosphate under acidic conditions. The formation of the green molybdophosphoric acid complex measured at 640 - 680 nm is directly related to the free inorganic phosphate concentration.

Solutions

- Malachite-green stopping solution

144.4 mg malachite green was dissolved in 80 mL distilled water, and 4.49 g ammonium heptamolybdate in 106.9 mL 4M HCl, while stirring. Ammonium heptamolybdate solution was poured slowly into the dye solution, and left for 30 minute at room temperature, until yellow-orange color was obtained. Finally, the solution was filtered and stored at 4 °C.

- 34 % sodium citrate solution
- 5XATPase buffer without detergent (250 mM Tris-HCl at pH 7.8, 10 mM $MgCl_2$)
- 3X and 1XATPase buffer with appropriate detergent (0.6 % and 0.2 %, respectively)
- 1 mM K_2HPO_4 solution for phosphate standards
- Protein samples diluted to 1 mg/mL in 1XATPase buffer with detergent

Procedure

Corresponding volumes of 3XATPase buffer with detergent, KCl, water and protein sample were mixed according to the *Table 1*, and kept on ice for 15 minutes. 100 µL 2 mM Na_2-ATP was added to each sample to start the reaction. Samples were incubated at 37 °C for 30 minutes. Meanwhile, 9 different phosphate standards were prepared, with amounts of phosphate between 0 and 24 nmol. Reaction stopping solution was prepared by mixing distilled water, malachite-green stopping solution and Tergitol type NP10 in a ratio of 1:1.5:0.033. At the end of the incubation time, samples were placed on ice and 400 µL of reaction stopping solution was added, followed by instant addition of 100 µL of 34 % Na-citrate. For the color stabilization, solutions were left at room temperature for 30 minutes. Finally, the absorbance was measured at 680 nm with a Perkin-Elmer Lambda 40 UV/VIS Spectrometer in disposable semi-micro plastic cuvettes.

ATP autohydrolysis	**KdpFABC without K^+**	**KdpFABC with 3.3 mM K^+**
100 µL 3X ATPase buffer with detergent	100 µL 3X ATPase buffer with detergent	100 µL 3X ATPase buffer with detergent
100 µL distilled water	100 µL distilled water	100 µL 10 mM KCl
-	1 µL 1 mg/mL protein	1 µL 1 mg/mL protein
100 µL 2 mM Na_2-ATP	100 µL 2 mM Na_2-ATP	100 µL 2 mM Na_2-ATP

Table 1. List of samples prepared for the malachite-green activity assay.

Each sample was measured in triplicate and the average absorbance was calculated. Measured values of the samples containing protein were corrected for the values of ATP autohydrolysis as background. The specific ATPase enzyme activity was determined as the difference in inorganic phosphate, P_i, produced per milligram of protein per minute from ATP hydrolysis by KdpFABC in the presence of saturating K^+ concentration, as well as in the nominal absence of K^+. The ratio between these two values represents the so-called induction factor, F_{ind}.

Minor modifications of described malachite green assay include:

- A higher K^+ concentration (33.3 mM) was necessary to achieve saturating conditions when β-DDM and Fos-choline 12 were used as detergent for KdpFABC purification. For all other used detergents, the previously noted concentration of 3.3 mM was sufficient.

- The determination of the ATPase activity of the KdpFABC complex reconstituted in E. *coli* lipid vesicles was performed in the absence of detergent, which means that only the activity of inside-out oriented proteins was detected. Also, due to the higher leak conductance of the vesicle membrane produced by chloride ions, all listed buffers were prepared with appropriate sulfate salts (*132*).

2.4. Reconstitution of the KdpFABC complex

Although detergents are vital for the isolation and purification of membrane proteins, in reality detergent-solubilized systems are a poor mimic of the native membrane environment in which such proteins are found *in vivo*. The complexity of the natural bilayer in which proteins are embedded makes the recreation of this exact surrounding impossible. A close resemblance, however, is achieved when lipids are included in the solubilized systems. Proteoliposomes are, therefore, a suitable tool to investigate structure and function of the membrane proteins. Several criteria should be fulfilled for proteoliposomes in order to allow a successful use as systems for functional biophysical studies, such as homogenous size distribution, even distribution of the protein, and preserved high activity of the reconstituted membrane protein (*133-135*). Furthermore, leak permeability of ions should be minimized, and all activated protein molecules must be inserted in a single orientation, to ensure that transport of different substrates occurs in the same direction.

Studies have shown that membrane protein reconstitution depends on the lipid mixture and the detergent used, and moreover, that the choice of detergent is crucial for the protein's functional incorporation in the membrane. The detergent used affects the result of the reconstitution in terms of protein distribution and orientation, as well as incorporation rate. In addition, it affects the size of vesicles and homogeneity (*136-138*). For the reconstitution of the KdpFABC complex in vesicles, a method was used that is based on a published method for the reconstitution of bacteriorhodopsin, which has been shown to be a successful model (*138*). Using this protocol, unilamellar proteoliposomes with an average diameter of approximately 120 nm are formed and ~50 % of the protein molecules reconstituted with the ATP-binding site facing outward.

For the vesicles preparation, the KdpFABC complex was isolated from membranes with 1 % (*w/v*) β-DDM, purified in one step using a HisTrap column, and finally resuspended in

50 mM Tris-HCl at pH 7.5, 2 mM $MgCl_2$, 130 mM imidazole, 150 mM NaCl and 0.2 % (*w/v*) β-DDM (*99*). For detergent removal, a technique was used that is based on a hydrophobic adsorption of detergent to beads, since the dialysis method was not suitable due to the low critical micelle concentration of DDM (0.01 % at 25 °C) (*135*). Possible artifacts induced by the lipid composition could be avoided by using protein and lipids extracted from the same organism. Therefore, E. *coli* polar lipid extract was used for the reconstitution of the KdpFABC. The protein:lipid ratio has been optimized and the most suitable ratio was found to be 1:5.

Procedure for KdpFABC reconstitution into E. *coli* lipid vesicles

An appropriate amount of E. *coli* polar lipid extract dissolved in chloroform (Avanti Polar Lipids, Alabaster, USA) was transferred into a glass flask and vacuum-dried while rotating for 30 minutes. The obtained thin lipid film was solubilized with 2 % (*w/v*) β-DDM and 2 % (*w/v*) $C_{12}E_8$ dialysis buffer containing 25 mM imidazole, 1 mM EDTA, 5 mM $MgSO_4$, and 70 mM K_2SO_4 at pH 7.2 (H_2SO_4). The final lipid concentration was adjusted to 10 mg/mL. The lipid/detergent mix was sonicated for 3-5 minutes, and kept at room temperature until a clear solution was obtained. To avoid lipid peroxidation, all steps were performed under N_2 atmosphere. Equal volumes of the solubilized E. *coli* lipids and a 2 mg/mL protein sample were mixed, with a final protein:lipid ratio of 1:5, followed by the addition of 200 mg BioBeads SM-2 (Bio-Rad), pretreated with dialysis buffer, per 600 µL solution. During an overnight incubation at 4 °C, the suspension was rotated at 40 rpm. Finally, the resulting vesicle suspension was separated from the BioBeads by aspiration with a capillary tip (Biozym Scientific GmbH), and stored on ice for 3 h before being used in fluorescence measurements.

The activity of the reconstituted KdpFABC protein was determined by the malachite green assay with the appropriate modifications (2.3.3.), in the presence and absence of 1 µM valinomycin. The K^+ ionophore was applied to prevent depletion of K^+ ions inside the vesicles. To determine the size distribution of formed vesicles, dynamic light scattering measurements were performed at room temperature, using a DLS Viscotek 802 spectrometer. Vesicles were diluted to achieve a final concentration of approximately 0.1 mg of lipid/mL of buffer, filtered with a 0.45 µm PVDF centrifugal filter (Millipore), and transferred to a 12 µL square cuvette (Viscotek, 802DLS quartz cell). Distilled water and

dialysis buffer were filtered with 0.02 µm inorganic membrane filters (Whatman). Intensity distributions of the scattered light were recorded and analyzed with Omnisize version 2.0 to obtain the corresponding vesicle-diameters distribution.

2.5. Voltage-sensitive dyes

Detailed studies of the P-type ATPases have revealed the existence of pump cycles in which different ion species are transported across the membranes in several distinguishable reaction steps. The majority of pumps move different ions in opposite directions with the same Ping-Pong mechanism (*5*). Theoretically, the ions could be transported across membrane in each of the described step (1.3.), although investigations have shown that a charge movement mainly occurs during the ion binding and release steps, accordingly referred to as "electrogenic" steps (*50;139*). Detection and further investigation of these steps require adequate techniques. So far, well-established techniques include the electrophysiological study of native cells or capacitive coupling of open membrane fragments adsorbed to lipid bilayers (*140;141*). An alternative optical method, employing various fluorescent probes, has been introduced and successfully used to detect charge movements in the Na^+,K^+-ATPase, SR Ca^{2+}-ATPase and H^+,K^+-ATPase (*142-148*).

2.5.1. Introduction into the principles of fluorescence

During the last 20 years, the use of fluorescence in biological sciences has been remarkably expanded. Because of a high detection sensitivity and the avoidance of handling radioactive tracers frequently used in the past, fluorescence spectroscopy has become a principal investigation method in biophysics and biochemistry. Particularly, various techniques based on fluorescence have been developed and successfully employed in the investigation of the P-type ATPases, providing insight in the overall transport mechanism and in its detailed characterization.

Fluorescence represents a form of luminescence (*149*). This phenomenon includes processes of light emission from any substance, and occurs from electronically exited states. One of many possible sources of excitation (*e.g.* mechanical actions, chemical reaction and heat) is photoexcitation, and the corresponding photoluminescence can be described as an

excitation to a higher energy state with a subsequent return to a lower energy state accompanied by the emission of photons. Depending on the nature of the excited state, photoluminescence is formally divided on fluorescence and phosphorescence. Phosphorescence is emission of light from an excited triplet state, in which the electron has the same spin orientation as the ground-state electron. In this case, transition to the ground state is "forbidden", resulting in slow emission rates. Typical phosphorescence lifetimes are in the order of milliseconds to seconds or even longer. On the other hand, fluorescence is a result of singlet–singlet electronic relaxation, with high emission rates in the order of 10^8 s^{-1}, so that a typical fluorescence lifetime is in the range of ns. The processes that occur between the absorption and emission of light are usually illustrated by the Jablonski diagram, given in *Figure 17*.

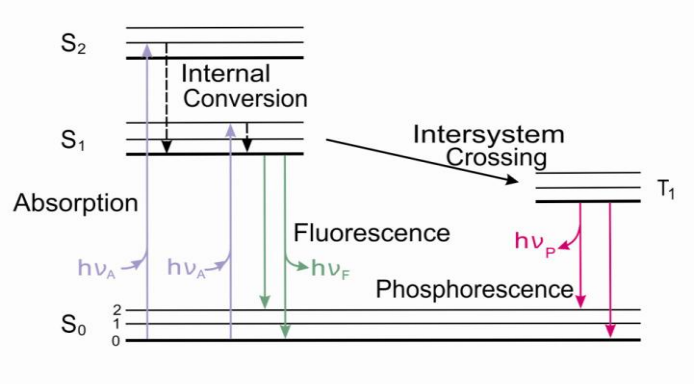

Figure 17. General form of a Jablonski diagram illustrating the light absorption and emission (*149*).

Transitions between states occur without displacement of nuclei, in accordance to Franck-Condon principle, and are shown as vertical lines. Upon light absorption, molecule is excited to one of the higher vibrational level of S_1 or S_2, followed by fast relaxation to the lowest vibrational energy level of S_1. This is known as internal conversions, and generally it is completed before emission. After emission, the molecule returns to a higher vibrational state of ground state level, which results in a vibrational structure in the emission spectrum. Molecules in the S_1 state can undergo a spin conversion into a triplet state, called intersystem crossing. Emission from T_1 to S_0 is forbidden, and as a result phosphorescence has rate constants significantly smaller than those for fluorescence. From the Jablonski diagram one can easily see that the energy of the emission is typically lower than the energy of absorption. In other words, the wavelength of the emitted radiation is longer than that of the exciting radiation. This phenomenon is known as the Stokes shift.

Fluorescence probes are important and widely used in the field of fluorescence spectroscopy. Fluorophores can be generally divided into *i)* intrinsic, that exist naturally such as aromatic amino acids, NADH and chlorophyll, and *ii)* extrinsic, added to the sample without fluorescence properties. Proteins contain three amino acid residues – tryptophan, tyrosine and phenylalanine that contribute to their intrinsic fluorescence. The dominant fluorophore is the indole group of tryptophan, which absorbs near 280 nm, while the emission spectrum is highly solvent dependent with a fluorescence maximum near 340 nm. The emission of tryptophan may be blue shifted if the residue is buried within a native conformation of a protein, and its emission maximum may be red shifted upon unfolding. When discussing fluorophores, there are two important characteristics. Firstly, *quantum yield* is defined as the number of emitted photons relative to the number of absorbed photons and it describes the efficiency of the fluorescence process. Secondly, *lifetime* refers to the average time in which the molecule stays in its excited state before emitting a photon, and it is important for practical applications of fluorescence.

Proteins can be covalently labeled with various fluorophores, producing fluorescent protein conjugates and that enable monitoring of protein structure and conformation. Membranes typically do not exhibit intrinsic fluorescence. Labeling membranes with fluorescent probes which spontaneously partition in the nonpolar region of the membrane provides methods to monitor membrane transport processes. Both protein- and membrane-bound dyes can be used in functional analysis of proteins. One of the examples successfully used in investigation of the functional properties of the Na^+,K^+-ATPase is fluorescein-5-isothiocyanate (FITC) (*150;151*). It binds to Lys501 in the ATP-binding site, consequently prohibiting ATP binding and enzyme phosphorylation. This allows studying the conformational transition between the E_1 and E_2 states, but not between the corresponding phosphorylated states. Since the ATP-binding site is highly conserved among the P-type ATPases, FITC labeling method can be applied also on other members of the family.

A special group of fluorophores are membrane-potential probes that are sensitive to the electrical potential. Different mechanisms are used to explain the voltage-sensitivity of these membrane probes. For example, carbocyanine dyes respond to potential by redistributing across the membranes, whereas styryl dyes respond directly to the electric field *via* an electrochromic mechanism (Stark effect). Voltage-sensitive dyes have been successfully used to record membrane potentials and investigate transport processes across the membranes. The use of potentiometric dyes offers broad possibilities for indirect studies of

translocation processes involving the P-type ATPases, especially in preparations not suitable for other well established biophysical techniques. Membrane-potential probes can be divided into two classes with respect to the speed and mechanism of the potential-dependent spectra into *fast dyes*, with respond times in the order of μs, and *slow dyes*, with much larger respond times of milliseconds to seconds (*5*). This is strictly functional, as some dyes can exhibit both types of response.

In this work, the mechanistic analysis of the KdpFABC transport properties was carried out using two voltage-sensitive dyes, RH421 and $DiSC_3(V)$, as members of the styryl and the cyanine group, respectively. Underlying principles of how these dyes work as membrane potential indicators will be discussed in more details.

2.5.2. Use of RH421 dye for characterization of the detergent-solubilized KdpFABC

The family of RH dyes includes various dialkylaminophenylpoly-enylpyridinium compounds, and they were introduced in the late seventies of the last century as optical probes to monitor membrane potentials (*152;153*). They can be classified as the "fast" dyes, considering that their response time on the change of a local electric field is less than microsecond. RH dyes have a delocalized positive charge in the pyridinium ring. Some members of this dye family carry a localized negative charge on the terminal sulfo group, as shown in *Figure 18*.

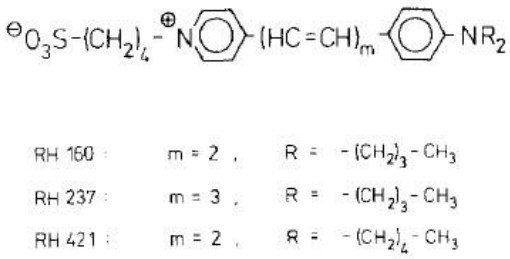

Figure 18. Structure of family of styryl dyes (*154*).

It was proposed that due to their amphiphilic structure, these dye molecules insert perpendicularly into the lipid bilayer, with the sulfo group facing the aqueous medium, while the rest of the molecule is embedded in the apolar membrane interior (*153*). This orientation of RH dye molecules is favorable for dye's spectral sensitivity to changes of the local electric field strength within the hydrophobic core of the membrane. The phenomenon

underlying its voltage-sensitivity is an *electrochromic effect*, derived from a dependence of the energy difference between the ground and excited state of the molecule on the local electric field strength. In the excited state, the delocalized positive charge of the dye is shifted towards the membrane interior, so that the positive electric field strength inside the membrane produces a blue shift in the absorption spectrum of the dye. Consequently, the emission spectrum of the dye is changed when excited at the red edge of the absorption spectrum, as illustrated in *Figure 19.*

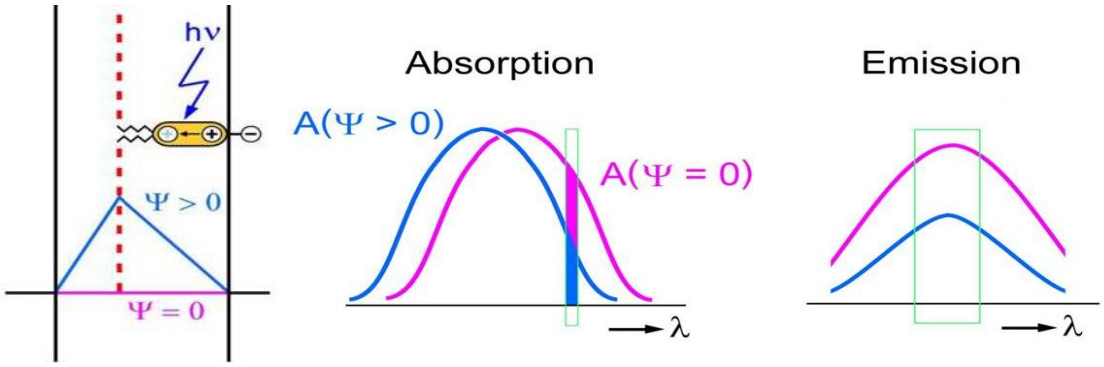

Figure 19. Illustration of the electrochromic effect of the RH421 styryl dye. Positive electric field Ψ in the membrane dielectric producing changes in the absorption and emission spectra of the dye.

The experimentally determined lipid/water partition coefficient of RH421 dye , γ, was found to be ~$2.5 \cdot 10^5$, implying that under the used experimental conditions more than 90 % of the dye is bound to the membrane, whereas the molar ratio of dye:protein was calculated to be ~3, in case of the Na^+,K^+-ATPase (*154*). Results obtained in experiments with hydrophobic ions tetraphenylborate (TPB^-) and tetraphenylphosphonium (TPP^+), which are able to modify the electrostatic potential at the lipid/water interface, strongly support the hypothesis that RH styryl dyes respond to the changes in the local field in the membrane. On the other hand, it was shown that partial reaction containing conformational transition but no net electric change, do not affect the fluorescence signal of the dye. Noteworthy is the observation that the RH421 dye does not affect the kinetic properties of the Na^+,K^+-ATPase at concentration up to 1 μM.

When open membrane fragments containing ATPase are suspended in aqueous solution, the two side of the membrane are short-circuited by the electrically conducting solution, and the transmembrane voltage remains zero under all conditions (*154-156*). As already mentioned, the detection mechanism is a consequence of the electric-field sensitive positive

charge shifting from the pyridinium ring to the aniline moiety. Therefore, time resolution is significantly higher than the time constants of the diffusion-controlled ion movements between aqueous media and ion-binding sites of the enzyme. The fluorescent signal of the dye is linearly dependent on the local electric field strength within the membrane, or in other words, on the number of charges in the binding-sites of the enzyme. Earlier work showed a limitation of the response of the RH421 dye arising from a requirement of high enough density of active proteins in the open membrane fragments (10^3-10^4 molecules/μm^2). However, the possibility to overcome this limitation was recently demonstrated and the application of the RH421 dye has been further extended to the detergent-solubilized Na^+,K^+-ATPase (*157*).

In this work, the RH421 dye was used to analyze the electrogenic steps of the detergent-solubilized KdpFABC transport cycle, primarily substrate(s) binding and release reactions under different experimental conditions. From these experiments, substrate-binding affinities in the E_1 and P-E_2 conformations were determined. Also, the so-called backdoor phosphorylation was investigated, triggered by the addition of inorganic phosphate, P_i (*158*).

2.5.2a. Steady-State fluorescent measurements using RH421 dye

The steady-state fluorescent measurements with detergent-solubilized KdpFABC were performed with a homemade setup using a HeNe laser (Laser 2000, Voltex, Inc., Colorado Spring, CO) with a wavelength of 594 nm to excite to fluorescence of the electrochromic styryl dye RH421, as previously described (*145;147*). The emitted light was collected at an angle perpendicular with respect to the incident light, filtered by a narrow-band interference filter (λ_{max}= 663 nm, half-width of 18 nm) and detected by a photomultiplier (R2066, Hamamatsu Photonic, Hamamtsu, Japan). The photocurrent was amplified by a Keithley 427 current amplifier (Keithley Instruments, Cleveland, OH) and further collected with a data-acquisition board of a personal computer (PCI-7112, Imtec, Backnang, Germany) at a sampling frequency between 1 and 10 Hz. The temperature of the cuvette was maintained by a thermostat at (20 ± 0.5) °C. The specific fluorescence changes depend on protein preparation, regarding protein density and lipid composition; therefore, some minor differences between different preparations are present.

The experiments were performed in buffer starting with 2 mL 50 mM Tris-HCl, 2 mM $MgCl_2$ (pH 7.8) in a cuvette made of optical glass (Helma). After 10 minutes of thermal

equilibration, 200 nM RH421 was added. Three minutes later while stirring, 9 µg/mL of the detergent-solubilized KdpFABC was added to the cuvette. When a stable fluorescence signal F_0 was reached, experiments were performed by adding small aliquots of indicated substrates from various concentrated stock solutions until signal saturation. Mg-ATP and Na_2-ATP were added from a buffered, pH-adjusted 0.5 M stock solutions. To allow comparison between different titration experiments, normalized fluorescence changes with the respect to the initial fluorescence level, $F_{0,}$ were calculated according to the equation $\Delta F/F_0 = (F - F_0)/F_0$. For the normalization of the signals, as well as for volume correction the Drifter program was used. For further evaluation of the results and fitting procedures, the data processing program, FigP 2.98, was used. An example of a steady-state experiment of potassium binding affinity of the KdpFABC in the E_1 conformation is shown in *Figure 20* (upper graph), with corresponding enlarged segment of K^+ titration (lower graph).

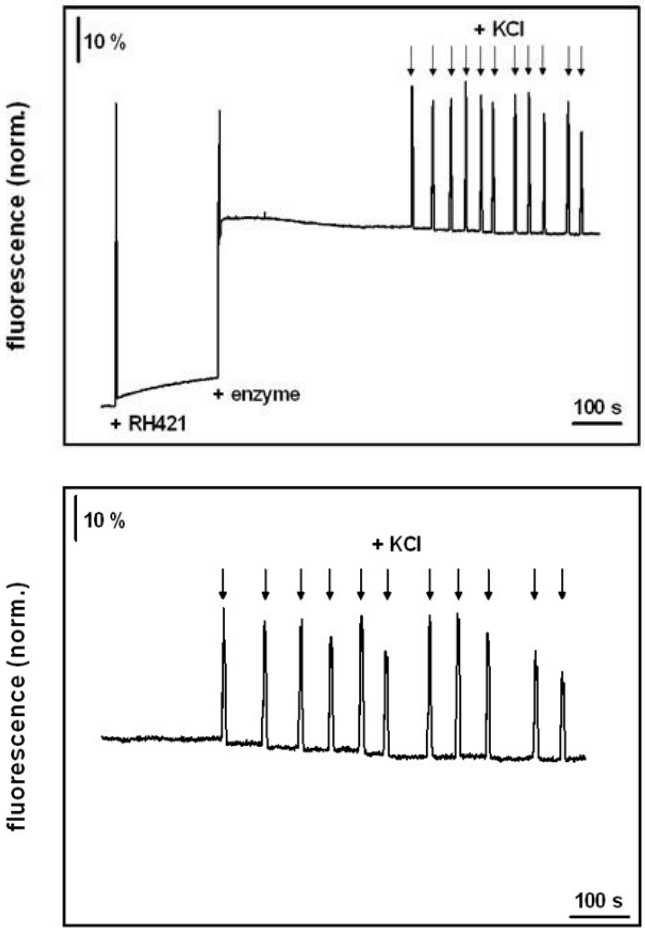

Figure 20. RH421 standard experiment of the detergent-solubilized KdpFABC. Complete trace of the experiment with respective additions of the dye, enzyme and upon achieving a stable fluorescent signal, small aliquots of KCl until signal saturation was obtained (upper graph). The enlarged trace of the K^+ titration is shown in the lower graph.

The substrate-dependent fluorescence change, F_{norm}, was fitted with a Hill function to obtain the half-saturating potassium concentration:

$$F_{\text{norm}}([X^+]) = F_0 + \Delta F_{\text{max}} / (1 + ([X^+]/K_{1/2})^{-n}) \qquad \text{(Eq. 2)}$$

where $[X^+]$ is the ion concentration, ΔF_{max} the maximum fluorescence change, $K_{1/2}$ the half saturating concentration, and n the Hill coefficient.

2.5.2b. Time-resolved measurements with caged ATP

Besides the ion-binding studies, the electrochromic dye RH421 can be used also for kinetic experiments (*159-161*), employing caged ATP. Caged ATP is a photolabile ATP precursor, allowing kinetic studies in intact biological systems, overcoming limitations coming from difficulties of adding the reactants to the system in a time shorter than the reaction time. Caged ATP is stable in water at pH 7, and not detectably photolyzed over minutes of daylight exposure. Upon activation with intensive UV-light flash, ATP is released with the time constant of 4.6 ms at pH 7 (*159*). The reaction mechanism of caged ATP photodissociation is given in *Figure 21*.

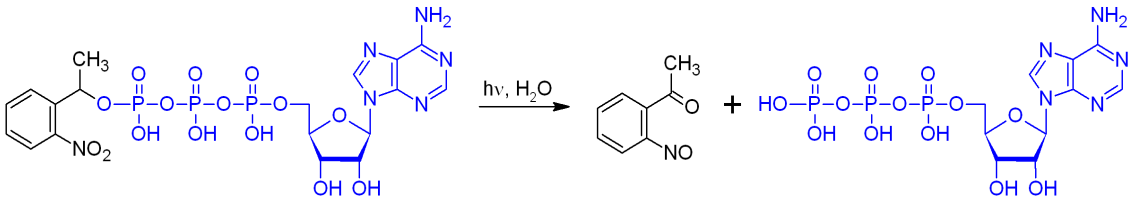

Figure 21. Reaction mechanism of photochemical release of ATP from caged ATP (P3-[1-(2-Nitrophenyl)ethyl]-ATP).

The kinetic experiments with the detergent-solubilized KdpFABC were performed with a homemade setup (*Figure 22*) (*162*). The photochemical release of ATP was triggered by a UV flash generated by an EMG 100 excimer laser (Lambda Physics, Göttingen, Germany; wavelength 351 nm, duration 14 ns, power 3.5 MW). A UV cut-off filter in front of the photomultiplier entrance window was used to reduce the effect of the UV flash on the fluorescence signal. RH421 was excited by a HeNe laser working at 594 nm. A quartz lens

widens the laser beam to illuminate the whole solution homogeneously. The emitted light was collected by an ellipsoidal mirror and converged onto the cathode of a photomultiplier (Mod. R928, Hamamatsu Photonics, Japan). An interference filter (663 ± 18) nm selects the emitted light of the styryl dye before it enters the photomultiplier. The output current is amplified and digitized by a 12-bit data acquisition board of a PC with sampling frequencies between 1 and 500 kHz. The bottom of the cuvette is in contact with a thermostated copper socket that also blocks the incident light. The experiments were performed in a darkened environment at (26 ± 1) °C. A cylindrical quartz cuvette (internal diameter 7.8 mm) is filled with 300 µL buffer containing 25 mM imidazole, 1 mM EDTA (pH 7.8), 5 mM $MgCl_2$, 200 nM RH421, 9 µg/mL of detergent-solubilized KdpFABC, 100 µM of caged ATP and various KCl concentrations. To remove traces of free ATP from the sample of caged ATP, Apyrase VI (1.4 x 10^{-3} units/mL) and 1.4 mM $MgCl_2$ were added to the 10 mM stock solution. Aliquots of caged ATP were flash-frozen in liquid N_2 and stored at -20 °C. During the experiments, caged ATP was kept on ice and protected from light. The cuvette was equilibrated for 10-15 min inside the instrument in the dark (to avoid photolysis of caged ATP). After equilibration, the shutter was opened and the experiment was triggered by a UV-light flash. About 10–20 % of caged ATP was photo-dissociated by a single flash.

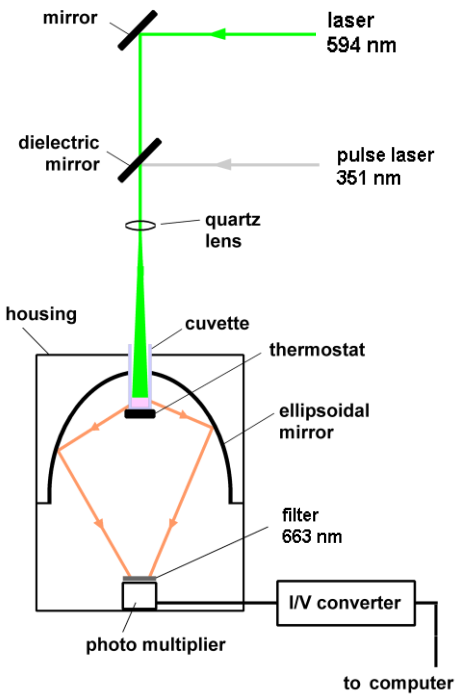

Figure 22. Schematic representation of the setup used for the measurements of transient fluorescence signals induced by photochemical release of ATP.

After the release of ATP, the enzyme is phosphorylated and undergoes the conformational transition from the E_1 state to P-E_2. At saturating ATP concentrations, ATP-binding and enzyme phosphorylation are fast compared to the conformational transition. The observed fluorescence decrease is a result of K^+ binding (*Figure 23*), and the signal was fitted with a single exponential function (Eq. 3). At saturating concentration of ATP, it is possible to calculate the rate constants of the conformational transition $E_1 \rightarrow$ P-E_2, under different conditions, such as pH, K^+ concentration and temperature. The investigation of role of protons in the reaction cycle was carried out, by performing experiment at different pH, in the absence and presence of saturating K^+ concentration. The ATP-binding affinity was determined from the set of experiments with various, non-saturating ATP concentrations. The exact concentration of ATP released was determined by the rapid firefly luciferin-luciferase kit (*163*).

The normalized fluorescence signal, $F_{norm}(t)$, was fitted with a single exponential function:

$$F_{norm}(t) = A \cdot (1 - e^{-t/\tau}) \qquad \text{(Eq. 3)}$$

where τ is the time constant of the normalized fluorescence decrease after ATP release. The first derivative of the function with the respect to time is at t = 0:

$$\left(\frac{dF_{norm}(t)}{dt}\right)_{t=0} = A \cdot \frac{1}{\tau} \cdot e^{-t/\tau}\Big|_{t=0} = \frac{A}{\tau} \qquad \text{(Eq. 4)}$$

Ratio between the amplitude and time constant, or the initial slope $\frac{A}{\tau}$, is proportional to the number of pumps activated by ATP, whereas the rate of substrate binding/release process is determined by the rate constant $k = \frac{1}{\tau}$. The reduction of the number of data points obtained from the experiment by the data-collection program DASYLab9 was performed with the Redulite2 program and procedure fit of the time course of the fluorescence signal has been performed with the data processing program FigP 2.98.

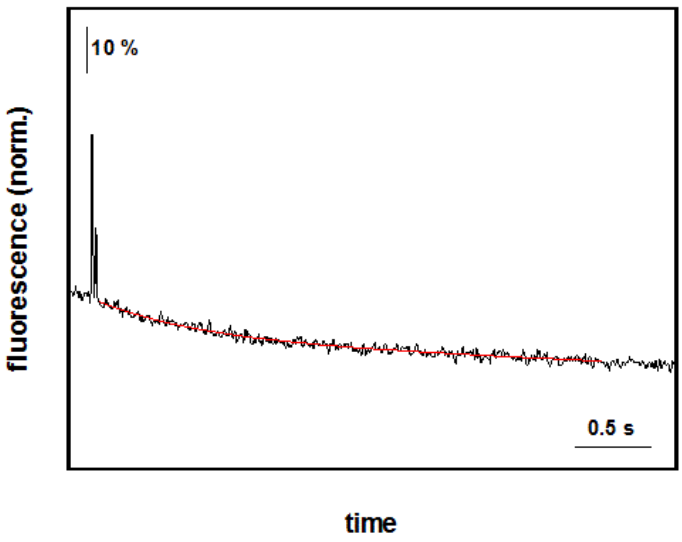

Figure 23. Fluorescence signal recorded after the photochemical release of ATP at saturating concentrations of K^+ ions and ATP, at pH 7.8.

2.5.3. The potential-sensitive fluorescent probe $DiSC_3(V)$

Two major groups of the so-called *slow dyes* which are successfully used as optical probes to measure changes in the electrical potential difference across membranes of cells, organelles and vesicles are cyanine and oxonol dyes (*164*). Oxonol VI has been successfully applied to detect ion transport of the reconstituted Na^+,K^+-ATPase, and it was shown that this dye is the most sensitive fluorescent probe to detect inside-positive electric potentials. In experiments with the KdpFABC reconstituted in vesicles, however, an inside-negative potential is observed upon ATP addition to the medium. This potential is generated by extrusion of K^+ ions by inside-out oriented pumps. Therefore the positively charged cyanine dye $DiSC_3(V)$ was introduced as an indicator of inside-negative electric potentials across the vesicle membrane, and it was successfully applied to detect the electrogenic pump activity of the KdpFABC reconstituted in vesicles (*90;99*).

The group of cyanine dyes was initially introduced as membrane potential probes for squid axon experiments by Hoffman & Laris (*165*). They are often referred to as accumulation or redistribution dyes, with respect to the mechanism of their response to the membrane potential change. The fluorescence response of this class of cationic dyes was shown to result from potential-dependent partition of dye molecules between the cell and extracellular medium. Changes in membrane potential making cells inside negative

(*hyperpolarization*) result in uptake of the positively charged cyanine dye molecule and decrease of the fluorescence. Upon depolarization, dye molecules are released, producing fluorescence increase. These dyes are highly membrane permeant, which is important property for dyes working by the redistribution mechanism in order to have reasonably fast responses to potential changes (*166;167*).

The structure of the 3,3'-dipropylthiadicarbocyanine iodide, $DiSC_3(V)$, used in this study is given in *Figure 24A*. Both absorption and emission spectra of $DiSC_3(V)$ depend on the nature of the solvents, ionic strength, and concentration of the dye. It was reported that changing from aqueous media to organic solvent both spectra were red-shifted by 17 nm. In dilute solutions, the monomeric form is predominant, whereas with increasing dye concentration, dimers and even higher aggregates are formed which have an extremely lower fluorescence yield. All spectroscopically different forms of the dye were found in cells and liposomes (*168*). In dilute dye solutions ($c < 1$ µM), the monomeric form of $DiSC_3(V)$ is predominant, with an excitation and emission maxima at 650 nm and 664 nm, respectively. An example of emission spectra of 300 nM $DiSC_3(V)$ in pure buffer containing 25 mM imidazole, 1 mM EDTA, 5 mM $MgSO_4$ and 70 mM K_2SO_4 at pH 7.2 (H_2SO_4), and in E. *coli* lipid vesicles suspension, is shown in *Figure 24B*. The experimental conditions were as follows: λ_{ex}=650 nm, slit=5 nm, integration time=1 s and temperature (18 ± 0.1) °C. Concentration of the E. *coli* lipid vesicles was 80 µg/mL, with an inside K^+ concentration of 140 mM. The observed red shift in the spectra recorded in vesicle suspension comes from quenching of the dye due to distribution between membrane and aqueous phase. Accordingly, a fluorescent decrease is observed (*Figure 24B*).

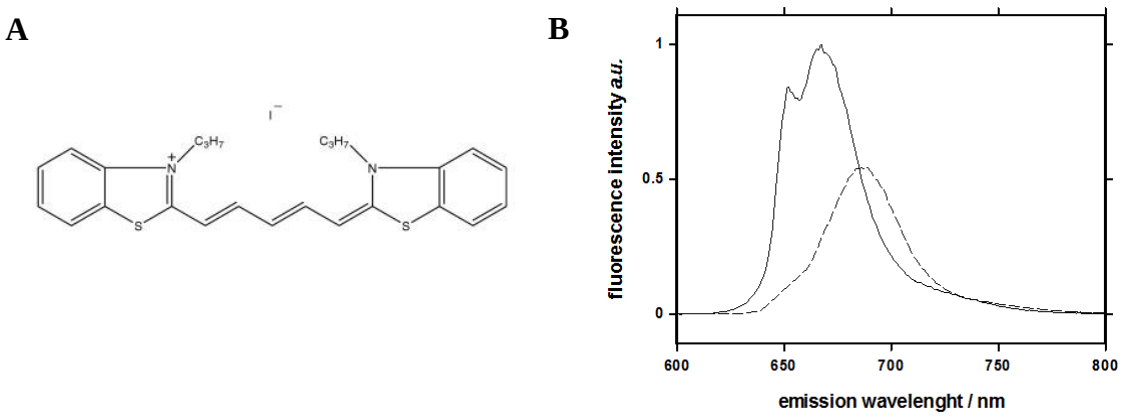

Figure 24. A: Structure of the $DiSC_3(V)$ dye **B:** Emission spectra of 300 nM $DiSC_3(V)$ resuspended in 25 mM imidazole, 1 mM EDTA, 5 mM $MgSO_4$ and 70 mM K_2SO_4 at pH 7.2 (full line), and in the presence of 80 µg/mL E. *coli* lipid vesicles (dashed line); $[K^+]_{in}=[K^+]_{out}$=140 mM.

Taking into consideration the mechanism of the potential sensing of $DiSC_3(V)$, the dye should be added to the vesicle suspension (and not *vice versa*). In this manner, a stable signal is reached already after 50 seconds, and quenching of the fluorescence signal due to the redistribution of the dye between the membrane and aqueous phase is avoided, as it was observed when the dye was added first (*Figure 25A*). To prevent the dye aggregation, which could lead to the formation of non-fluorescent dimers and higher aggregates, too high concentrations of the dye should be avoided. Therefore, it is essential to use the lowest amount of the dye producing an optimally measurable and stable signal (*Figure 25B*). The concentration of 300 nM $DiSC_3(V)$ was found to be the most appropriate, and it was used in all future experiments.

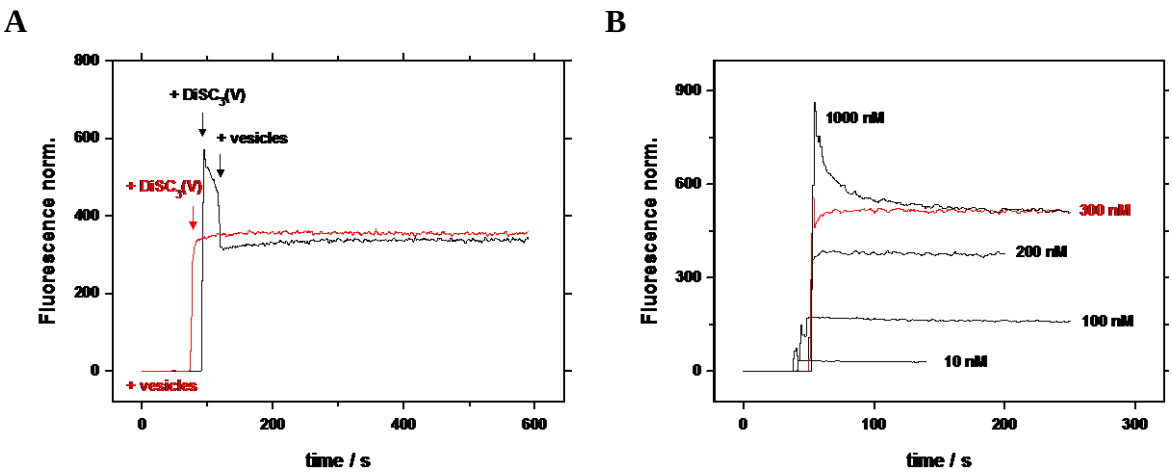

Figure 25. A: Stable fluorescence signal was reached after 50 s when 300 nM $DiSC_3(V)$ dye was added to the vesicle suspension. **B:** Fluorescence signal of different $DiSC_3(V)$ concentrations, added to the vesicles suspension. In all experiments the final lipid concentration was 80 µg/mL.

The application of $DiSC_3(V)$ in studying the ion transport across the lipid bilayer is limited by the low sensitivity for inside positive potentials. Instead of $DiSC_3(V)$, a more appropriate probe for those experiments would be one of the oxonol dyes. Another limitation is the interaction with a number of other membrane-embedded compounds, including CCCP and dinitrophenol, both commonly used ionophores, which tend to produce nonfluorescent complexes with $DiSC_3(V)$ (*164;169*).

2.5.3a. Investigation of the ion transport by KdpFABC reconstituted in lipid vesicles using $DiSC_3(V)$

The proteoliposomes prepared as previously described (2.4) contained 140 mM K^+. All experiments were performed in a Perkin-Elmer LS 50B fluorescence spectrometer. The fluorescence was excited at 650 nm (5 nm slit), and emission was detected at 675 nm (5 nm slit). 1 mL of buffer containing 25 mM imidazole, 1mM EDTA, 5 mM $MgSO_4$ and various concentrations of K_2SO_4 at pH 7.2 (H_2SO_4), was thermally equilibrated for 10 min in a optical-glass cuvette (Hellma). An aliquot of vesicles corresponding to the final concentration of 80 µg lipid /mL was added, followed by the addition of 300 nM $DiSC_3(V)$ from a 1 mM stock solution. A fluorescence signal increase was observed, as a result of the insertion of the dye into the vesicle membranes. When a stable signal was achieved (after ~50 s), 2.5 mM Mg-ATP was added, from a 0.5 M pH-adjusted stock solution, to trigger the pump activity. In this way, only pumps with ATP-binding sites facing outward were activated, and K^+ ions were pumped out of the vesicles. This extrusion of positive charge by KdpFABC generated inside-negative potential, reflected in a fluorescence decrease, that exponentially approached a steady-state level at which the pump current was compensated by the leak current due to the passive membrane conductance and the electric-potential gradient. Subsequent addition of 1 µM valinomycin, a highly selective potassium ionophore, caused a step change in fluorescence to a level indicating the Nernst potential determined by the actual K^+ concentration inside and outside the vesicles (*165*). To allow the comparison between different experiments, the fluorescent changes were normalized with respect to the fluorescence level, F_0, at a membrane voltage of 0, before the addition of ATP according to the equation $F_{norm}(t)=(F(t)–F_0) / F_0$, where $F_{norm}(t)$ is the normalized fluorescence amplitude and $F(t)$ is the measured fluorescence.

Alternatively, after the addition of Mg-ATP, 0.1 mM P-type ATPase inhibitor *o*-vanadate was added instead of valinomycin to evaluate the leak conductance of the membrane. As a result, the fluorescence signal increased exponentially due to the inhibition of the pump activity. Knowing the time constant, τ, of the exponential increase, allowed us to calculate the specific conductance of the membrane as $G_m = C_m / \tau$. Assuming that the specific membrane capacitance, C_m, is 1 µF/cm^2, the specific membrane conductance could be calculated as $G_m = 1$ µF/cm^2 /τ (*132*). A typical example of the fluorescence increase after addition of 0.1 mM *o*-vanadate is shown in *Figure 26*.

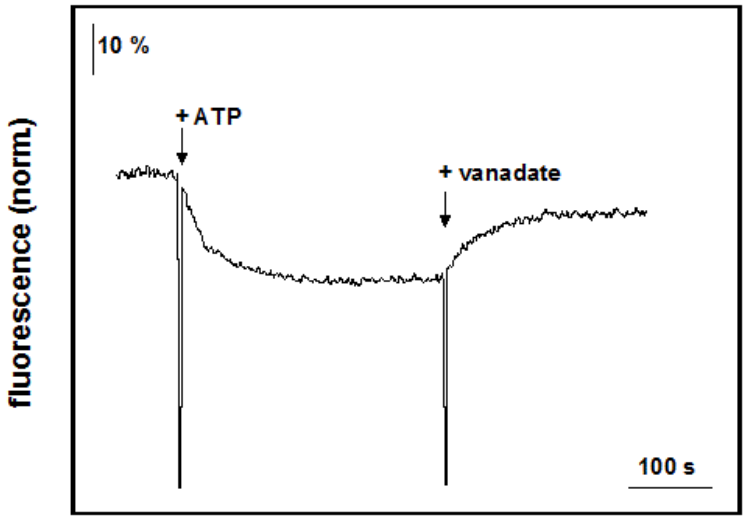

Figure 26. Fluorescence decrease after ATP addition as a result of extrusion of K^+ ions. After ~ 350 s a new steady-state is achieved. This is followed by an exponential increase of the fluorescence signal due to inhibition of the KdpFABC pumping activity by 0.1 mM *o*-vanadate.

The normalized fluorescence changes were fitted with a mono-exponential function:

$$F_{norm}(t) = A \cdot (1 - e^{-t/\tau}) + Residual \qquad \text{(Eq. 5)}$$

where $F_{norm}(t)$ is normalized fluorescence, A is the fluorescence amplitude, *Residual* is the normalized fluorescence level of the steady-state after ATP addition and τ is the time constant of the fluorescence decrease after ATP or increase after *o*-vanadate addition.

The initial slope of the fluorescence change, defined as the derivative of the signal with the respect to the time at t = 0, is directly proportional to the initial enzyme activity. This is correct at the early stage of the experiment, until the depletion of intravesicular K^+ becomes a limiting factor. The underlying theoretical principles are based on the consideration that the vesicle membrane can be described by an equivalent diagram with the capacitance, C_m, and the leak conductance, λ_L, of the lipid bilayer, whereas the pump is represented by a current generator, I_P, with a corresponding relationship (*170*):

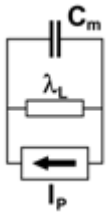

$$I = \frac{dQ}{dt} = C_m \cdot \frac{dU}{dt} \qquad \text{(Eq. 6)}$$

where Q is the electric charge on the membrane capacitor, U is the electric membrane potential and I is the current across the membrane. The net current through the vesicle membrane, I, is the sum of the pump current, I_P, and the leak current, I_L, flowing in the opposite directions:

$$I = I_P - I_L = n \cdot z \cdot e_0 \cdot \nu_P - \lambda_L \cdot U \qquad \text{(Eq. 7)}$$

where n is the number of pumps in the membrane, z is the number of charges transported per pump cycle, e_0 is the elementary charge and ν_P is the pump rate. Combining Eq. 6 and Eq. 7 leads to the inhomogeneous differential equation:

$$\frac{dU}{dt} = \frac{I_P}{C_m} - \frac{\lambda_L}{C_m} \cdot U \qquad \text{(Eq. 8)}$$

In the stationary phase, when the pump current is compensated by the leak current, valid at $t \rightarrow \infty$, the transmembrane voltage U_∞ is defined as:

$$I_P = I_L = \lambda_L \cdot U_\infty \qquad \text{(Eq. 9)}$$

The solution of the differential equation is

$$U(t) = U_\infty \cdot (1 - e^{-t/\tau}) \qquad \text{(Eq. 10)}$$

where $\tau = C_m / \lambda_L$ and $U_\infty = I_P / \lambda_L$. Finally, the derivative with respect to time at t=0 is defined as the initial slope:

$$\left(\frac{dU}{dt}\right)_{t=0} = U_{\infty} \cdot \frac{1}{\tau} \cdot e^{-t/\tau}\Big|_{t=0} = \frac{U_{\infty}}{\tau} \qquad \text{(Eq. 11)}$$

Taking into account that the fluorescence amplitude of the $DiSC_3(V)$ is proportional to the transmembrane potential (*166-168*), the initial pump activity is proportional to the initial slope of the fluorescence change. Results from the same vesicle preparation can be directly compared, since the proportionality factor could differ between different preparations. Normalization of signals, volume and drift corrections for these experiments were performed with the Drifter program and fitting of the data was performed with FigP 2.98.

3. RESULTS

3.1. Choice of detergent

One of the major challenges encountered when membrane proteins are studied is the difficulty in working outside the natural lipid environment, since various biophysical techniques, investigating both structure and function of membrane proteins, are impossible to be conducted under native conditions. Therefore, particular attention is focused on the establishment of the most suitable experimental conditions, especially on the choice of the detergent used for solubilization and purification of the desired protein. The goal is to identify conditions in which the stability and functional integrity of the protein is retained during solubilization and reconstitution by using the appropriate detergent.

To find the most appropriate conditions, KdpFABC was solubilized and purified, according to the protocol described in chapter 2.2, with six different detergents, Fos-choline 12, β-DDM, β-DM, PCC-α-M (*171*), LAPAO and Aminoxide WS-35. The concentration for the solubilization step was 1 % (*w/v*) and for the successive purification step 0.2 % (*w/v*), for each used detergent. Moreover, the same batch of E. *coli* membranes was used for all six detergents, in order to avoid possible differences between various cell membrane preparations and allow thus a direct comparison. The enzyme activity, E_A, of the ATPase and the half-saturating K^+ concentration, $K_{1/2}(K^+)$, chosen as characteristic parameters of the KdpFABC, were used for comparison of the different detergents' capabilities of maintaining a functional KdpFABC complex. The obtained results are summarized in *Table 2.*

The enzyme activity was measured using the malachite green activity test, and E_A represents the amount of inorganic phosphate, P_i, released by ATP hydrolysis of the detergent-solubilized KdpFABC complex, in a buffer containing 50 mM Tris-HCl (pH 7.8), 2 mM $MgCl_2$ and 0.2 % (*w/v*) of the respective detergent at 37 °C, in the nominal absence of and under saturation by KCl. According to the standard protocol described in 2.3.3, the final KCl concentration was 3.3 mM. Based on the results of the RH421 K^+-binding experiments, the half-saturating concentrations were lower than 3.3 mM in the case of β-DM, PCC-α-M, LAPAO and Aminoxide WS-35. 3.3 mM K^+ was, however, not sufficient for the experiments with Fos-choline 12 and β-DDM, therefore, the ATPase activity was measured in the presence of 10 fold higher KCl concentration, while all other conditions remained identical.

All tested detergents, except Aminoxide WS-35, are well-characterized compounds which are routinely used for solubilization, purification and crystallization of various membrane proteins. Aminoxide WS-35 is an industrial detergent, a mixture of C_7- to C_{17}-1-alkoylamino-3-dimethylamino propane-3-N-oxide, with LAPAO as its major component. More detailed structural information is, however, still lacking.

Detergent	**E_A / µmol P_i mg^{-1} min^{-1}**	**F_{ind}**	**$K_{1/2}(K^+)$ / mM**
Fos-choline 12	0.102 ± 0.024	1.2	14.95
β-DDM	0.534 ± 0.010	2.1	3.34
β-DM	0.554 ± 0.027	2.2	1.30
PCC-α-M	0.275 ± 0.013	2.6	0.16
LAPAO	0.628 ± 0.032	2.2	0.13
Aminoxide WS-35	0.868 ± 0.021	4.0	0.0065

Table 2. Effects of six different detergents used for purification of the KdpFABC complex. The enzyme activity, E_A, was determined in the presence of saturating K^+ concentration. The induction factor, F_{ind}, indicates the factor by which E_A increased when the K^+ concentration was increased from nominally 0 to a saturating concentration. $K_{1/2}(K^+)$ was determined by equilibrium-titration experiments with RH421 and represents the K^+ concentration at which K^+ binding was half-maximal.

Although the results show a good correlation in enzyme activity, induction factor and half-saturating K^+ concentration for each tested detergent, only one of them, Aminoxide WS-35, provided a solubilized KdpFABC complex with $K_{1/2}$ of 6.5 µM, which is comparable to the affinity found under physiological conditions (*67;79*). Interestingly, the major component of this complex mixture, LAPAO, did not provide enzyme with high K^+ binding affinity, although the enzyme ATPase activity was much closer to that obtained with the Aminoxide WS-35 solubilized KdpFABC. This observation indicates that KdpFABC obviously requires specific, yet unknown, component(s) to stabilize a properly functioning complex, in which the K^+-binding sites are arranged in the same manner as in the physiological membrane environment. The role of this unidentified component might be of a functional lipid, similar to the finding recently reported for the Na^+,K^+-ATPase (*172*). According to the presented results, all subsequent experiments were performed with protein complexes solubilized in Aminoxide WS-35.

3.2. Substrate dependence of the KdpFABC ATPase activity

The ATPase activity of detergent-solubilized KdpFABC in Aminoxide WS-35 was determined with the malachite green assay, in the presence of different K^+ concentrations, ranging from 0 to 3.3 mM, at pH 7.8. The results of K^+-dependent ATPase activity, shown in *Figure 27A,* could be fitted with by a simple Michaelis-Menten kinetics. The $K_{1/2}$ value of the K^+-induced activity was determined to be (2.03 ± 0.12) µM, which is in good agreement to previously reported value (*67;79*).

One approach to investigate the role of protons in KdpFABC reaction cycle was to measure the ATPase activity at different pH values between 6.0 and 8.5 in the presence of saturating 3.3 mM K^+ (*Figure 27B*). The observed pH dependence could be also fitted by a Michaelis-Menten kinetics, and a pK value of 7.8 was obtained at the saturating K^+ concentration. According to the fitting parameters a factor ~3 could be determined between the enzyme activity of the deprotonated and protonated state of the KdpFABC. This observation indicates that proton binding reduces the overall ATPase activity, by reducing the turnover number of the KdpFABC complex. Two possible explanations for this effect are an allosteric binding of proton to the KdpB subunit, thus affecting the enzyme activity, or competition between K^+ and H^+ at the binding sites located in the KdpA subunit. Assuming that proton is transported as a counterion, as in the case of the H^+,K^+-ATPase, the overall activity of the pump should decrease at high pH due to the lack of transported substrate. In contrast to this requirement, an increase in ATPase activity was observed at high pH and saturating K^+ concentration, indicating that proton cotransport is less likely in case of the KdpFABC.

On the other hand, the pH dependence of the enzyme ATPase activity in absence of K^+ showed overall lower level (*Figure 27B*). The maximal activity was found to be (0.18 ± 0.02) µmol P_i per mg protein per min at pH (7.5 ± 0.2). In order to confirm that the observed residual enzyme activity is not a result of a K^+ contamination in the double-distilled water used in these experiments, the same measurements were repeated with ultrapure water ($[K^+] \leq 10$ ppb), but no significant difference was detected, and the determined KdpFABC activity was (0.17 ± 0.01) µmol P_i per mg protein per min at pH 7.8 and in the absence K^+. According to the pH dependence of the enzyme activity in the presence of K^+, at lower pH also an activity decrease is observed, most likely produced by an allosteric effect, whilst at a pH higher than 7.8 the activity was only slightly reduced to ~0.14 µmol P_i per mg protein

per min (pH 8.8). Comparing the pH-dependent ATPase activity, both in the absence and presence of saturating 3.3 mM K^+, the activity reduction can be explained by the reduced binding of protons when no K^+ are present. These results are in agreement with the previously published observation that in the absence of K^+ the KdpFABC complex is also capable of transporting protons, although to lesser extent (*90*).

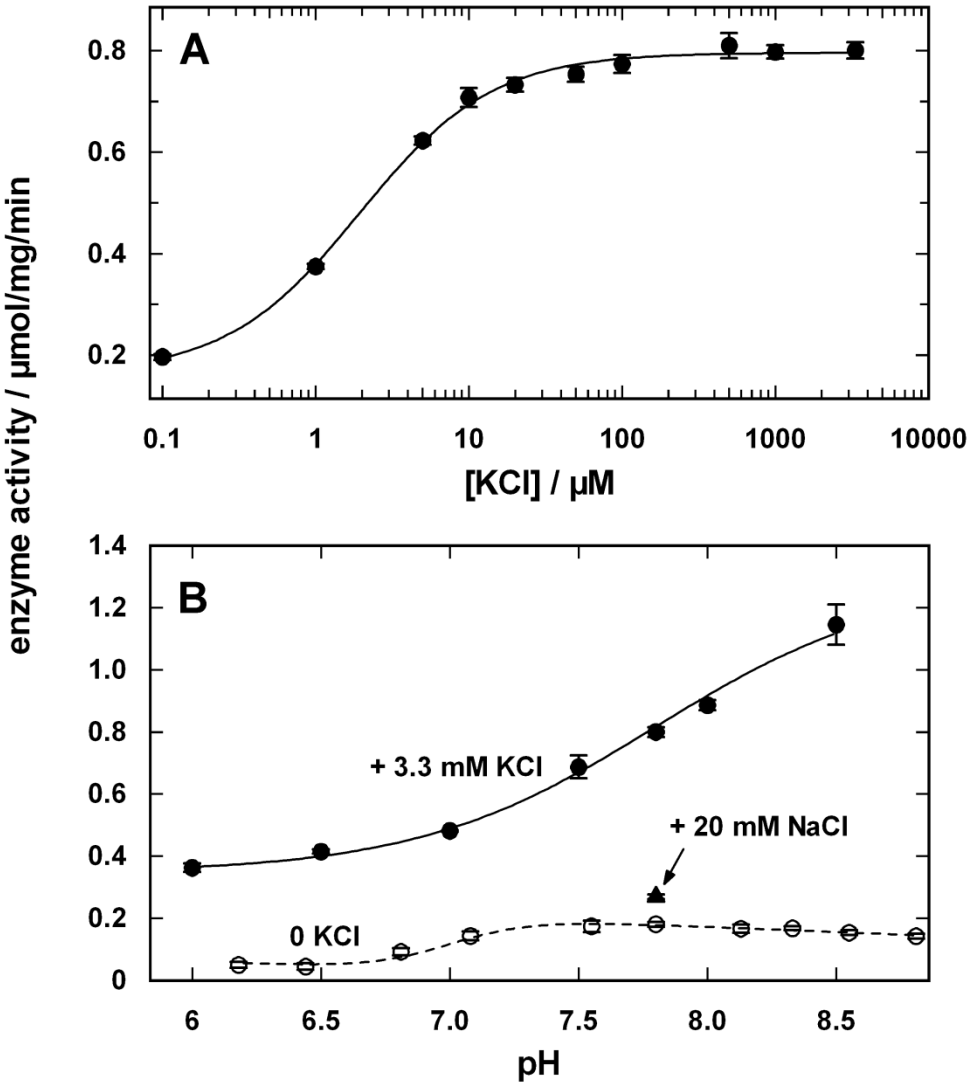

Figure 27. K^+ and pH dependence of the KdpFABC complex activity solubilized in Aminoxide WS-35. **A:** K^+-induced ATPase activity at pH 7.8 with a $K_{1/2}$ of (2.03 ± 0.12) µM. **B:** pH dependence of the enzyme activity in the presence of 3.3 mM K^+, fitted with a simple binding isotherm with a pK of 7.8. The pH dependence of enzyme activity in the absence of K^+ is shown by open circles and a dashed line. The activity at pH 7.8 in the presence of 20 mM NaCl is represented with a solid triangle.

The ATPase activity was also measured in the presence of 20 mM NaCl (suprapur® quality), and in the absence of K^+ at pH 7.8. The measured Na^+-induced enzyme activity was found to be (0.27 ± 0.1) µmol P_i per mg protein per min (*Figure 27B*). This result confirms previous observations that KdpFABC is able to transport also Na^+ in absence of K^+, although with lower affinity and extent. In summary, in absence of K^+, both H^+ and Na^+ act as weak congeners of potassium (*90*).

To determine the ATP binding affinity of KdpFABC, a set of experiments was carried out varying ATP concentration, at constant pH 7.8 and saturating K^+ concentration. The Na_2-ATP concentration ranged between 1 µM and 5 mM, while the pH in the buffered electrolyte after addition of ATP did not vary more than ± 0.1 (*Figure 28*, in black). The data were fitted with a sum of two Hill functions (Eq. 2). In the range of ATP concentrations lower than 500 µM, the enzyme activity increased with increasing ATP concentration, with a calculated $K_{1/2,1}$ of (65 ± 18) µM and n = 0.9, and a maximum activity of ~0.8 µmol P_i per mg protein per min. This value is in good agreement with previously reported ATP binding affinities, varying between 50 and 80 µM, obtained with different techniques. At ATP concentrations higher than 500 µM an activity decrease was observed, with a respective $K_{1/2,2}$ of (1.54 ± 0.13) mM and n = 2.1. In order to exclude the effects of possible Na^+-induced artifacts, measurements were repeated with Mg-ATP, under the same conditions. An almost identical behavior of the enzyme activity was found, therefore, suggesting that observed effects are produced by ATP (*Figure 28*, in red).

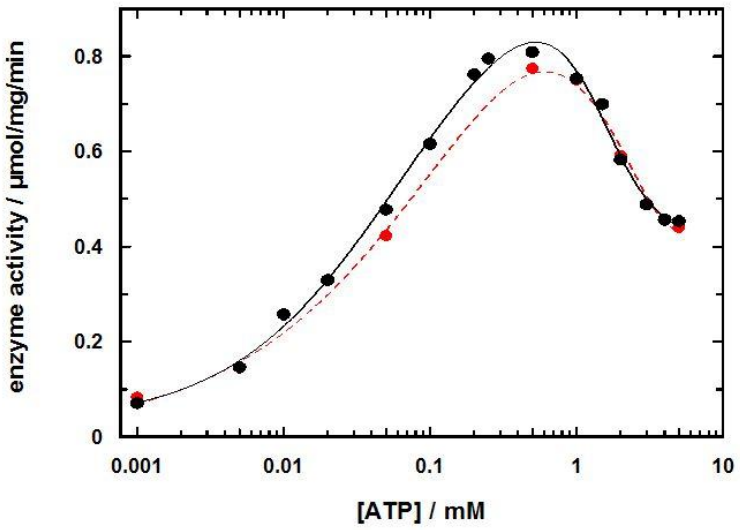

Figure 28. ATP dependence of the KdpFABC complex activity solubilized in Aminoxide WS-35. When Na_2-ATP was used (in black), data were fitted by the sum of two Hill functions with $K_{1/2,1}$ = (65 ± 18) µM and $K_{1/2,2}$ = (1.54 ± 0.13) mM. An almost identical behavior was determined when Mg-ATP was used (in red), with corresponding $K_{1/2,1}$ = (74± 12) µM and $K_{1/2,2}$ = (1.55 ± 0.27) mM.

3.3. RH421 steady-state experiments with the detergent-solubilized KdpFABC

3.3.1. Standard experiments

The so-called standard experiment, a basic approach of the steady-state technique (2.5.2a.), can be used to characterize the electrogenic ion-binding properties of the KdpFABC in both conformational states, E_1 and P-E_2. In this set of experiments, the fluorescence response of the RH421 dye was monitored, at various pH of the buffer and in the presence of different substrates that stabilize specific stationary states of the enzyme throughout the reaction cycle. In the absence of ATP, the KdpFABC is supposed to be stabilized in its E_1 conformation, and binding of K^+ and possibly H^+, is assumed to occur at the cytoplasmic side. Upon addition of saturating 1 mM Mg-ATP, the enzyme proceeds to the P-E_2 state, in which the ion binding is assumed to take place at the extracellular side. Another possibility to trap the enzyme in E_2-P state is *via* the so-called backdoor phosphorylation, triggered by addition of inorganic phosphate, P_i, which reverses the direction of dephosphorylation step in the transport cycle, $E_1 + P_i \rightarrow E_2$-P (*158*). Corresponding experiments were performed to study the electrogenicity of ion binding in the unphosphorylated state, after phosphorylation by 1 mM Mg-ATP and by 1 mM Tris-phosphate (P_i).

An important observation necessary to mention before presenting obtained results is the requirement of pH jumps from pH 8 down to pH 6 and backward for stabilization of the fluorescence signal before any subsequent experimental studies. First results involving pH changes of the buffer were misleading, suggesting strong proton binding by solubilized KdpFABC complex. An example of proton titration experiment, in the absence of K^+, ATP and P_i, shown in *Figure 29A*, reveals a fluorescence decrease of ~20 % as a result of binding of H^+, whereas a maximal fluorescence decrease was ~5 % in case of the K^+ binding (see text further below). Since the fluorescence change is a measure of the positive charge bound to the membrane domain of KdpFABC, this observation would indicate binding of four times as many protons as K^+ ions. This assumption is not in agreement with any known behavior described for P-type ATPases so far, and it is highly unlikely to be the case for the KdpFABC mode of work. A possible explanation for this observation, however, could be the conformational rearrangement of the dye/lipid system induced by forward and backward pH jumps that leads to a new equilibrium state, and finally produces a stable fluorescence

signal. Therefore, all RH421 experiments were carried out with initial pH decrease from 8 to 6 (by adding HCl) and successive, instantaneous increase back to pH 8 (by adding NaOH). After these pH jumps, successive H^+ titration resulted in florescence decrease of ~5 % (*Figure 29B*) that are comparable to the steps obtained for addition of saturating K^+ concentrations.

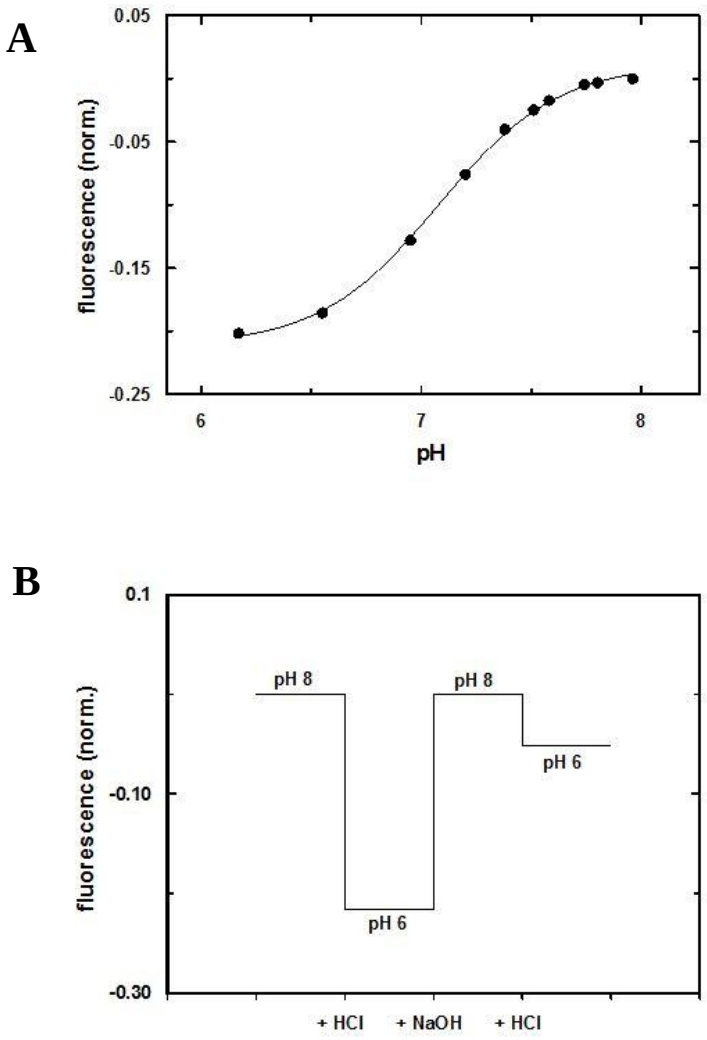

Figure 29. Effect of pH on the fluorescence signal of RH421, most likely induced by conformational rearrangement in the RH421/lipid system induced by sudden pH jumps. **A:** H^+ titration in the absence of K^+, showing ~20 % fluorescence decrease upon reaching pH 6. **B:** Forward and backward pH jumps followed by decreasing the pH back to 6 (by adding HCl), only now producing a fluorescence decrease of ~5 % due to proton binding.

According to the described protocol, a cuvette with 2 mL buffer of 50 mM Tris-HCl (pH 8) and 2 mM $MgCl_2$ was thermally equilibrated, before 200 nM RH421 dye and 9 µg/mL detergent-solubilized KdpFABC were added. After achieving a stable fluorescence signal

(10-15 minutes), aliquots of HCl were added to adjust the desired pH value of the buffer, followed by the addition of saturating concentrations of 1 mM ATP (pH adjusted) and 250 µM KCl. Addition of ATP did not alter the pH of the buffer more than ± 0.1. An example of the single fluorescence signal trace is shown in *Figure 30A*, whereas the corresponding set of HCl, ATP and KCl additions is given is *Figure 30B.*

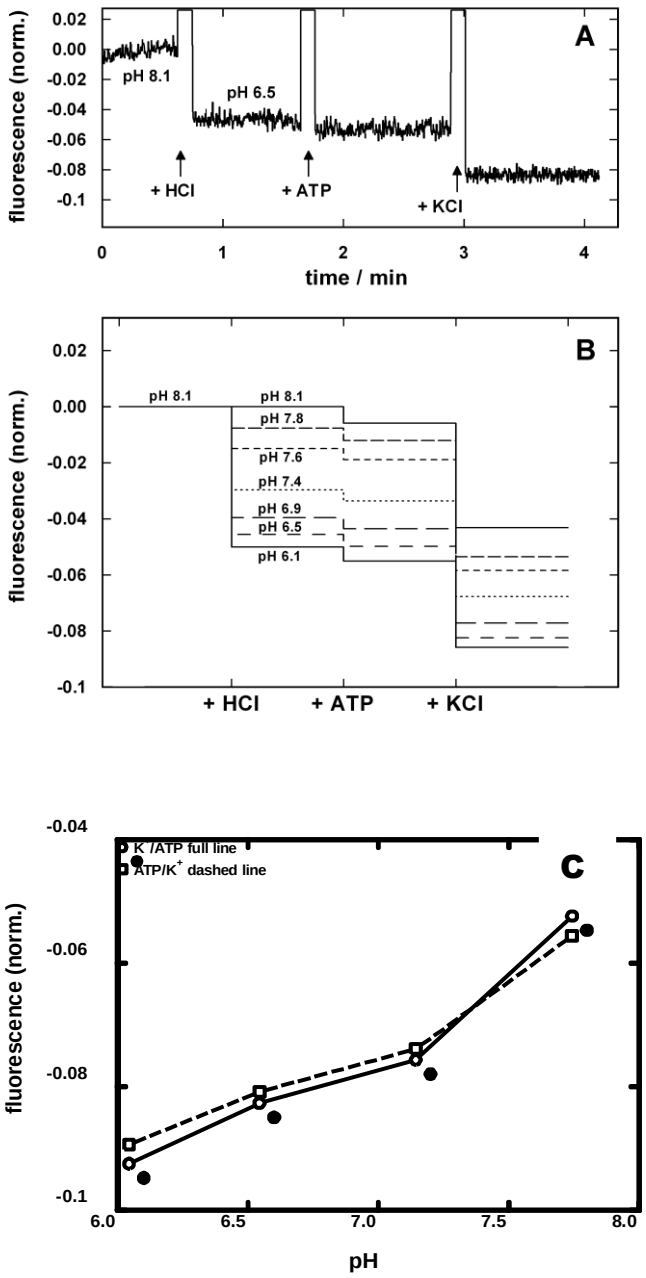

Figure 30. RH421 standard experiment to reveal the electrogenic contributions of substrate additions to the KdpFABC complex. **A:** Fluorescence trace induced by the addition of HCl to obtain pH 6.5 (6.5 µl HCl 4 M), 1 mM ATP and 250 µM KCl. **B:** Schematic representation of the fluorescence changes detected after addition of various amounts of HCl to obtain the indicated pH, followed by the addition of ATP and KCl. **C:** Changing the order of substrate addition revealed no significant difference in the substrate-induced fluorescence decreases.

Additions of both H^+ and K^+, and to a minor extent ATP, generated a fluorescence decrease. To check whether there is a mutual effect on the binding behavior, in the next set of experiments, the order of ATP and HCl additions was reversed (*Figure 30C*). There was no significant difference in the substrate-induced fluorescence decreases.

The further evaluation of the results obtained from standard experiments is given in *Figure 31*. The substrate-induced decreases of the RH421 fluorescence indicate that binding of both ion species, K^+ and H^+, is an electrogenic process in the unphosphorylated as well as in the phosphorylated states of the KdpFABC. This implies that the ions are bound to sites located in a protein domain embedded in the membrane dielectric.

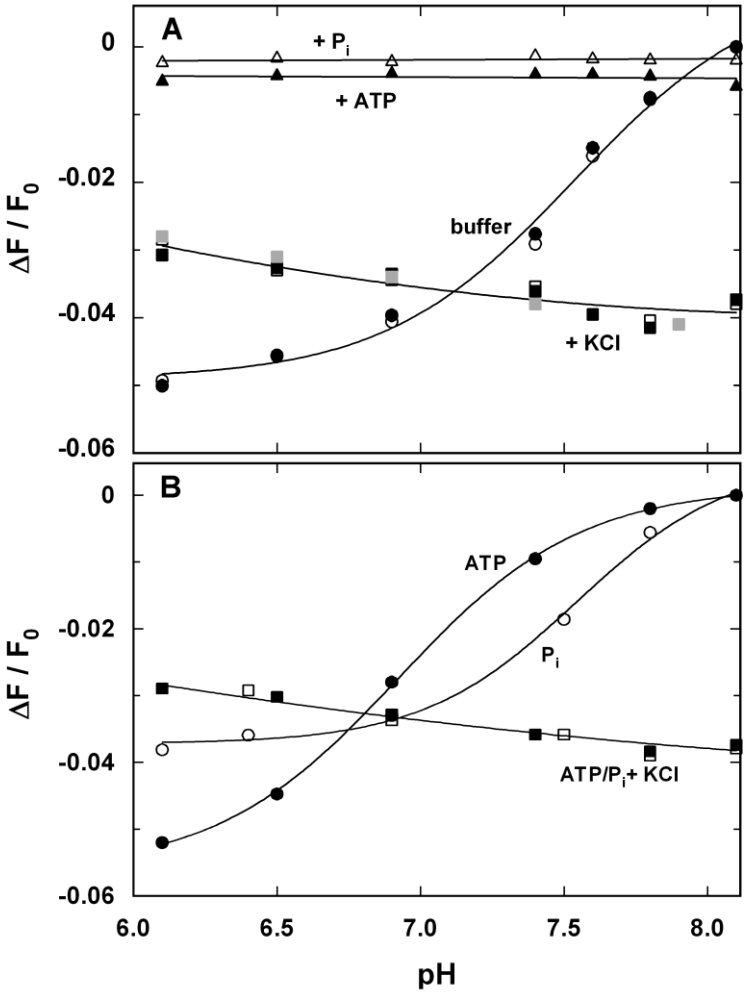

Figure 31. Analysis of the electrogenicity of substrate binding to the KdpFABC complex. **A:** pH dependence of the fluorescence changes induced by the additions of aliquots of HCl, 1 mM ATP or P_i, and 250 µM KCl. Solid symbols: experiments with addition of ATP; open symbols: experiments with addition of P_i, grey squares: K^+ titration experiments in E_1. **B:** pH dependence of the fluorescence changes induced by the additions of 1 mM ATP or P_i first, then appropriate aliquots of HCl, and finally 250 µM KCl. The lines were drawn to guide the eye.

Results presented in *Figure 31A* show that only a very small fluorescence change (<0.5 %) is produced during the phosphorylation step both by ATP and P_i, indicating that no significant charge movements occur during the corresponding reaction steps. Further on, it was demonstrated that the H^+ concentration affects the amount of electrochemically bound K^+, and that the H^+-binding kinetics differs in the unphosphorylated and phosphorylated state of the KdpFABC, produced both by ATP and P_i. On the other hand, binding of K^+ was not significantly dependent neither on the pH of the buffer nor the specific state of the enzyme, E_1 or E_2-P. The addition of saturating KCl and HCl concentrations produced a fluorescence decrease of up to ~5 % (*Figure 31B*).

3.3.2. Ion-binding titrations

To determine the affinities of the KdpFABC binding sites for both ion species, K^+ and H^+, a set of titration experiments was performed. Starting with 2 mL buffer containing 50 mM Tris-HCl (pH 7.8), 2 mM $MgCl_2$, after thermal equilibration 200 mM RH421 and 9 µg/mL detergent-solubilized enzyme, and subsequently KCl or HCl was added in appropriately small aliquots from stock-solutions until the fluorescence signal saturated. In this manner the existing binding site(s) were titrated, allowing a determination of the half-saturating concentration for K^+ or protons, $K_{1/2}$ and pK, respectively. These experiments were started in the buffer, in which KdpFABC is assumed to be in its unphosphorylated E_1 state, or in a phosphorylated state produced by addition of either Mg-ATP or Tris-P_i. All titration experiments were repeated 3-5 times and the corresponding averaged values of normalized fluorescence levels were plotted against pH or K^+ concentration.

Results shown in *Figure 32A* represent K^+ titration in the buffer at pH 7.8, and after addition of 1 mM ATP or 1 mM P_i, when KdpFABC is supposed to adopt the E_1 and E_2-P conformations, respectively. The K^+-concentration dependence in the E_1 conformation of the KdpFABC (*Figure 32A*, full circles), was fitted by a Hill function with half-saturating concentration $K_{1/2}$ of (6.5 ± 0.3) µM and a Hill coefficient n of 2.3 ± 0.3 (*Figure 32A*, solid line). Hill coefficient larger than 2 indicates a cooperative binding of more than one K^+. No satisfying fit could be obtained using a simple Michaelis-Menten kinetics (*Figure 32A*, dashed line).

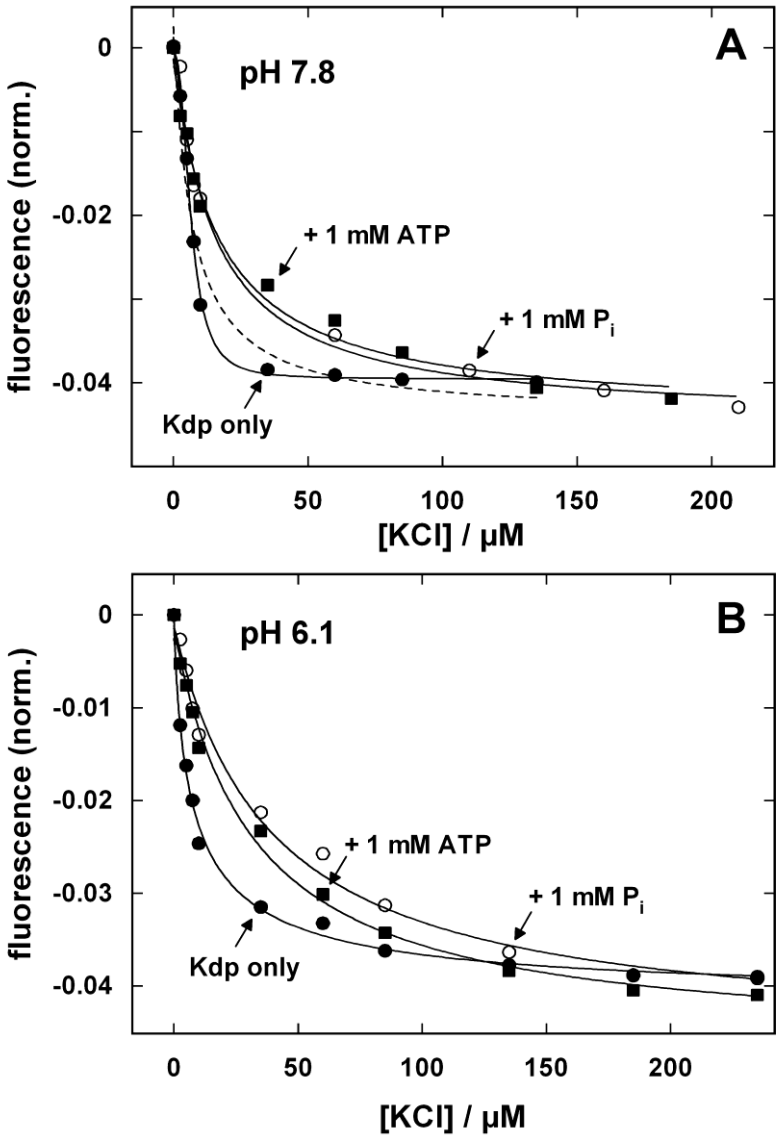

Figure 32. Electrogenic binding of K^+ ions in buffer (E_1 state, noted as Kdp only) and after addition of 1 mM Mg-ATP or 1 mM P_i ($P\text{-}E_2$ state). **A:** K^+ titrations at pH 7.8 with calculated $K_{1/2}$ values of 6.5 µM (Kdp only), 14.4 µM (P_i), and 16.8 µM (ATP). **B:** Similar experiments performed at pH 6.1. The half-saturating concentrations $K_{1/2}$ were 7.9 µM (Kdp only), 39.1 µM (P_i), and 31.6 µM (ATP). The lines drawn through the data were fits with either a Hill function of a Michaelis-Menten binding isotherm.

In the second set of experiments, phosphorylation of the KdpFABC was triggered by addition of 1 mM Mg-ATP, converting the enzyme to the $P\text{-}E_2$ conformation, followed by a KCl titration. In this case, the K^+ dependence could be fit with a Michaelis-Menten kinetics, providing the half-saturating concentration $K_{1/2}$ of (16.8 ± 3.0) µM. In the presence of ATP and KCl, the pump works in its turnover mode, and it is not completely clear if the KdpFABC is preferentially in the $P\text{-}E_2$ conformation under these conditions. Therefore, another approach to investigate the K^+ binding affinity in the phosphorylated state of the

enzyme is addition of 1 mM Tris-phosphate, instead of ATP, before the corresponding KCl titration was performed. Under these conditions, KdpFABC is supposed to be trapped in a P-E_2 state, similar to behavior already known for other members of P-type ATPases. The results of K^+-titration experiments in the presence of 1 mM Tris-P_i were also fitted with a simple Michaelis-Menten kinetics (*Figure 32A*, open circles), providing a half-saturating concentration of (14.4 ± 2.6) µM. Comparing the values obtained for the K^+-binding affinity for phosphorylated KdpFABC complex, produced by ATP and P_i, no significant difference was observed. This result is not unexpected, since the K^+ binding kinetics should not depend on the phosphorylation method. On the other hand, from the obtained agreement of the half-saturating concentrations it can be assumed that the enzyme complex adopts preferentially the P-E_2 conformation in both sets of measurements. The apparent K^+-binding affinity was, however, decreased by a factor of ~2 with the respect to the half-saturation determined in the unphosphorylated state (E_1). Noteworthy is the observation that in all KCl titration experiments, performed under three different conditions, the maximum fluorescence decrease of ~0.04 was nearly identical. This implies that the same number of K^+ ions bind to the membrane domain of the KdpFABC complex, independently of the conformational state of the enzyme.

To investigate to effect of possible proton binding on K^+ binding affinity, the titration experiments were repeated at pH 6.1. For adjusting the desired pH HCl was used, prior additions of other substrates. KCl titrations were performed in buffer (E_1 state) and P-E_2 conformation, achieved by addition of either 1 mM Mg-ATP or 1 mM Tris-P_i (*Figure 32B*). The pH measured at the end of experiments did not differ more than ± 0.1 from the initial pH. All three data sets could be fitted by a simple Michaelis-Menten kinetics. In the E_1 conformation (*Figure 32B*, full circles) the calculated $K_{1/2}$ value of (7.9 ± 0.7) µM, was slightly increased with respect to the value obtained at pH 7.8. This observation indicates that higher proton concentration reduces the K^+ binding affinity in E_1 state. This effect is even more pronounced in the P-E_2 conformation of the enzyme, triggered both by ATP and P_i. In this case, the presence of more protons significantly increased half-saturating concentrations to (31.6 ± 1.1) µM and (39.1 ± 7.3) µM, in the presence of ATP (full squares) and P_i (open circles), respectively. Similar to the behavior observed at pH 7.8, the same number of K^+ ions is bound inside the membrane domain of the KdpFABC complex since the maximum fluorescence decrease was almost the same in all three cases, and furthermore, almost identical to the decrease produced by K^+ binding at pH 7.8. The

presence of higher H^+ concentration, however, reduced the apparent K^+ binding affinity only to a minor extent in the unphosphorylated state, whilst the apparent K^+ binding affinity in the phosphorylated, P-E_2, state was significantly reduced, resulting in approximately twofold $K_{1/2}$ values.

To further investigate the effect of protons in the KdpFABC pumping cycle, proton titrations were carried out correspondingly under different conditions (*Figure 33A*). Starting with buffer pH 8.0 - 8.1, aliquots of HCl were added until a pH of 6.1 was achieved. The relative fluorescence changes upon proton titration and the pK values for the proton binding were determined by fitting the pH dependence with the Hill function. Proton titration experiments performed in the E_1 state of the enzyme and in the absence of K^+ (Kdp only, full circles), were fitted with a pK of 7.55 ± 0.05 and a Hill coefficient of n > 1.4. When proton titration was performed in the P-E_2 state in the absence of K^+, determined pK values were 6.78 ± 0.20 and 7.34 ± 0.04, when the phosphorylated state was produced by 1 mM Mg-ATP or 1 mM Tris-P_i, respectively. The results presented in *Figure 33B* show the dependence of the pK values on the KCl concentration up to 500 µM in the unphosphorylated state of the enzyme. These data indicate that the K^+ concentration in the buffer has no significant effect on the pK value. If K^+ binding would compete with protons, the apparent pK values should decrease with increasing KCl concentrations. At the highest used KCl concentration of 500 µM, which is significantly higher than saturating K^+ concentration, the pK value was 7.65 ± 0.20. As for the fluorescence decrease at the lowest tested pH ~ 6 upon H^+ titration dependence on KCl concentration, similar effect was observed (*Figure 33C*). It was found that maximal fluorescence decrease was independent on the K^+ concentration present in the buffer, with ΔF_{max}(pH~ 6) of -0.057 ± 0.002 at 0 K^+, and -0.050 ± 0.01 at 500 µM K^+. Obtained values of the K^+ and H^+ binding affinities under various conditions are summarized in *Table 3*.

Comparing the results compiled in *Table 3*, it is apparent that the K^+ binding affinity in the phosphorylated state of the KdpFABC complex is generally lower than in the unphosphorylated conformation. Higher proton concentration reduces the K^+ binding affinity, and this effect is stronger in the P-E_2 state, achieved either by ATP or P_i. In contrast, there are no significant differences in pK in the absence and presence of K^+ in all three tested states. Additionally, it was found that pK values were strongly dependent of the phosphorylation method. The pK value in phosphorylated state achieved by addition of ATP was found to be 5.70 ± 0.30, whereas upon back-door phosphorylation it was 7.20 ± 0.20.

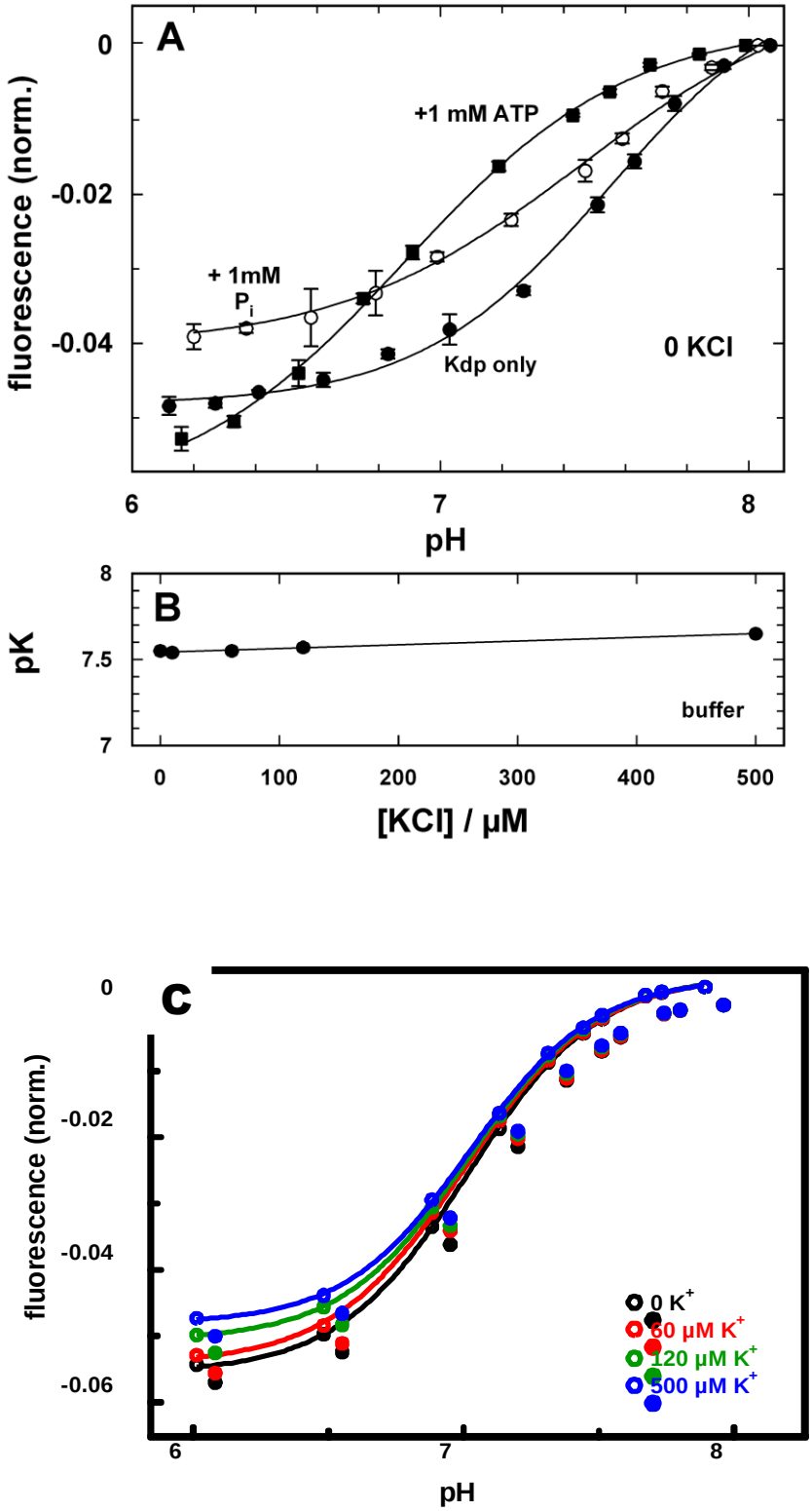

Figure 33. pH titration experiments with the detergent-solubilized KdpFABC complex in different conformations, in the absence and presence of different K^+ concentrations. **A**: In the E_1 conformation (Kdp only) a pK of 7.55 could be determined, whereas in the P-E_2 conformation pK values of 6.78 (+ATP) and 7.34 (+ Pi) were determined. The lines drawn represent fits with the Hill function. **B**: Distribution of pK values obtained in corresponding pH titrations in the presence of different K^+ concentrations. The pK increased only slightly from 7.55 (0 KCl) to 7.65 (500 µM KCl). **C:** pH titration experiments in the presence of different K^+ concentrations, showing that maximal fluorescence decrease was independent on the K^+ concentration present in the buffer.

		Buffer	+ 1 mM ATP	+ 1 mM P_i
$K_{1/2}$ / µM	pH 7.8	6.5 ± 0.3	16.8 ± 3.0	14.4 ± 2.6
	pH 6.1	7.9 ± 0.7	31.6 ± 1.1	39.1 ± 7.3
pK	0 K^+	7.55 ± 0.05	6.78 ± 0.28	7.34 ± 0.04
	500 µM K^+	7.65± 0.20	5.70 ± 0.30	7.20 ± 0.20

Table 3. Comparison of ion-binding properties of detergent-solubilized KdpFABC. Half-saturating K^+ concentrations were determined at pH 7.8 and pH 6.1 for both the unphosphorylated and phosphorylated state induced by the addition of either Mg-ATP or inorganic phosphate (P_i). Apparent pK values were obtained in the absence and presence of saturating 500 µM KCl.

To investigate this remarkable asymmetry of K^+ and H^+ competition, the K^+ binding kinetics in the E_1 state was analyzed in terms of a Lineweaver-Burk plot. K^+ titrations at five different pH values in the range of 6.1 – 7.8 are shown in *Figure 34*. The interception of the linear-regression lines through the data points is above the $1/[K^+]$ axis, and it indicates a mixed inhibition of K^+ binding by protons. This finding suggests that at least two different mechanisms contribute to the inhibitory effect.

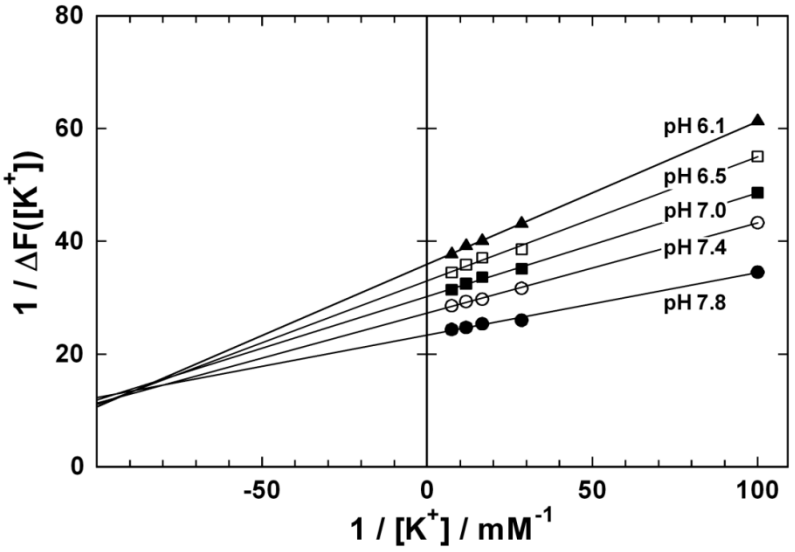

Figure 34. Lineweaver-Burk plot of K^+ binding to solubilized KdpFABC in its E_1 conformation at different pH values. The interception of the regression lines through the data points above the $1/[K^+]$ axis indicates a mixed inhibition of K^+ binding by H^+.

It was already reported that KdpFABC is capable of transporting Na^+, as well as other cations (*90*), in the absence of K^+. To test whether Na^+ ions are able bind to the K^+-binding sites, corresponding Na^+-titration experiments were performed (*Figure 35*). Starting from 2 mL buffer, containing 50 mM Tris-HCl (pH 7.8), 2 mM $MgCl_2$, 200 nM RH421 and 9 µg/mL detergent-solubilized KdpFABC, appropriate aliquots of NaCl stock-solution were added. The concentration dependence could be fit with a simple Michaelis-Menten kinetics, with half-saturating concentration $K_{1/2}(Na^+)$ of (4.3 ± 0.2) mM. Interestingly, the maximal fluorescence decrease of ~5 % was nearly identical as in the case of corresponding K^+ titration, although the binding affinity is lower by a factor of ~660.

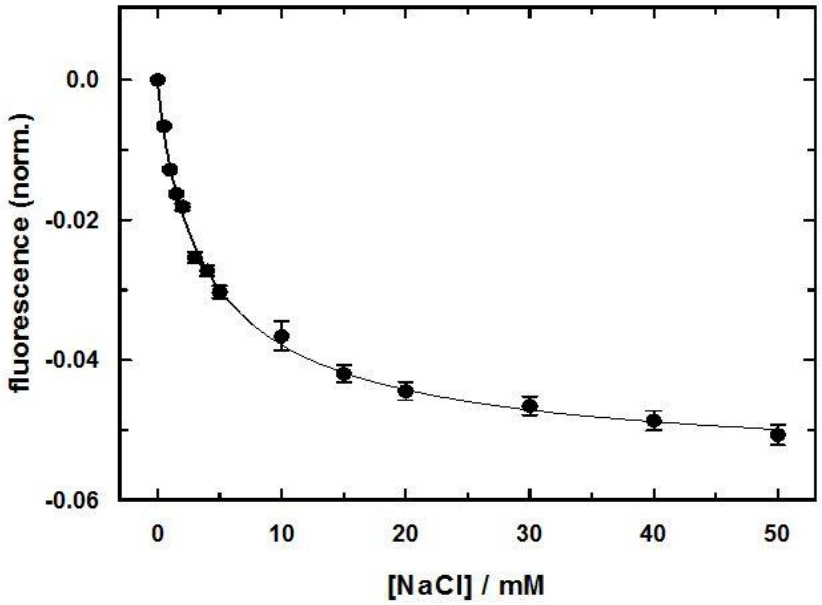

Figure 35. Na^+ titration of the solubilized KdpFABC at pH 7.8 in the absence of K^+. Data were fitted with a simple Michaelis-Menten binding kinetics, with $K_{1/2}(Na^+)$ of (4.3 ± 0.2) mM.

3.3.3. Effect of Mg^{2+} ions on K^+-binding affinity

In case of the Na^+,K^+-ATPase it has been demonstrated that increasing concentration of Mg^{2+} ions have the tendency to reduce the Na^+-binding affinity (*173*). This effect was investigated also for the KdpFABC K^+-binding affinity in the E_1 conformation. For this purpose, KCl titrations were performed at pH 7.8, in the presence of various $MgCl_2$ concentrations. The results were fitted with a Hill function, and the calculated half-saturating K^+ concentrations, $K_{1/2}$, and the maximum fluorescence changes, ΔF_{max}, were

plotted against respective Mg^{2+} concentration (*Figure 36*). From the results shown in *Figure 36A*, it is apparent that the K^+-binding affinity of the KdpFABC is reduced with increasing Mg^{2+} concentration, similar to the observation reported for the Na^+,K^+-ATPase. The apparent decrease of the Na^+-binding affinity in the case of the Na^+,K^+-ATPase has been assigned to the Gouy-Chapman effect induced by a Mg^{2+} ion bound in the vicinity of the entrance of the access channel to the ion-binding sites. This explanation can also be proposed for the results found for K^+-binding affinity dependence on Mg^{2+} of the KdpFABC complex. According to the results shown in *Figure 36A*, half saturating concentrations, $K_{1/2}(K^+)$, increased by a factor of ~3 with increasing Mg^{2+} concentration from 0 to 20 mM. In addition, the affinity of the assumed Mg^{2+}-binding site was calculated to be (6.6 ± 0.2) mM. Results presented in the *Figure 36B* show that under the same experimental conditions, the amplitude of the maximal fluorescence decrease upon K^+ binding, ΔF_{max}, increases by a factor larger than 2. Taking into account that this parameter, ΔF_{max}, is a measure of the total amount of positive charge bound to the membrane domain (*154;157*), the obtained results indicated that in the presence of Mg^{2+} more positive charge is bound.

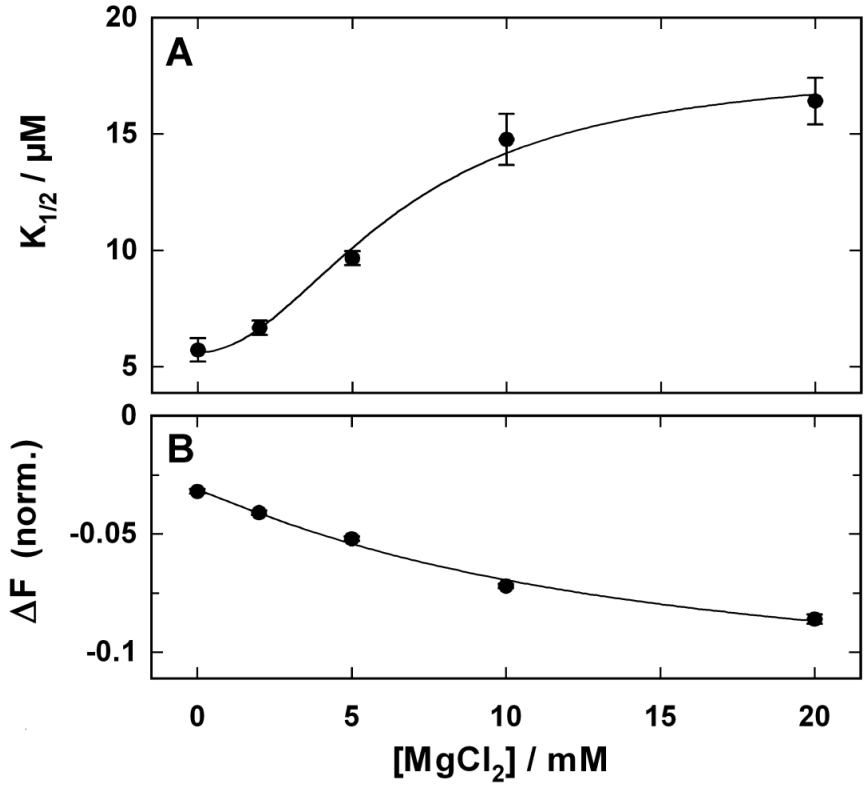

Figure 36. Effect of Mg^{2+} ions on K^+ binding in the E_1 conformation of the KdpFABC complex. **A:** The apparent affinity of K^+ binding is reduced with increasing Mg^{2+} concentrations. **B:** The maximal fluorescence amplitude, ΔF_{max}, obtained by the addition of a saturating K^+ concentration (*174*) increased with the Mg^{2+} concentration and indicates the binding of a higher amount of positive electric charge.

It is unlikely, however, that the presence of Mg^{2+} ions directly raises the number of K^+-binding sites located in the membrane domain of KdpFABC complex, therefore, a plausible explanations for this finding is that, in the absence of K^+ and Mg^{2+}, the binding site are at least partially occupied by H^+. The presence of Mg^{2+} ions leads to a displacement of protons from the binding sites caused by the Gouy-Chapman effect. To check this assumption, $MgCl_2$ titrations of the solubilized KdpFABC were performed at pH 7.8 in the absence of K^+. The results presented in *Figure 37* show a fluorescence increase assigned to the release of positive charge, protons, from the ion-binding sites within the membrane domain, induced by the Mg^{2+} titration. Consequently, in the presence of increasing Mg^{2+} concentrations, the process of K^+ binding at saturating concentrations is no longer an electroneutral exchange of H^+ by K^+, but rather a net uptake of K^+, reflected as an increase of the fluorescence change, ΔF_{max}.

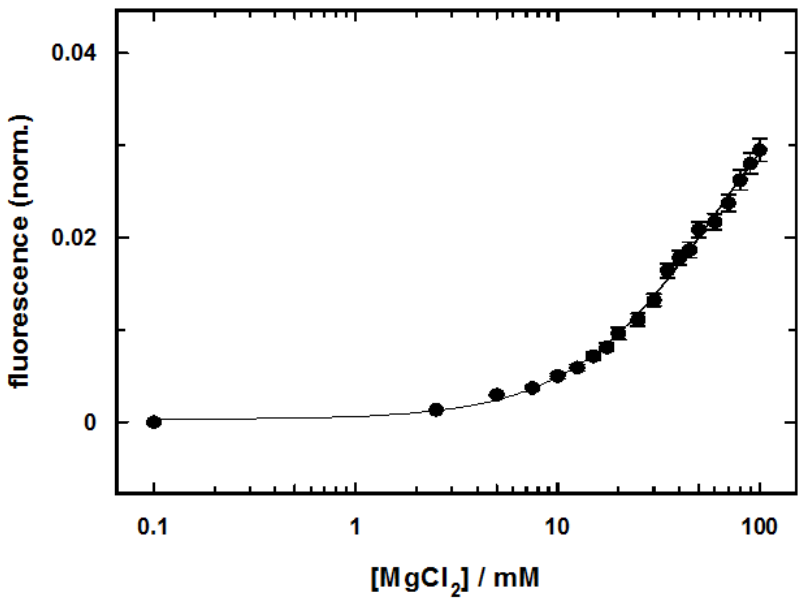

Figure 37. Mg^{2+} titration of the solubilized KdpFABC in the absence of K^+ at pH 7.8. The presence of Mg^{2+} ions induced the displacement of H^+ from the binding sites. This is reflected by a corresponding increase of the fluorescence signal of the RH421. The line is drawn to guide the eye.

3.4. $DiSC_3(V)$-fluorescence measurements with KdpFABC reconstituted in lipid vesicles

For characterization of the KdpFABC-containing vesicles, the size distribution determined by dynamic light scattering was found to be (117 ± 21) nm (*Figure 38*). The K^+-stimulated ATPase activity of the proteoliposomes determined by the malachite green assay was found to be (0.282 ± 0.008) µmol P_i mg^{-1} min^{-1}. The comparison with the enzymatic activity of the detergent-solubilized complex in β-DDM (*Table 2*) confirmed that ~50 % of the KdpFABC was incorporated into the vesicles with inside-out orientation. Interestingly, almost identical ATPase activity was measured in the presence and absence of valinomycin, similarly to a previous observation (*99*).

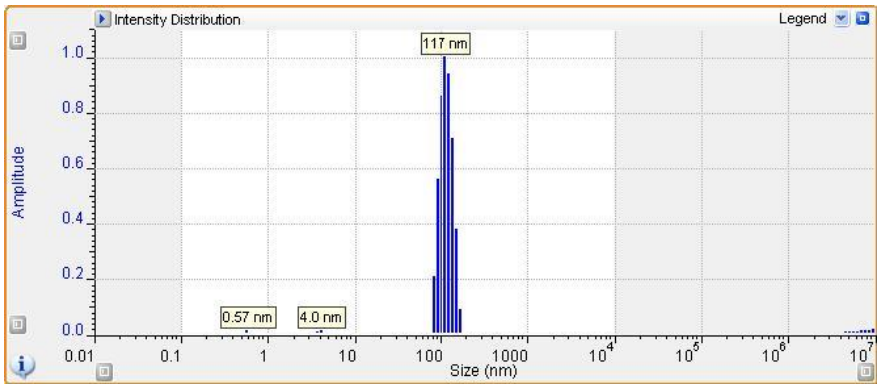

Figure 38. An example of the recorded distribution of the scattered light with KdpFABC-containing vesicles, analyzed with Omnisize 2.0. The size distribution was found to be (117 ± 21) nm. Procedure of the dynamic light scattering measurement is described in 2.4.

3.4.1. Calibration of the fluorescence signal of the $DiSC_3(V)$ dye

First set of experiments was performed with plain lipid vesicles, prepared according to the protocol described in paragraph 2.4, to calibrate the fluorescence signal of the $DiSC_3(V)$ dye, necessary for the later measurements in order to verify the direction of the ATP-induced fluorescence signals. For this purpose, a gradient of potassium concentrations is maintained across the vesicle membrane in the presence of K^+ ionophore valinomycin. 10 mg/mL E. *coli* lipid vesicles with 140 mM K^+ inside were added to the thermally equilibrated 1 mL buffer containing 25 mM imidazole, 1mM EDTA and 0.14 mM K_2SO_4 (pH 7.2), to a final lipid concentration of 80 µg/mL, followed by the addition 300 nM

$DiSC_3(V)$. An efflux of K^+ ions was initiated by the addition of 1 µM valinomycin. When a steady-state fluorescence was reached, small aliquots of 0.5 M K_2SO_4 were added, thus increasing the concentrations of K^+ ions in the external medium. The respective fluorescence signal trace is given as the inset in *Figure 39*. After addition of each aliquot, a new steady-state fluorescence level is reached instantaneously, and resulting fluorescence levels were plotted against the corresponding K^+ equilibrium potential, E_K, calculated using the Nernst equation (Eq. 1), where $[K^+]_{in}$ and $[K^+]_{out}$ are respective potassium concentrations of the internal and external medium. The results are given in *Figure 39*, and they show a linear relationship between equilibrium potential, E_K, and the fluorescence level in the voltage range between -120 mV and -40 mV. This observation is in good agreement with previously published results (*164*). A further conclusion is that the valinomycin-induced efflux of positive charge from the vesicles produces inside-negative electric potential, which is reflected in a decrease of the fluorescence signal of $DiSC_3(V)$.

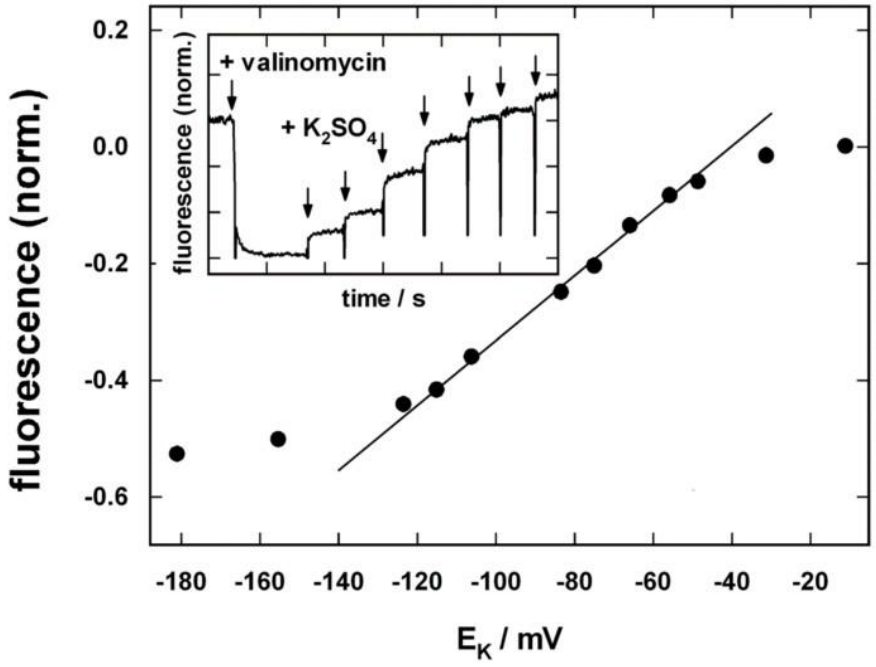

Figure 39. Calibration of the fluorescence responses of $DiSC_3(V)$ dye. Plain lipid vesicles loaded with 140 mM K^+ were analyzed in buffer starting with 0.14 mM K^+. After equilibration, 1 µM valinomycin and subsequently aliquots of K_2SO_4 were added (as indicated by arrows in the inset). The equilibrium potential, E_K, was calculated from the K^+ concentrations inside and outside, and the fluorescence levels were plotted against the respective E_K. The regression line through the data point was used as calibration curve to estimate the membrane potential obtained in various experiments.

3.4.2. Electrogenicity of the K^+ transport by the KdpFABC

KdpFABC was reconstituted into E. *coli* lipid vesicles as described in paragraph 2.4. Starting with 1 mL buffer containing 25 mM imidazole, 1 mM EDTA, 5 mM $MgSO_4$, pH 7.2 and 140 mM K^+, upon thermal equilibration an aliquot of proteoliposomes were added corresponding to a final lipid concentration of 80 µg/mL and 300 nM $DiSC_3(V)$. The concentration of K_2SO_4 was identical inside and outside of the vesicles. The high K^+ concentration was chosen to ensure a prolonged pump activity without depletion of K^+. After a stable fluorescence signal was obtained, 2.5 mM Mg-ATP was added to start ATP-driven K^+ export across the vesicle membrane. Under these conditions, only the inside-out oriented KdpFABC fraction is activated by ATP addition to the external medium. The response of ATP-induced K^+ pumping by KdpFABC is shown in *Figure 40A.*

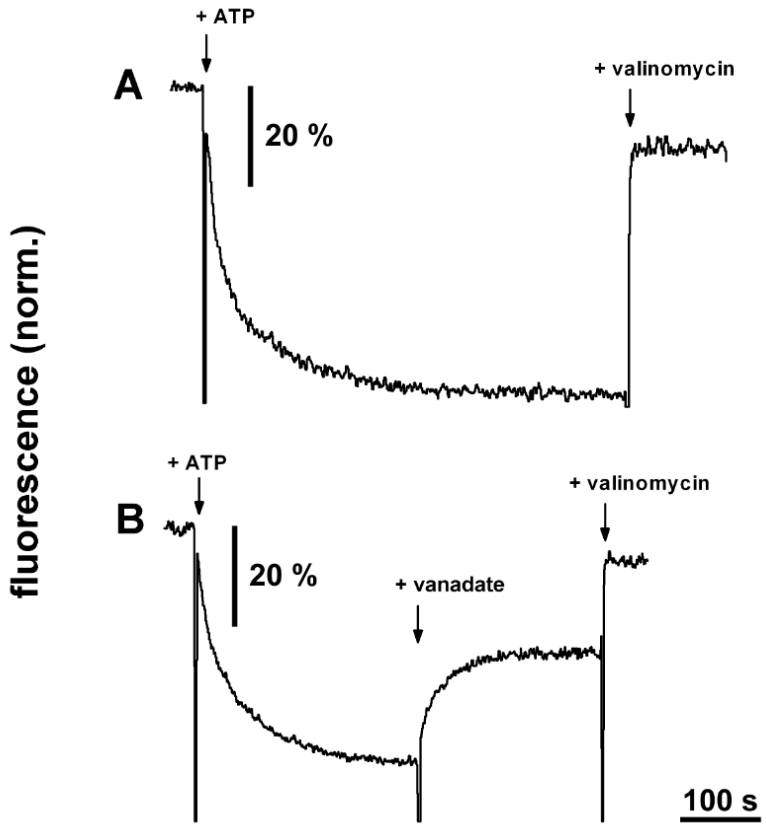

Figure 40. Electrogenic pump activity of KdpFABC containing proteoliposomes detected by the fluorescent membrane-potential indicator $DiSC_3(V)$. **A:** Initially, the internal K^+ equals the outside K^+ of 140 mM. Addition of 2.5 mM Mg-ATP triggers K^+-pumping of KdpFABC resulting in K^+ export out of the vesicles. The increasing inside negative potential is reflected by a fluorescence decrease. Addition of 1 µM valinomycin abolishes KdpFABC pump activity and stabilizes the fluorescence level at the Nernst potential, which is controlled by the ratio of K^+ concentrations inside and outside the vesicles. **B:** When the ATP-induced steady state was reached, 0.1 mM of the P-type ATPase inhibitor *o*-vanadate was added. Consequently, the membrane potential breaks down according to the reduced pump activity and the leak conductance of the membrane until a new steady state level is obtained.

The results presented in *Figures 39* and *40* confirm that ATP-induced pumping of K^+ is an electrogenic process, and that K^+ is transported out of the vesicles, which is in correspondence to previously published results (*99;175*). Upon addition of ATP, a new stationary fluorescence level was reached after ~250 seconds. This level is controlled by a compensation of the pump current by the oppositely directed leak current that increases with the membrane potential generated by the pump activity. The achieved stationary fluorescence level represents a measure of the pump current. Addition of 1 µM valinomycin induced a high K^+ conductance across the membrane, leading to the fluorescence level that approaches a level corresponding to the K^+ equilibrium potential (Eq. 1).

Addition of 0.1 mM of *o*-vanadate, a specific P-type ATPase inhibitor, upon a stable ATP-induced steady-state was reached, resulted in an inhibition of the KdpFABC pump activity. The inhibition is reflected in an exponential increase of the fluorescence signal to a new steady-state (*Figure 40B*). The increase of the fluorescence signal could be fitted with a mono-exponential function with a time constant of 47.8 s, corresponding to a specific membrane conductance of 21 pS/cm^2 (assuming a specific capacitance C_m of 1 $\mu F/cm^2$).

Another set of experiments was performed with different concentrations of Mg-ATP (pH adjusted) used to induce the KdpFABC pump activity. The conditions were the same as previously described in the experiments shown in *Figure 40*. The achieved steady-state fluorescence levels, which are a measure of the pump current, were plotted against the respective ATP concentrations. The plot was fitted with a Hill function, providing a half-saturating ATP concentration of (59.1 ± 7.3) µM and a Hill coefficient of 0.74 ± 0.07 (*Figure 41*). The calculated value of half-saturating ATP concentration is in good agreement with the concentration obtained in previous ATPase activity measurements performed with detergent-solubilized KdpFABC.

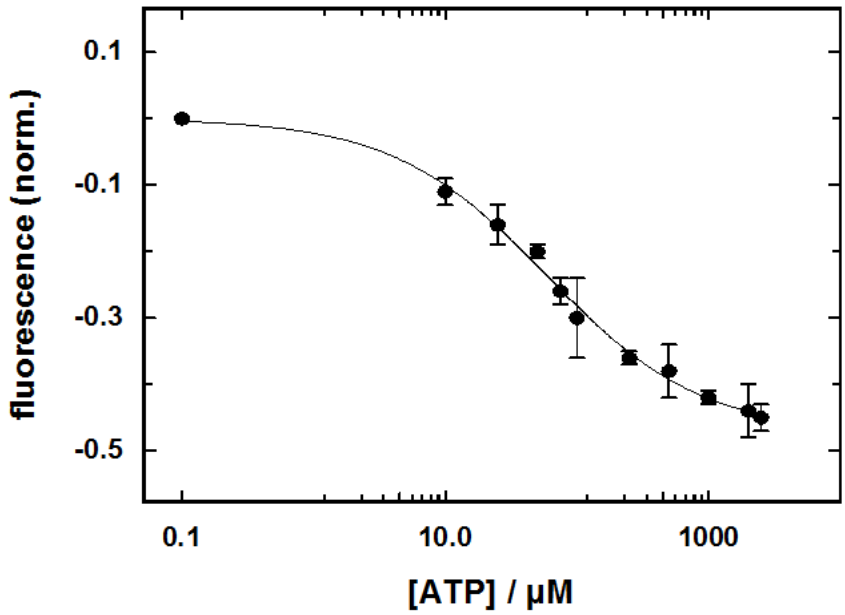

Figure 41. Steady-state fluorescence levels reached after K^+ export induced by the addition of different Mg-ATP concentrations. Intra- and extravesicular K^+ concentrations were 140 mM at pH 7.2. The obtained data were fitted with a Hill function with half-saturating ATP concentration of (59.1 ± 7.3) µM.

3.4.3. Role of H^+ in the transport process of KdpFABC

A first step in investigation of the role of protons in the pumping process performed by KdpFABC complex was to obtain the pH dependence of the ATP-induced pump current. For this purpose, experiments similar to those shown in *Figure 40A* were carried out, under the same conditions except for the pH of the external medium that was varied between 6.4 and 7.8. The concentration of K^+ was the same inside and outside of the KdpFABC-containing vesicles. After addition of 2.5 mM Mg-ATP, a stable fluorescence decrease was reached upon which 0.1 mM of *o*-vanadate was added to inhibit the pump current. For each pH value, at least three measurements were performed, and the average value of the final steady-state level was calculated. Furthermore, the calculated time constants of fluorescence increases upon inhibition by *o*-vanadate were used to evaluate the influence of pH on membrane conductance. It is important to notice that the specific membrane conductance did not significantly differ in the pH range 6.2 – 8.2, with an average leak current of (20 ± 2) pS/cm^2. Therefore, varying the pH of the buffer did not interfere with the further pH-dependent pump-current properties. The maximum steady-state fluorescence levels, as a measure of the pump current, were plotted against the respective buffer pH, as shown in *Figure 42*. The fluorescence decrease – and therefore the pump current – was found to be

maximal in the pH range of 7.3 - 7.4, whereas, both at higher and lower pH, the pump current was diminished significantly. The overall pH dependence could be fit with the sum of two Hill functions, with calculated pK values of 7.21 and 7.50. The respective Hill coefficients were found to be larger than 2, indicating that cooperative binding of more than one proton controls the pump current. A possible conclusion is that at low pH binding of protons reduces the electrogenic pump activity, while at high pH the release of protons inhibits the pump current.

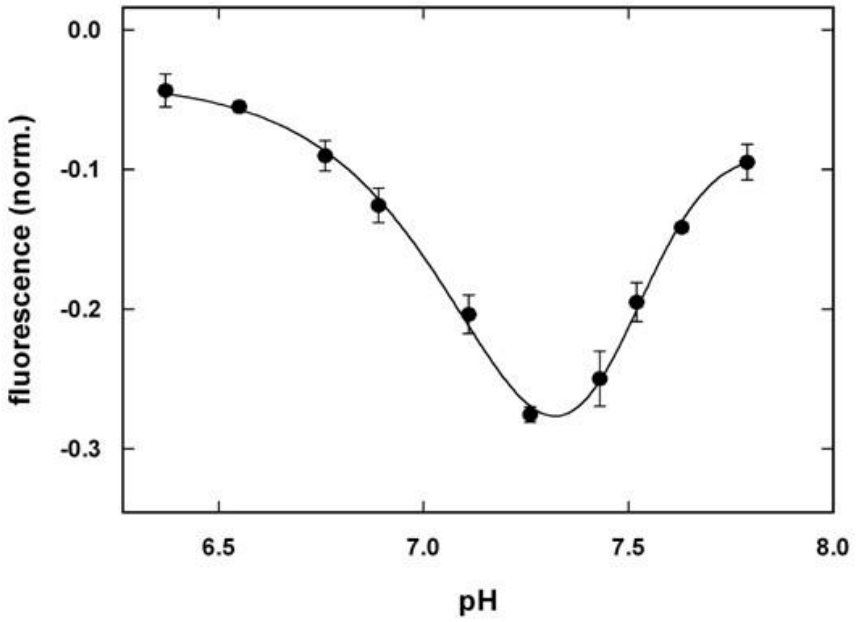

Figure 42. pH dependence of the steady-state fluorescence level obtained after addition of 2.5 mM ATP to vesicles with reconstituted KdpFABC and 140 mM K^+ inside and outside. Since there is a linear relation between the fluorescence level and the electric membrane potential, E_K (*Figure 39*), and at the steady-state condition $I_{pump} = I_{leak} = \lambda_{leak} \times E_K$, in consequence the pump current is proportional to the steady-state fluorescence level. The data were fitted with the sum of two Hill functions with pK_1 of 7.21 ± 0.02 and pK_2 7.50 ± 0.02.

When ATPase activity of detergent-solubilized KdpFABC was measured at different pH and in the absence of K^+ ions (*Figure 27B*, dashed line), a residual H^+-induced pump activity was observed. Therefore, a possible electrogenic H^+ transport of KdpFABC reconstituted in E. *coli* lipid vesicles was studied. KdpFABC-containing vesicles were prepared in absence of K^+, using only ultrapure chemicals and water, and no pH electrode was immersed in the solutions, in order to reduce K^+ contamination. Similar to the previously conducted experiments, 1 mL buffer containing 25 mM imidazole, 1 mM EDTA,

5 mM $MgSO_4$ at pH 7.2 was thermally equilibrated, followed by addition of an aliquot of proteoliposomes corresponding to 80 µg/mL and 300 nM $DiSC_3(V)$. Upon achieving a stable fluorescence signal, 2.5 mM Mg-ATP was added, triggering the KdpFABC pump activity. According to the results shown on *Figure 43A*, a minor fluorescence increase, in the order of ~5 %, was observed upon ATP addition, followed by an extremely slow fluorescence decrease. As previously mentioned, an increase of the fluorescence signal of the $DiSC_3(V)$ dye is a result of an uptake of positive charge inside the vesicles. Since no other cations are present in the solution, the obtained result indicates transfer of protons into the vesicles. As a result of this ATP-induced H^+ transport, the intravesicular protons concentration becomes higher than outside. This observation is confirmed by the subsequent addition of the uncoupler SF 6847 (*176*), that led to a drop of the fluorescence to a signal below the initial level, indicating an intravesicular negative potential as a result of H^+ export.

To exclude possible artifacts produced by Mg-ATP and the uncoupler SF 6847, control experiments were performed. The first experiment was performed in the absence of Mg^{2+} and by addition of Na_2-ATP instead of Mg-ATP. Under these conditions, KdpFABC could not be activated, since Mg^{2+} is an essential cofactor for enzyme phosphorylation. Therefore, no ion transport can occur. According to obtained result (*Figure 43B*), no fluorescence signal change was observed, confirming that no pump current was generated in the absence of Mg^{2+} in the solution, and that addition of ATP does not induce any fluorescence artifacts.

In the second control experiment, the addition of Mg-ATP and uncoupler SF 6847 was reversed (*Figure 43C*). The addition of 10 nM SF 6847 did not produce any significant fluorescence signal change, indicating that no pH gradient is present across the vesicle membrane. Subsequent addition of Mg-ATP induced no significant fluorescence change, as a consequence of vesicle membrane short-circuited for protons in the presence of the uncoupler SF 6847. The acquired results strongly indicate a limited ATP-induced H^+ uptake, resulting in an inside-positive potential, and a pH gradient produced by addition of the SF 6847. Interestingly, the direction of the proposed proton transfer would oppose that of K^+ pumping.

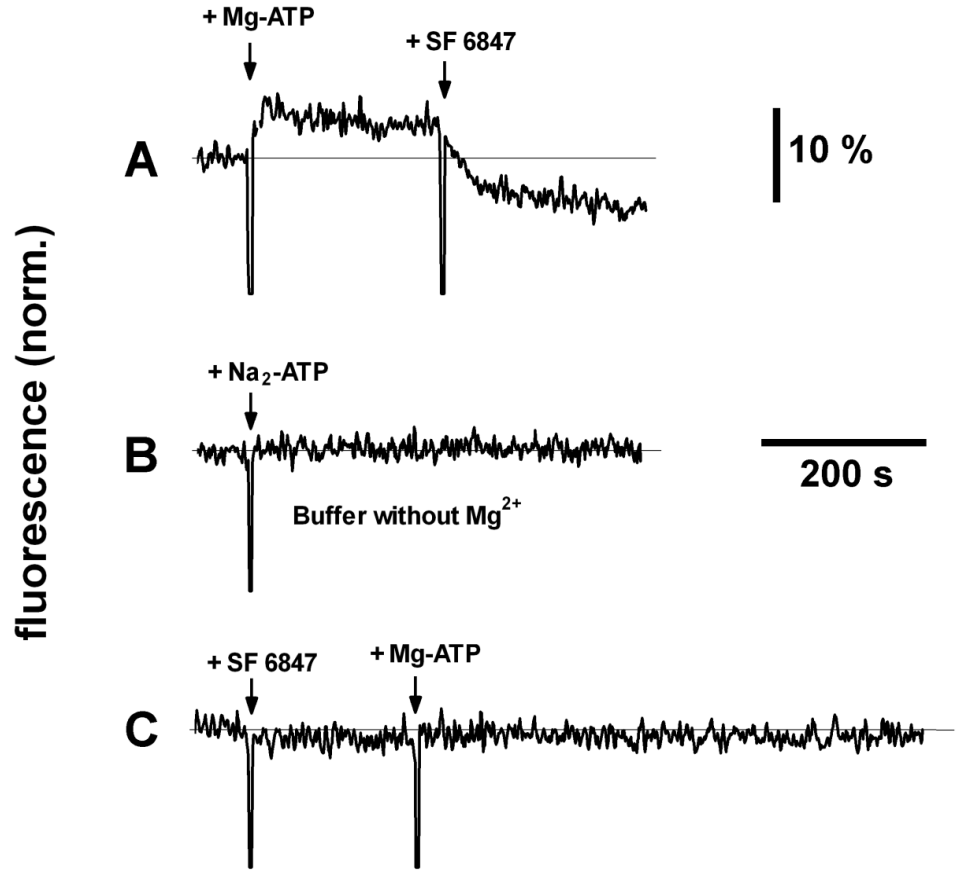

Figure 43. Proton transport in reconstituted KdpFABC vesicles prepared in the absence of K^+. **A:** Addition of 1 mM Mg-ATP produced a small fluorescence increase that was stabilized until 10 nM uncoupler SF 6847 was added, leading to a decrease of the fluorescence below the initial level. **B:** When in the absence of Mg^{2+}, 1 mM Na_2-ATP was added, no pump activity was possible and no fluorescence change could be detected. **C:** The initial addition of 10 nM uncoupler SF 6847 resulted in vesicle membranes short-circuited for protons. Subsequent addition of Mg-ATP induced no significant fluorescence change, thus, no ion transport occurred due to short-circuited membrane for protons.

3.4.4. Effect of extravesicular K^+ and Mg^{2+} concentrations on the pumping activity of the KdpFABC complex

The transport activity of reconstituted KdpFABC complex in E. *coli* lipid vesicles was investigated also with respect to different K^+ concentrations present in the external medium. Vesicles were prepared with 140 mM K^+ inside at pH 7.2, according to the previously described protocol. The external concentration of K^+ was varied in the range from 0.14 mM to 140 mM, and the only anion was sulfate. The ionic strength of the external solution was

kept constant by addition of $Tris^+$. Activation of the KdpFABC pump was induced by the addition of 1 mM Mg-ATP (pH adjusted) and the respective fluorescence decrease was a result of K^+ extrusion from the vesicles. Fluorescence changes were fitted with a mono-exponential function, and initial slope was calculated as the time derivative at $t \rightarrow 0$ (paragraph 2.5.3a.), a condition under which the depletion of the intravesicular K^+ concentration is not the limiting factor for the KdpFABC pumping and under the assumption that the vesicles are of uniform size. As already mentioned, the initial slope of the fluorescence signal change reflects the initial pump activity. In *Figure 44* calculated initial slopes were plotted as a function of the external K^+ concentration. From the obtained data, the initial pumping activity of the reconstituted KdpFABC complex decreases with increasing K^+ concentration of the external medium, indicating an inhibitory effect of the extravesicular (cytoplasmic) potassium concentration. The results were fitted with a Hill function and as a result an inhibition constant, $K_i(K^+)_{ex}$, is determined, as a concentration of the external K^+ at which the inhibition of the KdpFABC pumping activity is half-maximal. The obtained values are $K_i(K^+)_{ex}=(23 \pm 2)$ mM and a Hill coefficient of $n=1.5 \pm 0.2$. The similar inhibitory effect of K^+ was reported also in the case of Na^+,K^+-ATPase (*177*).

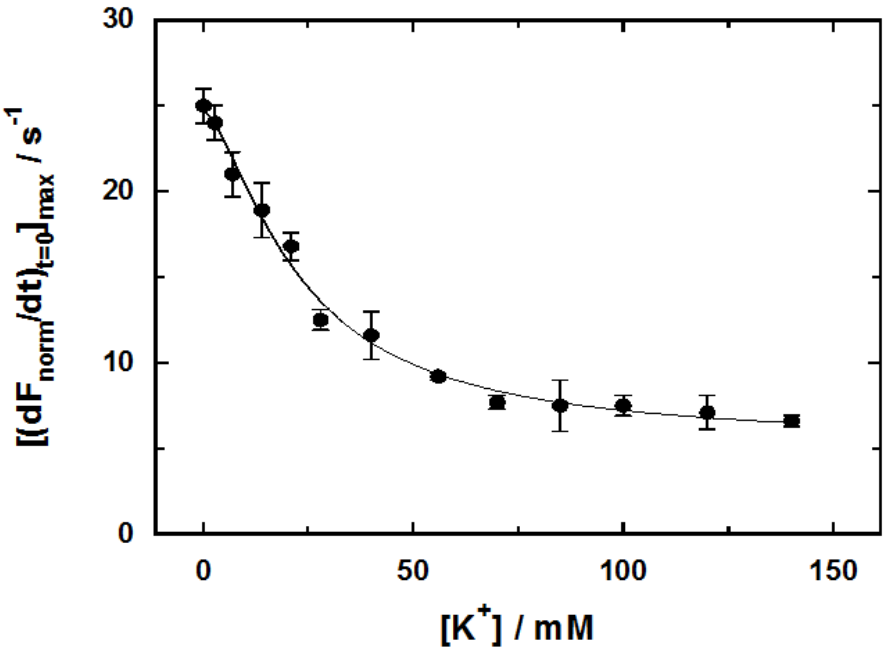

Figure 44. Initial slopes of the ATP-induced fluorescence decrease as a function of K^+ concentration present in the external medium. The initial slope reflects the KdpFABC pump activity. The intravesicular K^+ concentration was constant 140 mM at pH 7.2. The concentration dependence was fitted with a Hill function, with a $K_i(K^+_{ex}) =(23 \pm 2)$ mM and a Hill coefficient of $n = 1.5 \pm 0.2$.

In another set of experiments, the Mg^{2+} concentration was varied in the external medium. The magnesium ion acts as a cofactor required for the phosphorylation step and pumping activity. In the case of other P-type ATPases it was shown that it can be replaced by other divalent cations, although none acts as effective as magnesium. To investigate the effect of magnesium on the pumping activity of the reconstituted KdpFABC, vesicles were prepared in the buffer containing 25 mM imidazole, 1mM EDTA and 140 mM K^+ at pH 7.2. Buffer of the same content was used as external medium with different $MgSO_4$ concentrations between 0 and 20 mM. The pump activity was induced by addition of 1 mM Na_2-ATP (pH adjusted). In the absence of magnesium no pump activity was measured. The fluorescence decrease in the presence of respective Mg^{2+} concentrations was fitted with a mono-exponential function, and the pump activity reflected by the initial slope was determined as characteristic parameter. As mentioned previously, under this condition the decline of the intravesicular K^+ concentration was no limiting factor for the pump activity. The dependence of the initial pump current on the extravesicular magnesium concentration is shown in the *Figure 45*. It was fitted with a Hill function and the corresponding $K_{1/2}(Mg^{2+})$ was found to be (1.73 ± 0.05) mM. The presented results reveal that the pumping activity of the reconstituted KdpFABC increased with increasing Mg^{2+} concentration up to 20 mM. The obtained half-saturating constant of 1.73 mM is almost three time higher than the value reported in the case of the Na^+,K^+-ATPase (*177*).

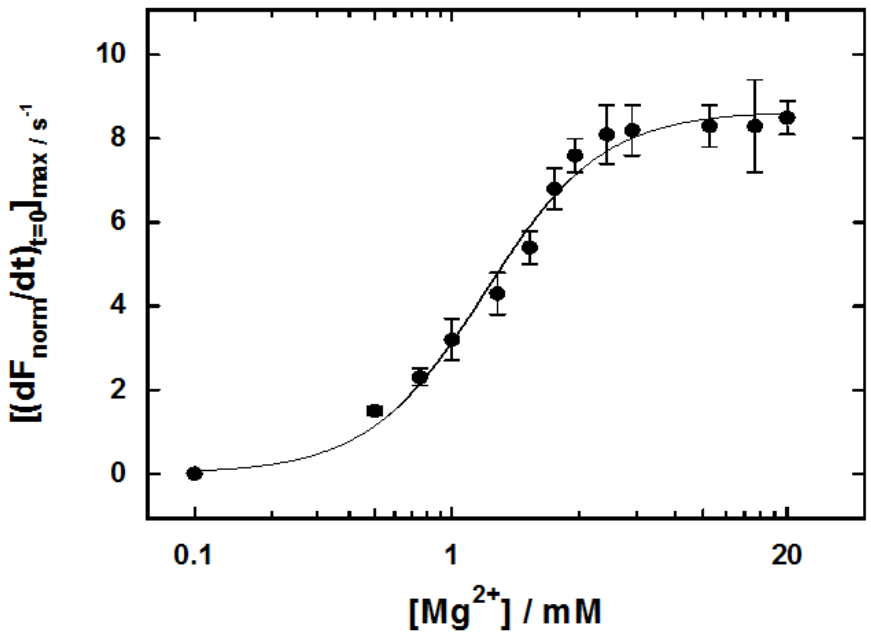

Figure 45. Calculated initial slopes, reflecting the initial KdpFABC pump activity, as a function of external Mg^{2+} concentration at pH 7.2. The K^+ concentration of 140 mM was the same inside and outside of the vesicles. The data were fitted with a Hill function, providing the $K_{1/2}(Mg^{2+})$ of (1.73 ± 0.05) mM.

3.4.5. Effect of ADP and inorganic phosphate on the pumping activity of the KdpFABC complex

KdpFABC transports K^+ ions across the membrane utilizing the energy released during the enzymatic ATP hydrolysis performed the KdpB subunit. The actual value of the Gibbs energy for ATP varies, and under normal physiological conditions has the value close to -50 kJ/mol. Products of ATP hydrolysis, ADP and inorganic phosphate, P_i, should affect the KdpFABC pumping process. Besides the direct competition at the ATP binding site, the presence of ADP in the medium may also reverse the phosphorylation step, thus decreasing the turnover rate of the KdpFABC. In the same manner, inorganic phosphate may affect the turnover rate by slowing the dephosphorylation step by shifting the equilibrium toward the E_2-P state. In order to investigate the effects of the ADP and P_i on the K^+ transport, KdpFABC was reconstituted into E. *coli* lipid vesicles, with 140 mM K^+ inside and outside of the vesicles. All other conditions were the same as in the previous preparations. Starting with 1 mL buffer containing 25 mM imidazole, 1 mM EDTA, 5mM $MgSO_4$ (pH 7.2), an aliquot of vesicles corresponding to the 80 µg lipids/mL and 300 nM $DiSC_3(V)$ were added. After achieving a stable fluorescence signal, different aliquots of concentrated stock-solutions of ADP or P_i were added, followed by the addition of 1 mM Mg-ATP (pH adjusted). Upon KdpFABC activation by ATP, the fluorescence signal decreased to a new steady-state state. Corresponding time-depended fluorescence traces of ATP-driven K^+ extrusion at different ADP concentrations in the external medium are shown in *Figure 46.*

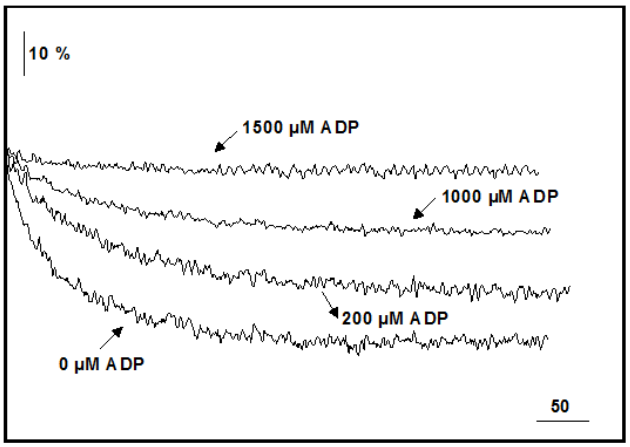

Figure 46. ATP-induced K^+ transport at different ADP concentrations in the external medium. The K^+ concentration was 140 mM (inside an outside of the vesicles), pH 7.2. Addition of ADP prior ATP addition did not produce significant fluorescence change. The maximal fluorescence decrease shows clear decrease with increasing ADP concentration.

The calculated half-maximal inhibiting concentrations of ADP and P_i were K_i (134 ± 15) µM and K_i (268 ± 35) µM, and Hill coefficients 0.84 ± 0.11 and 0.63 ± 0.05, respectively (*Figure 47*). The amplitudes of the fluorescence decrease upon ATP-activation decreased with increasing both ADP and P_i concentrations (*Figure 46*, in the case of ADP). Respective concentrations in case of the Na^+,K^+-ATPase previously reported were 80 -100 µM for ADP and 14 mM for P_i inhibition (*178*). In comparison with the results obtained for the KdpFABC it was found that the kinetics of inhibition seems to be similar for ADP, since the half-maximal inhibitory concentration are in the same order of magnitude. On the other hand, whereas inhibition of Na^+,K^+-ATPase by inorganic phosphate was found to be only weak, a much stronger inhibitory effect was observed for the KdpFABC complex.

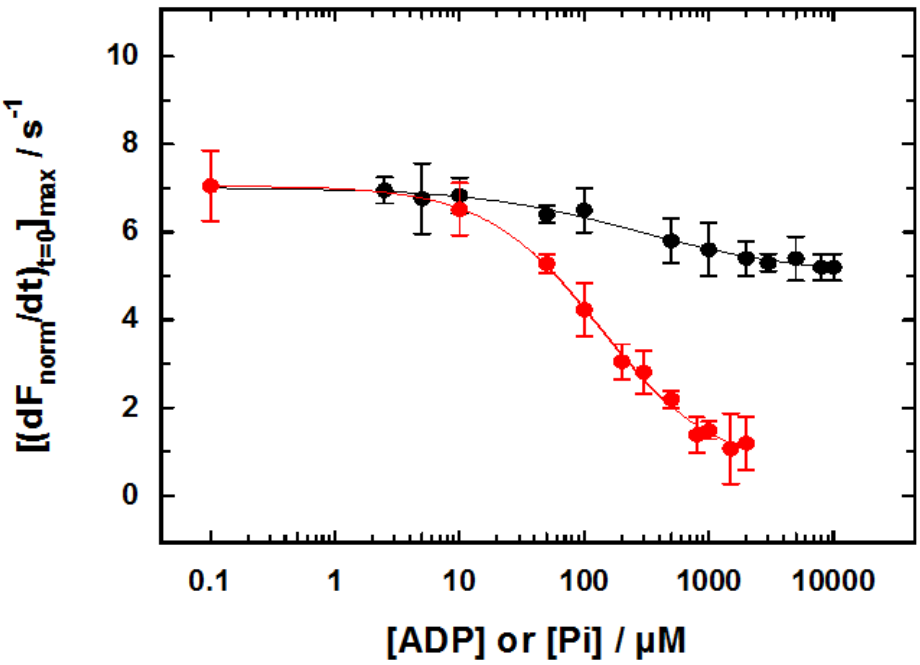

Figure 47. Initial slope $[(dF_{norm}/dt)_{t=0}]_{max}$ as a function of ADP (in red) and P_i (in black). The ATP concentration was 1 mM, whereas internal and external K^+ concentration was 140 mM. Data were fitted with a Hill function, with K_i(ADP) of (134 ± 15) µM and a Hill coefficient of 0.84 ± 0.11, and $K_i(P_i)$ of (268 ± 35) µM and a Hill coefficient of 0.63 ± 0.05.

3.5. KdpFABC activity inhibition by *o*-vanadate

It is long known that a phosphate-analogue, *o*-vanadate, acts as a specific inhibitor of the P-type ATPases (*179;180*). Vanadate binds to the E_2 state of the enzymatic reaction cycle, thereby mimicking the E_2-P transition state, as shown in the simplified reaction scheme of the KdpFABC (*Figure 48*). Sensitivity to *o*-vanadate indicates that the pump is capable of performing a full reaction cycle with respective $E_1 \rightarrow E_2$ transition. The specific inhibition of enzymatic and therefore also of the transport activity of KdpFABC by *o*-vanadate was tested both with detergent-solubilized complex with β-DDM and reconstituted KdpFABC into E. *coli* vesicles.

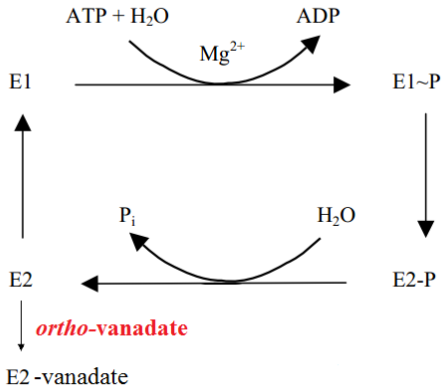

Figure 48. Simplified scheme of the enzymatic KdpFABC reaction cycle, with *o*-vanadate inhibition shown in red.

The first set of experiments consisted of the malachite green ATPase assay of detergent-solubilized enzyme in Aminoxide WS-35 in the presence of different *o*-vanadate concentration ranging from 0 to 1 mM, whereas the ATP concentration was constant 0.67 mM (*Figure 49A*). For each *o*-vanadate concentration three different measurements were performed and the average activity was calculated, while the error is given as s.e.m. The concentration dependence of the activity was fitted by a Hill function, with a K_i of (0.98 ± 0.12) µM, corresponding to the half-maximal activity inhibition, and a Hill coefficient was 1.2 ± 0.2. The enzyme activity of the detergent-solubilized KdpFABC in DDM was 0.55 µmol P_i mg^{-1} min^{-1} in the presence of 0.1 µM *o*-vanadate, revealing activity loss of approximately 50 %.

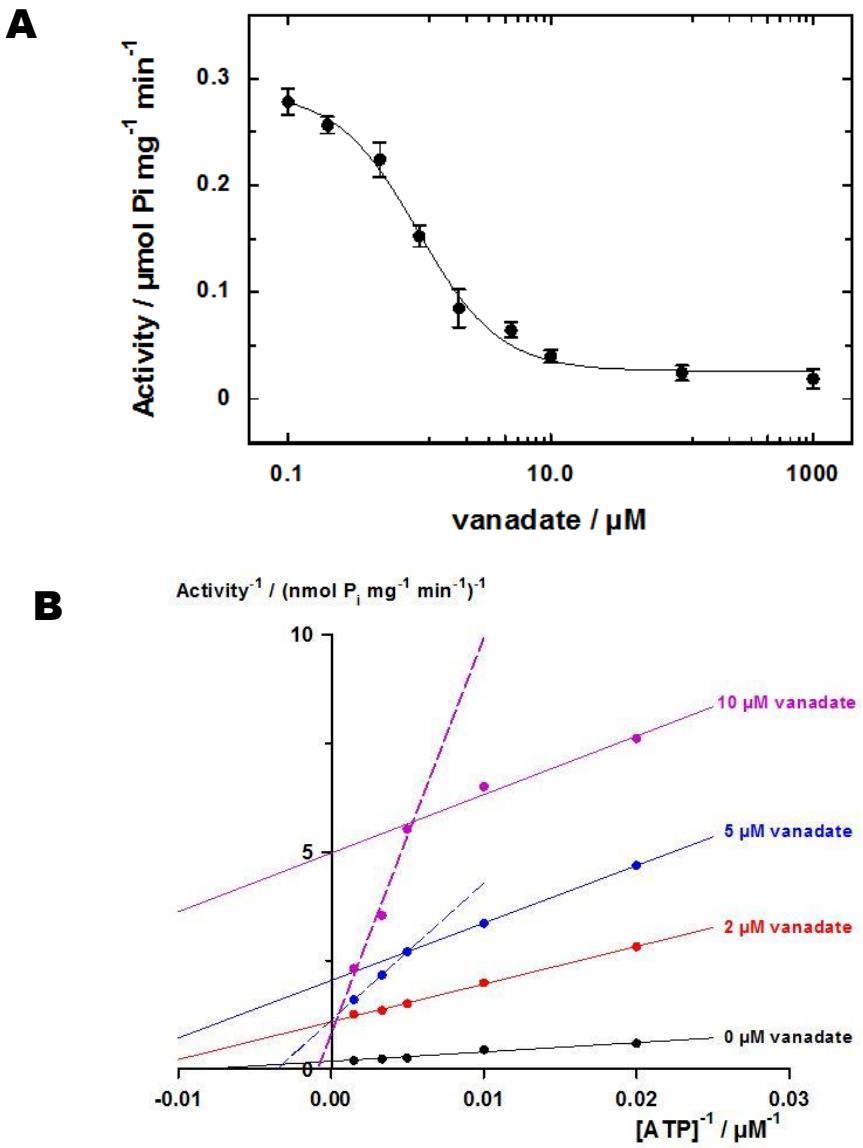

Figure 49. Inhibition of ATPase activity of β-DDM-solubilized KdpFABC by *o*-vanadate. **A:** Malachite green activity assay preformed at different *o*-vanadate concentrations. Data were fitted with a Hill function and respective half-maximal inhibitory concentration K_i of (0.98 ± 0.12) µM. **B:** Lineweaver-Burk plot of ATP-dependent KdpFABC activity at different *o*-vanadate concentrations. From the interception of the respective regression curves, a complex kinetics of inhibition by *o*-vanadate is indicated. At high ATP concentration, a mechanism corresponds to a competitive binding, whereas at low ATP concentrations, a "partial" uncompetitive kinetics is indicated.

In the second set of experiments, the inhibition kinetics of *o*-vanadate towards the ATP hydrolysis was investigated. The malachite green assay experiments were performed in the presence of different *o*-vanadate concentrations, 0, 2, 5 and 10 µM, and the ATP hydrolysis was measured when the ATP concentration was varied between 0 and saturating 667 µM. All other conditions were kept identical to the protocol described previously. From the

obtained data, a competition between ATP and *o*-vanadate was analyzed using a Lineweaver-Burk plot (*Figure 49B*). Reciprocal values of measured ATPase activity were plotted against the reciprocal ATP concentration for all four *o*-vanadate concentrations used. The obtained results indicated a complex inhibition of ATP hydrolysis by *o*-vanadate. However, at lower ATP concentrations, the linearly fitted curves for different *o*-vanadate concentrations indicate a behavior similar to an uncompetitive binding kinetics. The true uncompetitive binding kinetics, however, is not completely certain, since the regression curves are not absolutely parallel. The consideration of "partial" uncompetitive binding kinetics would mean that *o*-vanadate binds only to the enzyme-substrate complex, to some extent. At higher ATP concentration, the regression lines intercept on the y axis, suggesting competitive binding kinetics between ATP and *o*-vanadate, thereby binding of an inhibitor to the active binding site of the KdpFABC prevents binding of the ATP.

The inhibitory effect of the *o*-vanadate was also tested in the case of KdpFABC reconstituted into E. *coli* lipid vesicles. The malachite-green ATPase activity assay was performed with the modifications described previously. The concentration of *o*-vanadate was varied between 0 and 5 mM, while the ATP concentration was 0.67 mM. The experiments at each *o*-vanadate concentration were performed in triplicate, and the average ATPase activity was calculated. Obtained results were fitted with a Hill function, shown in a *Figure 50A*, with a K_i of (62 ± 6) μM and a Hill coefficient n of 0.77 ± 0.05. The malachite green assay experiments were also performed in the presence of different *o*-vanadate concentrations, 0, 10 and 100 μM, and the ATP hydrolysis was measured when the ATP concentration was varied between 0 and saturating 667 μM. All other conditions were kept identical to the protocol described previously. From the obtained data, a competition between ATP and *o*-vanadate was analyzed using a Lineweaver-Burk plot (*Figure 50B*). Reciprocal values of measured ATPase activity were plotted against the reciprocal ATP concentration for all four *o*-vanadate concentrations used. The obtained results suggest simpler inhibition kinetics than one found in the case of detergent-solubilized KdpFABC. In this case, a true uncompetitive inhibition is indicated, which means that *o*-vanadate binds to the enzyme-substrate complex. The fraction of the competitive binding kinetics indicated for detergent-solubilized KdpFABC at ATP concentration higher than 0.1 mM (*Figure 49B*) was not observed in the case of reconstituted KdpFABC. A possible explanation for this finding could be a lower sensitivity of the reconstituted KdpFABC, thus the contribution of the competitive inhibition of *o*-vanadate toward ATP hydrolysis is decreased or even lost.

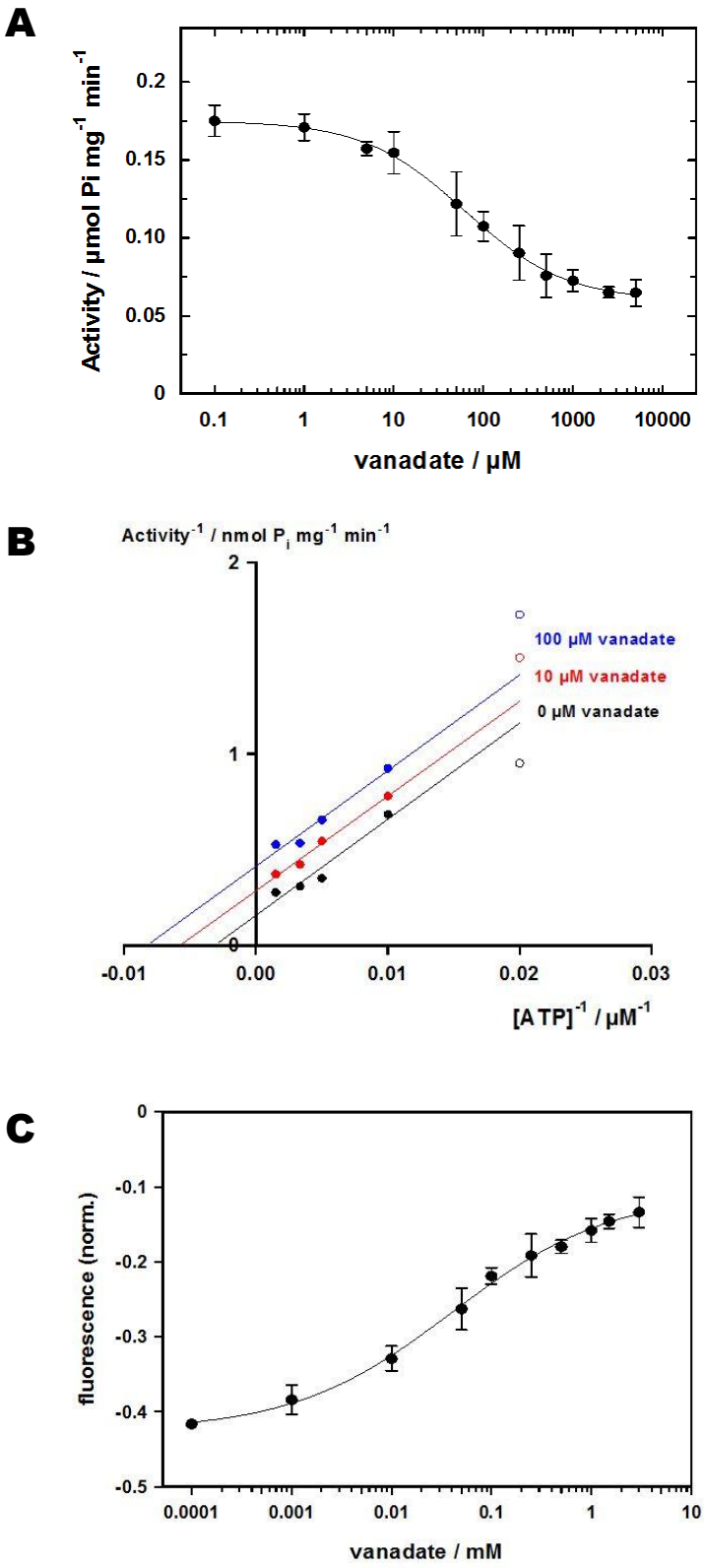

Figure 50. Inhibition of the ATPase activity of reconstituted KdpFABC into E. *coli* lipid vesicles by *o*-vanadate. **A:** The malachite green activity assay preformed at different *o*-vanadate concentrations. The data were fitted with a Hill function and the respective half-maximal inhibitory concentration K_i was (62 ± 6) µM. **B:** Lineweaver-Burk plot of ATP-dependent KdpFABC activity at different *o*-vanadate concentrations. Interception of the respective regression curves indicates an uncompetitive binding kinetics. **C:** Fluorescence increase upon addition *o*-vanadate in small aliquots. The data were fitted with a Hill function and a K_i of (40 ± 7) µM was determined.

Another approach to investigate the inhibitory effect of *o*-vanadate was carried out using the $DiSC_3(V)$ and the reconstituted KdpFABC complex. Vesicles were formed according to the protocol (2.4), with potassium concentrations of 140 mM inside and outside. Starting with 1 mL buffer, containing 25 mM imidazole,1 mM EDTA and 5 mM $MgSO_4$ (pH 7.2), an aliquot of vesicles corresponding to the 80 µg lipid/mL and 300 nM dye were added. After achieving a stable signal, 1 mM Mg-ATP was added, inducing K^+ export. When a stable fluorescence was reached, aliquots of *o*-vanadate stock-solution were added, resulting in the fluorescence signal increase to a new steady-state. Amplitudes of normalized fluorescence signal changes were plotted against respective *o*-vanadate concentrations (*Figure 50C*). Data were fitted with a Hill function with a concentration corresponding to the half-maximal inhibition K_i of (40 ± 7) µM. Calculated values suggest that reconstituted KdpFABC is only partially sensitive in comparison to detergent-solubilized complex.

3.6. Temperature dependence of the KdpFABC activity

Beside structural and kinetics properties, another important aspect in understanding of the ion transport performed by ion pumps is the energetics of the transport. One approach to gain insight into the energetics of the KdpFABC is the temperature dependence of enzymatic and transport function. The malachite green activity assay of the β-DDM-solubilized KdpFABC was performed at different temperatures in order to determine the activation energy under turnover conditions. The assay was performed according to the modified protocol, and the samples were incubated at temperatures between 6 °C and 40 °C for 30 minutes. At higher temperatures (>40 °C) measured activity showed decrease, probably due to denaturation of the KdpFABC complex and consequently a loss of activity. For each temperature three measurements were performed and the average ATPase activity was calculated. The ATPase activity was plotted against the respective temperature, exhibiting exponential dependence (*Figure 51A*). For calculation of the activation energy, the logarithmic activity, ln A, was plotted against reciprocal temperature, according to the Arrhenius equation (*Figure 51B*). Data were fitted with linear regression and provided an activation energy of E_a = (55 ± 1) kJ/mol.

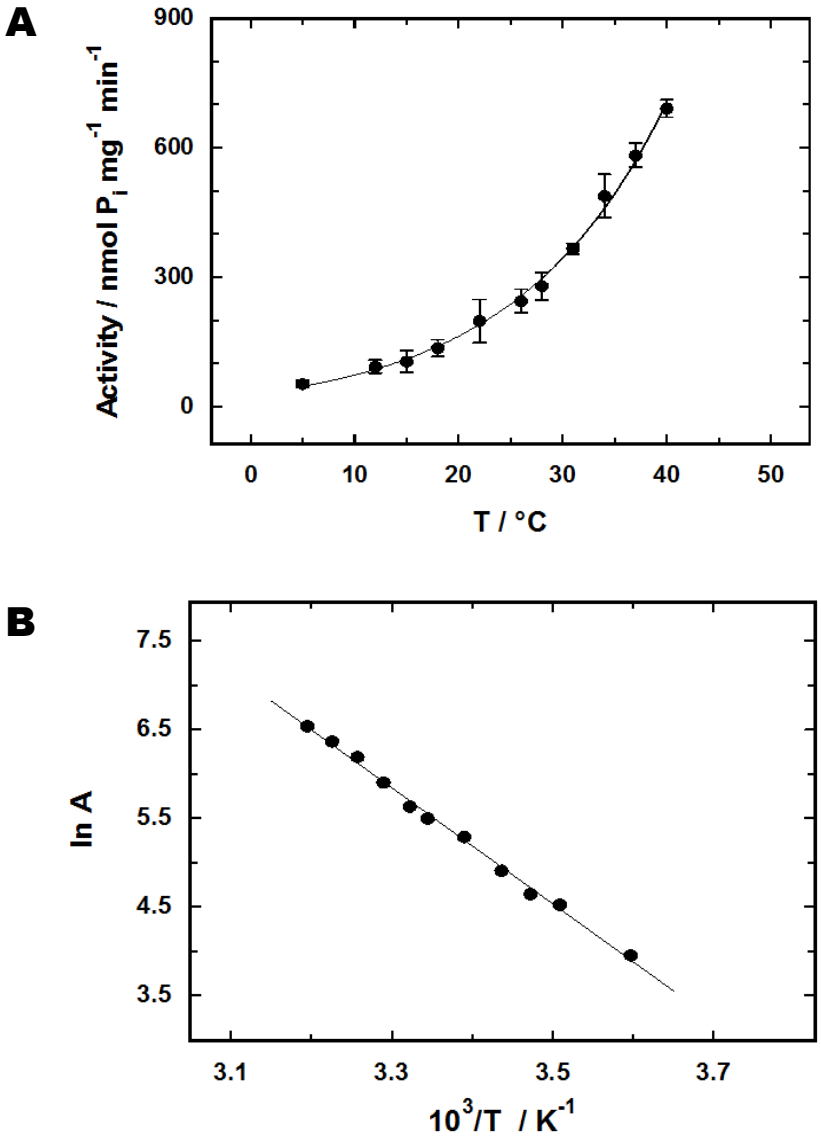

Figure 51. ATPase activity of detergent-solubilized KdpFABC in β-DDM at different temperatures. **A:** Exponential profile of the temperature-dependent ATPase activity measured by the malachite green assay. **B:** Temperature dependent ATPase activity represented as Arrhenius plot. The calculated activation energy was (55 ± 1) kJ/mol.

To determine the activation energy of ATP-driven K^+ transport across the membrane, fluorescence measurements with $DiSC_3(V)$ were carried out at various temperatures. Vesicles were prepared according to the previously described protocol, containing 140 mM K^+. The thermostated cuvette was filled with 1 mL buffer containing 25 mM imidazole, 1 mM EDTA and 5 mM $MgSO_4$ (pH 7.2), followed by the addition of an aliquot of vesicles and 300 nM dye. Upon the subsequent addition of 1 mM Mg-ATP, the fluorescence signal

decreased, finally achieving a new steady-state. The temperature was set between 9 °C and 40 °C, and for each temperature 3 experiments were performed, and the average fluorescence decrease was calculated. The ATP-induced fluorescence decrease was fitted with a mono-exponential function, enabling calculation of the initial slope. The initial slope was proportional to the initial KdpFABC-pump activity, and it was plotted against respective temperature (*Figure 52A*). Since the data exhibited a typical exponential profile, they were further evaluated as Arrhenius plot (*Figure 52B*), with the y axis representing the logarithm of the initial slopes, ln k, and the x axis representing the reciprocal values of the temperatures. The calculated activation energy was (111 ± 5) kJ/mol.

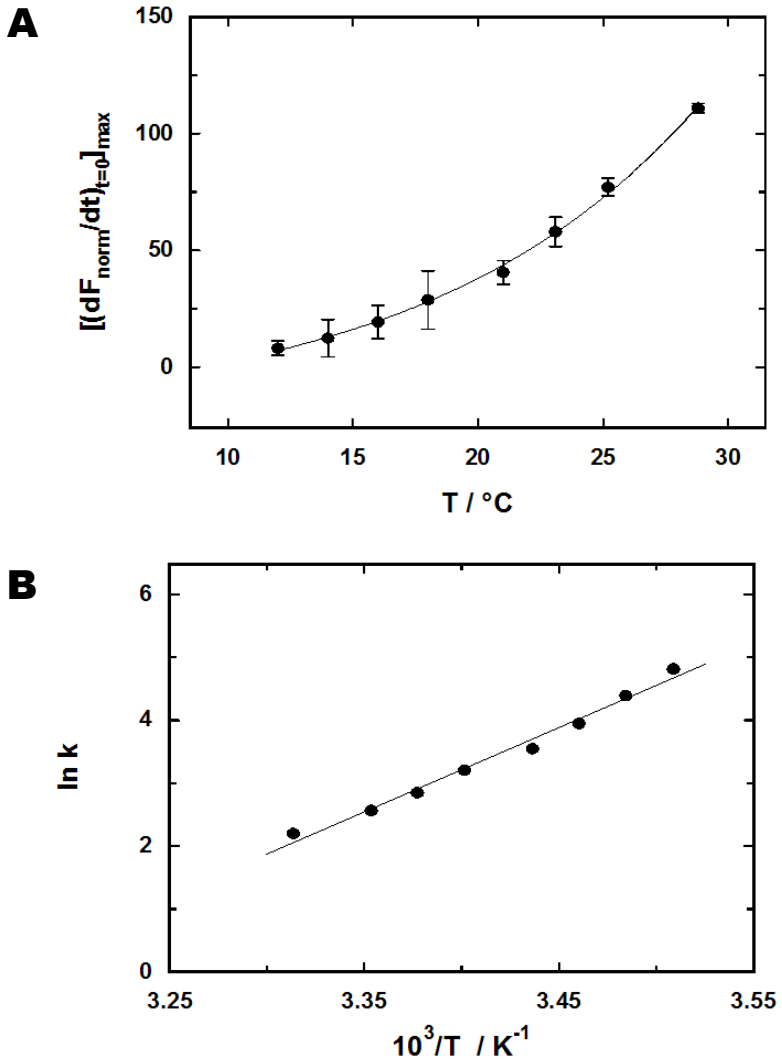

Figure 52. Temperature dependence of K^+ pumping activity of the reconstituted KdpFABC complex in E. *coli* lipid vesicles. **A:** A typical exponential dependence of initial pump activity, represented by the initial slope as function of the temperature. **B:** Temperature dependence of K^+ extrusion on temperature represented as Arrhenius plot. The calculated activation energy was (111 ± 5) kJ/mol.

3.7. Time-resolved kinetics experiments with detergent-solubilized KdpFABC

To gain more insight into the kinetics of the reaction steps of the KdpFABC pump cycle, various experiments using caged ATP and RH421 fluorescence dye were carried out. The first set of experiments was performed at a saturating concentration of caged ATP and various KCl concentrations in the buffer. Under these conditions, the conformational change E_1-P → P-E_2 is assumed to be the rate-determining step of the ATP-induced reaction sequence. After photochemical release of ATP, a fluorescence decrease was observed as a result of K^+ binding to the solubilized KdpFABC complex. All experiments were performed at least 3 times, and the average fluorescence decrease was calculated. The fluorescence decrease was fitted with a mono-exponential function, and the obtained time constants, τ, were plotted against the respective K^+ concentrations (*Figure 53*). The time constant did not change significantly with the K^+ concentration that was varied by a factor of 10^4. The average value was found to be (592 ± 23) ms. Important to note is that the determined time constant is by a factor of 100 greater than the one of the ATP-release reaction (2.5.2b.), and therefore hardly affected by the caged ATP photo-dissociation process.

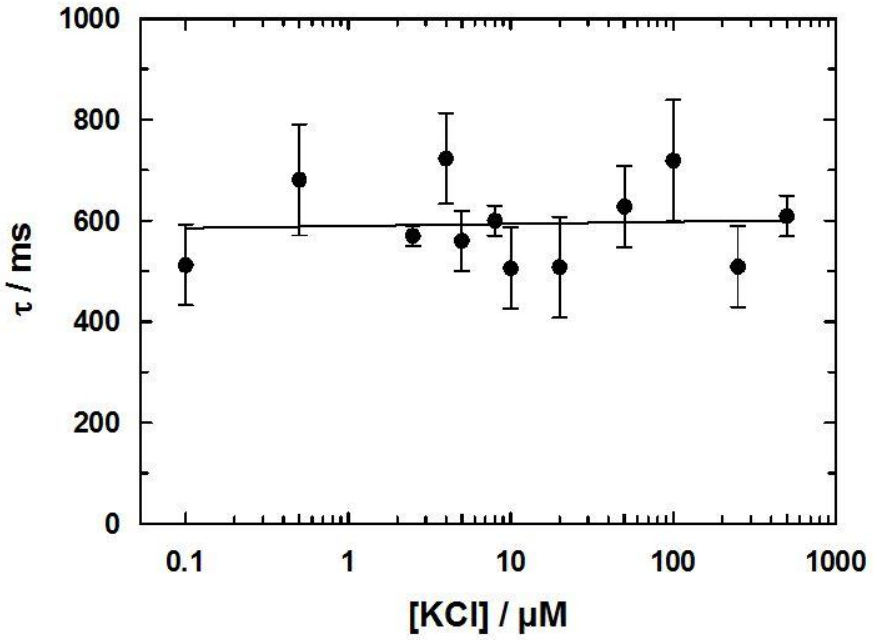

Figure 53. Dependence of the time constant, τ, of the fluorescence decrease upon photorelease of ATP as a function of K^+ concentration, at pH 7.8 and 25 °C. The line through the data is a linear fit, indicating the absence of a significant K^+ dependence.

Another parameter determined from these experiments is the ratio between the amplitude of the fluorescence signal decrease and the time constant, A / τ, reflecting the fraction of the solubilized KdpFABC complexes activated by the photochemically released ATP (2.5.2b.). Ratios were plotted against KCl concentrations and were fitted with a Hill function, providing a half-saturating K^+ concentration, $K_{1/2}$, of (5.27 ± 0.24) µM and a Hill coefficient of 2.3 ± 0.2, as shown in *Figure 54*.

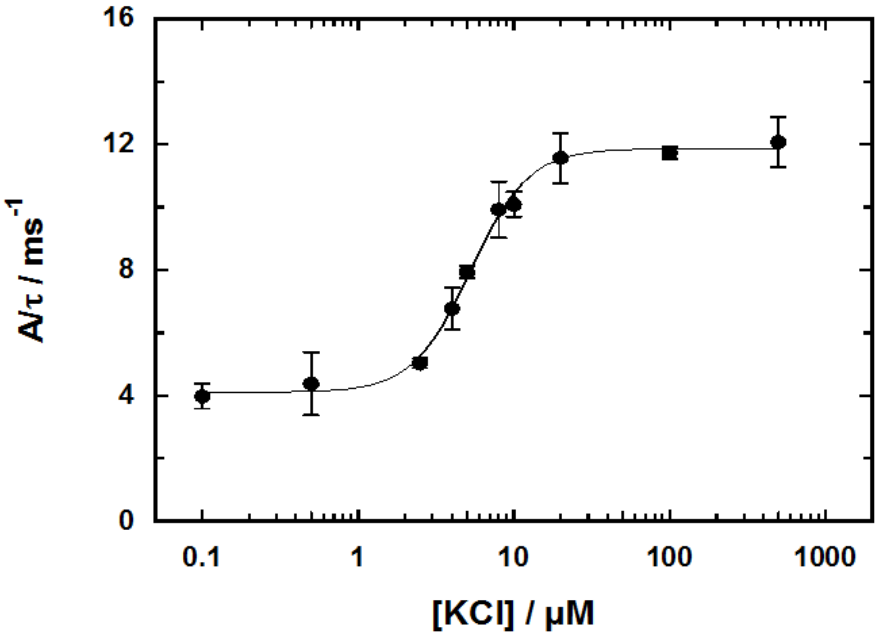

Figure 54. Dependence of the ratio between the amplitude of the fluorescence signal decrease, A, and respective time constant, τ, obtained from the fit of the fluorescence decrease by a mono-exponential function, at pH 7.8 and 25 °C. The concentration dependence was fitted with a Hill function with $K_{1/2}$ of (5.27 ± 0.24) µM and n 2.3 ± 0.2.

The second set of experiments was performed at different pH, in the absence and presence of saturating 100 µM K^+, and saturating concentration of caged ATP. All experiments were performed at least 3 times, and the average fluorescence decrease was calculated. The fluorescence decrease was fitted with a mono-exponential function, and the obtained rate constants, k = 1 / τ, were plotted against the respective pH (*Figure 55*). pH-dependance of determined time constant in the absence of K^+ was fitted by the sum of two Hill functions, with corresponding pK_1 of 7.41 ± 0.01 (n = 6.1 ± 0.5) and pK_2 of 6.98 ± 0.01 (n = 4.2 ± 0.4). The highest rate constant was found to be at pH ~7.2. The results obtained in the presence of saturating K^+, could be fitted with a single Hill function with a pK of 6.70 ± 0.10 and a Hill coefficient of n = 2.0 ± 1.0.

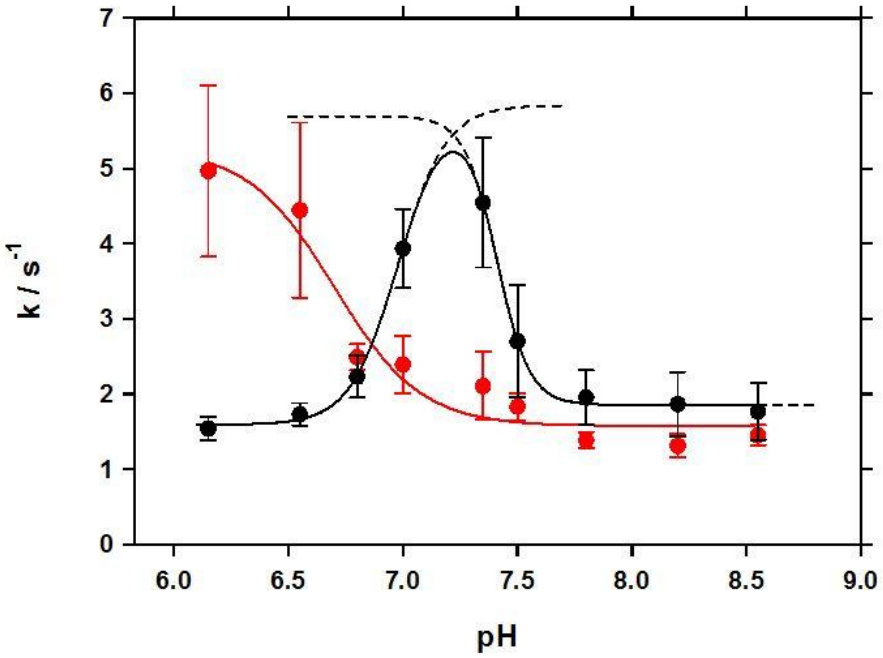

Figure 55. pH-dependence of the rate constant, k, of the fluorescence decrease upon photorelease of ATP, in the absence (black) and in the presence of 100 µM K^+ (red). The results of the pH-dependance in the absence of K^+ were fitted by the sum of two Hill functions with pK_1 of 7.41 ± 0.01 (n = 6.1 ± 0.5), and pK_2 of 6.98 ± 0.01 (n = 4.2 ± 0.4). The obtained results in the presence of 100 µM K^+ were fitted with a Hill function with pK of 6.7 ±0.1 (n = 2.0 ± 1.0).

To evaluate the real effect of H^+ on the rate constant of the conformational transition of KdpFABC, a possible artifact produced by the pH-dependent ATP-release should be discussed. ATP-release kinetics is given by the equation:

$$[ATP] = \theta \cdot [\text{caged ATP}] \cdot (1 - e^{-\lambda t}) \qquad \text{(Eq. 12)}$$

where [caged ATP] and [ATP] are concentrations of caged ATP and released ATP, respectively, θ is a quantum yield of the photo reaction, t is time, and λ is a characteristic parameter of ATP-release process, described as (*181-183*):

$$\lambda = 2.2 \cdot 10^{9} \cdot 10^{-pH} \qquad \text{(Eq. 13)}$$

The time constant (in milliseconds) of the ATP-release process can be calculated according to:

$$\tau = 1 / \lambda = 4.55 \cdot 10^{-7} \cdot 10^{pH} \qquad \text{(Eq. 14)}$$

The ATP-release time constants are 0.455 ms (pH 6), 4.55 ms (pH 7) and 45.5 ms (pH 8). The time constant of the conformational transition is in the order of 700 ms at pH 8 (*Figure 55*), which is (in the worst case) ~15 times higher than that of ATP-release process at pH 8. Therefore, an effect of the pH-dependent ATP-release kinetics on the conformational

transition process of KdpFABC may be neglected in the pH range covered in the experiments.

As previously mentioned, at saturating ATP concentrations, ATP-binding and KdpFABC phosphorylation are faster than the conformational transition. At non-saturating ATP concentrations, however, ATP-binding becomes rate-limiting process. The time constant of the fluorescence decrease under this condition reflects the rate of the ATP-binding reaction. In the next set of experiments, the apparent ATP-binding concentration of the solubilized KdpFABC was determined, in the presence of saturating 100 µM KCl at pH 7.8, and various concentrations of caged ATP between 1 and 400 µM. The luciferin-luciferase assay was used to determine concentration of released ATP, and the calibration curve is given as the inset in *Figure 56*. The fluorescence decreases were fitted with a mono-exponential function, and time constants were plotted against the concentration of photochemically released ATP upon single laser pulse (*Figure 56*).

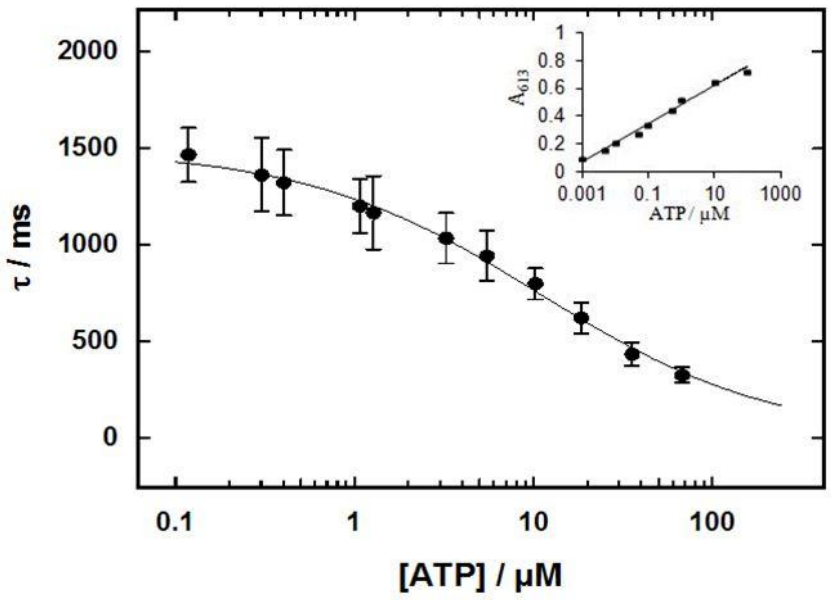

Figure 56. Concentration dependence of ATP binding with detergent-solubilized KdpFABC in Aminoxide WS-35. The RH421 method was used to determine the concentration dependence relaxation-time constant, τ, of the fluorescence decrease. The calibration curve obtained with luciferin-luciferase assay is given as the inset, showing a linear dependence in the ATP concentration range between 0.001 and 100 µM. The apparent ATP-binding constant was determined to be (59 ± 3) µM and a Hill coefficient of 0.66 ± 0.05.

The ATP-binding constant was determined using a Hill fit, and it was found to be (59 ± 3) µM with a Hill coefficient of 0.66 ± 0.05. A problem encountered in these measurements was that the upper limit of the caged ATP concentration used was 400 µM, and higher concentrations were avoided because of possible artifacts caused by the high absorption of the caged ATP in the solution that prevented a homogeneous illumination and therefore a homogeneous release of ATP. Moreover, the inhibition constant of caged ATP for the KdpFABC complex was determined previously with electrical experiments and found to be 630 µM (*99*), in the presence of saturating K^+ concentration, indicating that caged ATP acts as a weak competitive inhibitor of ATP binding.

4. DISCUSSION

The KdpFABC complex of E. *coli*, a member of P-type ATPase superfamily, is a high affinity potassium uptake system, expressed as an emergency transport system under potassium-limiting conditions. Only the largest KdpB subunit exhibits an explicit homology to other P-type ATPases and represents the catalytic subunit that performs ATP hydrolysis, whereas the KdpA subunit binds and transports K^+ and shows similarities to KcsA-like K^+-channels. The essential function of P-type ATPases consists of coupling between the energy-releasing ATP hydrolysis and the energy-consuming ion transport across membranes. The ion transport process is performed by enzyme phosphorylation and dephosphorylation, followed by sequential substrate binding or release, as summarized in Post-Albers scheme (*Figure 6*). In this project, the ultimate goal was to characterize the mechanistic aspect of the KdpFABC pump cycle. To obtain such functional information on the molecular mechanism of KdpFABC complex, several questions were addressed. First, the nature of the ion-binding partial reactions of the pump cycle of the detergent-solubilized KdpFABC was investigated. For this purpose a fluorescence technique was employed that is based on the voltage-sensitive dye RH421. It enables monitoring of ion movements in the membrane domain of the KdpFABC complex. Based on this method, the electrogenicity of H^+ and K^+ binding was investigated, in unphosphorylated E_1 and phosphorylated E_2-P conformation, the latter achieved by addition of either ATP or inorganic phosphate, P_i. K^+-binding titrations were carried out under different conditions, to examine the effects of H^+ and Mg^{2+} in the electrolyte. To compare the transport and the enzyme activity, the dependence of ATP hydrolysis on the proton concentration was measured. The data available from a few well-studied members of the family, such as Na^+,K^+-ATPase and SR Ca^{2+}-ATPase, strongly suggest that countertransport is essential for all P-type ATPases (*184*). Secondly, the KdpFABC was reconstituted in E. *coli* lipid vesicles, and the electrogenic pump activity was studied using the fluorescent potential indicator $DiSC_3(V)$. With this approach, the proposed proton transport was investigated. Effects of different substrates/inhibitors on the ATP-induced K^+ export were studied. In the third part, time-resolved experiments with detergent-solubilized KdpFABC were carried out, providing additional kinetic information about the reaction cycle. The obtained results will finally allow us to build-up an appropriate Post-Albers model for the KdpFABC pump cycle.

ATPase activity and RH421 experiments with detergent-solubilized KdpFABC

The initial step of this study was to identify the most appropriate detergent which preserves functional integrity of the KdpFABC complex upon its solubilization and purification. In total, six different detergents were tested to obtain protein/detergent complexes with biochemical properties as close to the physiological state as possible. The obtained results (*Table 2*) revealed that only an unspecified mixture of detergents, Aminoxide WS-35, provided a functional complex with a $K_{1/2}(K^+)$ of 6.5 µM that is in the same order as previously reported values for the ion pump in its native environment. The KdpFABC complex purified with other detergents, which are commonly used for the purification of various other membrane proteins, resulted in both lower ATPase activities and K^+-binding affinities, the latter more significantly affected. Furthermore, the major component in this mixture, 3-Laurylamido-N,N'-dimethylpropyl amine oxide (LAPAO), alone was not sufficient to preserve the functional properties of the KdpFABC. Although the enzyme activity was found to be close to one obtained with Aminoxide WS-35, the K^+-binding affinity was lower by a factor of 20. This observation suggests that a minor, not yet identified component present in the Aminoxide WS-35 detergent mixture is crucial for proper enzyme function, possibly playing the role of a functional lipid. A similar finding has been determined for the Na^+,K^+-ATPase to which a functional PS lipid is bound to support a stable structure of the functional ion pump (*172*). Mass-spectrometric analyses are underway to identify the specific component(s) and the mechanism by which they stabilize the functional KdpFABC complex. According to the results summarized in *Table 2*, the effect of the detergents is much lower on the overall enzyme activity (a factor of ~8.5 comparing activities in the presence of Fos-choline 12 and Aminoxide WS-35), than on the K^+-binding affinity (the corresponding factor is ~2300). This means that obviously the structure of the ion-binding site of the KdpA subunit inside the membrane is more severely affected by the detergent/lipid environment, than the enzymatic function in KdpB which is located in the cytoplasmic part of the subunit. In addition, the coupling mechanism between the KdpB and KdpA must be also affected, since the induction factor (which may be interpreted as a measure of coupling between ATP hydrolysis in KdpB and ion binding and transport in KdpA) differs by a factor of ~4 between Fos-choline 12 and Aminoxide WS-35. Coupling is also assumed to occur inside the membrane domain. On the other hand, the lower induction factor, F_{ind}, in Fos-choline 12 indicates that the ATPase function must be less strictly

coupled to the ion-transporting domain, since the saturating K^+ concentrations increase the enzyme activity less strongly compared to the observation in case of the Aminoxide WS-35 solubilized complex.

Substrate dependence of the KdpFABC ATPase activity

Results of the K^+-dependent enzyme activity (*Figure 27A*) were fitted with a Michaelis-Menten kinetics providing a $K_{1/2}$ of (2.03 ± 0.12) µM that is, together with the respective value of RH421 K^+-binding titration (*Table 2*), in agreement with previously published data (*54;67;114*). Furthermore, the enzyme activity could be stimulated not only by the presence of the transported K^+ ions but also by H^+ and Na^+, although to a significantly lesser extent. The maximal activity was found to be (0.18 ± 0.02) µmol P_i per mg protein per min for H^+, and (0.27 ± 0.10) µmol P_i per mg protein per min for Na^+ at pH 7.8. These activities correspond to 21 % and 31 %, respectively, of the maximal activity in the presence of saturating 3.3 mM K^+ at pH 7.8. In the absence of K^+ both ion species seem to act as weak congeners of K^+, with respect to stimulate the ATPase activity (*Figure 27B*). This has been already demonstrated for all alkali ions and not only for the native protein but also for mutant G232D within the KdpA subunit (*90*). The residue G232 was found to be of crucial importance for both K^+ affinity and selectivity, and it is the first residue within the highly conserved GGG motif, that forms a selectivity filter-like sequence similar to that found in the KcsA K^+ channel (*91*). In the RH421 ion-binding experiments with detergent-solubilized KdpFABC complexes it was demonstrated that binding of K^+, as well as of both H^+ and Na^+, produced a fluorescence decrease. The fluorescence decrease, which is a result of an uptake of positive charge into binding sites inside membrane domain of the KdpFABC, was observed in both unphosphorylated and phosphorylated conformation of the enzyme (*Figures 30-32, 35*).

The effect of pH on the K^+-induced enzyme activity was investigated to address the question of the role of protons in the function of the pump (*Figure 27B*). If H^+ is able to bind competitively to the ion-binding site(s) and would be transported as a counterion, an overall decrease of the ATPase activity is expected at high pH due to the lack of the transported substrate. According to the results shown in *Figure 27B* this is not the case. Therefore, the proton countertransport is less likely in case of the KdpFABC. Another observation is that increased H^+ concentrations obviously reduce the turnover number of the

KdpFABC complex even at saturating K^+ concentration. To include both effects of H^+ on the enzyme activity two possible explanations are suggested. On the one hand, numerous amino-acid side chains are prone to protonation/deprotonation and may affect the enzyme and/or transport function in an unspecific manner. On the other hand, since in the absence of K^+ a small but significant enzyme activity was detected (*Figure 27B*, open circles and dashed line), H^+ could bind also to specific sites, thereby generating either an allosteric effects on the KdpB subunit or direct competition in the K^+-binding sites of the KdpA.

The ATP-dependent enzyme activity (*Figure 28*) demonstrated a complex behavior. The activity increase was observed at ATP concentrations lower than 500 µM, with a $K_{1/2,1}$ of 65 µM, which is in agreement with already reported ATP affinities (*99;115*). At ATP concentrations higher than 500 µM, the enzyme activity showed a decrease and the concentration dependence was fitted by a Hill function with a $K_{1/2,2}$ of 1.54 mM and a Hill coefficient of 2.1. Although a Hill coefficient higher than 2 indicates that this inhibitory effect of ATP depends on a cooperative action of at least two ATP molecules, a mechanistic explanation for this observation cannot be given so far. An almost identical behavior was found for both Na_2-ATP and Mg-ATP, confirming that effect is indeed produced by ATP. A recent analysis of the ATP binding mechanism of KdpFABC does not reflect the potential involvement of two ATP molecules, but rather include formation of a transient KdpBN/$KdpC_{sol}$/ATP ternary complex at a 1:1:1 stoichiometry (*117*).

Ion-binding titrations

Results of the RH421 titration experiments performed in both E_1 and E_2 state, achieved by addition of either ATP or Tris-P_i (*Figures 31-33*), provide information on the ion-binding and release reactions of KdpFABC. The ion-binding affinity for both ions, K^+ and H^+, was found to differ in the unphosphorylated and phosphorylated conformation. Furthermore, the results revealed an asymmetric mutual interference between K^+ and H^+, with partially dependent half-saturating concentrations on the phosphorylation mechanism (*Table 3*). According to the presented experimental data, several important conclusions can be drawn. Since the amplitude of the fluorescence decrease induced by K^+ is basically unaffected by H^+ and *vice versa*, K^+ and H^+ bind preferentially to different sites in the membrane domain, and an electroneutral exchange of K^+ for H^+ contributes only to a small fraction to this process. In the unphosphorylated state, an increase of the H^+ concentration by a factor of

100 decreased the amount of K^+ bound electrogenically only by ~20 % (*Figure 31*). Similarly, an increase in K^+ concentration from 0 to 500 µM decreased the amount of electrogenically bound H^+ only by ~15 % (*Figure 33C*). This observation indicates that at least ~80 % of K^+ and H^+ binding occurs independently, *i.e.* at different binding sites. The phosphorylation of KdpFABC by either ATP or P_i, in the presence of saturating K^+, produced no significant fluorescence changes. Therefore, it can be concluded that the location of the binding site(s) inside the KdpA subunit is not significantly displaced during the phosphorylation and dephosphorylation reaction step of the KdpFABC complex, and in the P-E_2 conformation the binding sites remain occupied by K^+ ions. According to the *Figure 32*, it can be observed that the binding of K^+ and H^+ in both the phosphorylated (produced by both ATP and P_i) and the unphosphorylated state resulted in a maximal fluorescence decrease of ~4 %. This implies that in both partial reactions the amount of positive charge in the binding sites is constant when the same pH and saturating K^+ concentration are present on both sides of the membrane.

The half-saturating K^+ concentration, $K_{1/2}$, increased by a factor of ~2.2 - 2.6 when phosphorylated at pH 7.8, whereas at pH 6.1 this effect was even more pronounced, with a respective factor of ~4.0 - 4.9 (*Table 3*). There was no significant difference whether the phosphorylation was performed by ATP or P_i. The Lineweaver-Burk plot (*Figure 34*) demonstrated a mixed inhibition for K^+ binding with the respect to the H^+ in the E_1 conformation. As already mentioned above, the direct competition between H^+ and K^+ contributes only with a minor fraction to the observed inhibitory effect. A possible mechanism of the major non-competitive fraction of inhibition could be an electrostatic Coulomb interaction, in a way that the presence of the positively charged H^+, bound to independent sites within the KdpA subunit, generates a Debye-Hückel type repulsion of K^+ which is reflected by the apparently lower affinity of the K^+-binding sites at low pH.

In the absence of K^+, the half-saturating proton binding concentration, pK, of ~7.55 in the unphosphorylated state of the enzyme was reduced to ~7.34 when the enzyme was phosphorylated by P_i, and to ~6.78 when phosphorylated by ATP. The difference with respect to the origin of the phosphate is remarkable, since it implies that higher H^+ concentrations are necessary to stabilize H^+ binding in the phosphorylated state under turnover conditions (*i.e.* when the enzyme is phosphorylated by ATP). This dependence is even more pronounced at saturating K^+ concentration (*Table 3*). Under this condition, the pK value did not significantly change in the E_1 state (~7.65) and upon backdoor

phosphorylation (~7.20). When the enzyme was phosphorylated by ATP, however, a pK of ~5.70 was determined. A straightforward interpretation of this finding is that H^+ ions are able to bind in the phosphorylated state but that this state is short-lived under turnover conditions when the H^+-binding sites are less protonated or even deprotonated, and the enzyme can be dephosphorylated after K^+ binding from the extracellular side. Therefore, higher H^+ concentrations stabilize the phosphorylated state in which H^+ ions are bound. Furthermore, this behavior provides the additional evidence that H^+ is not released from these sites since their presence is required for stabilization of the phosphorylated state of the enzyme.

Similar to what has been found for the Na^+,K^+-ATPase, the $K_{1/2}$ of K^+ binding showed an increase with increasing Mg^{2+} concentrations (*Figure 36*). The apparent reduction of the K^+-binding affinity may be assigned, as in case of the Na^+,K^+-ATPase, to a Gouy-Chapman effect induced by a Mg^{2+} ion bound in the vicinity of the entrance of the access channel to the ion binding site located in the KdpA subunit. Since the amplitude of the maximal fluorescence change, ΔF, reflects the amount of charge taken up within the membrane domain, the observation that ΔF increased upon K^+ binding by more than a factor of 2 with increasing Mg^{2+} concentration (*Figure 36B*), implies that the presence of Mg^{2+} leads to a higher amount of bound positive charge. It is unlikely that the presence of Mg^{2+} increases the number of ion-binding sites. Addition of Mg^{2+} in the absence of K^+ leads to an increase of the fluorescence (*Figure 37*), which can be explained by a displacement of positive charge from the binding site(s). An obvious explanation would be that the binding site(s) are at least partially occupied by H^+ in the absence of K^+ and Mg^{2+}, and that the Gouy-Chapman effect induced by the presence of Mg^{2+}induces the H^+ displacement. This effect allows subsequently a larger net charge uptake when the K^+ titration is performed, as has been observed in *Figure 36B.*

$DiSC_3(V)$ measurements with the KdpFABC reconstituted in E. *coli* lipid vesicles

The size distribution of the KdpFABC–containing vesicles determined by dynamic light scattering was found to be (117 ± 21) nm, and with approximately 50 % of the incorporated enzyme with inside-out orientation. The observation that activity of the reconstituted enzyme was the same in the absence and presence of valinomycin could mean that the decrease of the intravesicular K^+ concentration, as a result of the pump activity, is not

significant, thereby has no effect on the pump activity during the experiment. Knowing the vesicle's diameter and the total K^+ concentration present in the electrolyte (140 mM), the corresponding K^+ concentration in a single vesicle can be calculated to be $\sim 1 \cdot 10^{-18}$ mol. Assuming five pumps per vesicle (and a molecular mass of 150 kDa), according to the transport rate of 150 µmol g^{-1} min^{-1} and 30 min duration of the malachite green experiment, total amount of the exported K^+ from the vesicles is $\sim 1 \cdot 10^{-20}$ mol. Comparing the values of the initial and exported K^+ suggests that depletion of K^+ during the activity measurement is not the limiting factor, thus, the pump works independently of valinomycin presence.

The calibration experiments performed with plain lipid vesicles and various rates of K^+ concentrations present inside and outside of the vesicles, showed that $DiSC_3(V)$ dye is suitable to monitor inside-negative potentials (*Figure 39*). Furthermore, a linear relationship between Nernst potential for K^+ and the produced fluorescence signal of the dye was found to exist in the voltage range between -120 mV and -40 mV. The initial experiment with KdpFABC-containing vesicles (*Figure 40A*) confirmed that KdpFABC pump is electrogenic and produces a net extrusion of positive charge from the vesicles, as has been published before (*99;100*). From the corresponding experiment with *o*-vanadate (*Figure 40B*), the time constant was determined to be 47.8 s, which corresponds to a specific membrane conductance of 21 pS/cm^2, and it was found to be constant over a pH range between 6.2 and 8.2.

According to the ATP-dependent K^+ export (*Figure 41*), the half-saturating ATP concentration was determined to be ~59 µM, and it is in good agreement with one obtained from the enzyme activity measurements of the detergent-solubilized KdpFABC (*Figure 28*). The observed activity inhibition at ATP concentrations higher than 500 µM, however, was not detected in experiments performed with the reconstituted enzyme. The reason for this difference is not clear so far. The difference between both experimental conditions was that in the vesicle experiments ATP was present only on the cytoplasmic side, whereas in the experiments with detergent-solubilized KdpFABC the protein was not embedded in a lipid bilayer but surrounded by an annulus consisting preferentially of detergent molecules. Reasonable is to assume that the unphysiological condition of the detergent environment provides sites on the protein surface that allow binding of additional ATP molecules.

Investigation of the pH-dependent K^+ transport across the vesicle membrane revealed that cooperative binding of more than one proton controls the pump current (*Figure 42*). The maximal fluorescence amplitude, ΔF_{max}, which is reached as steady state after addition of ATP can be used as measure of the pump current : $I_{pump} = \lambda_{leak} \cdot U = C \cdot \Delta F_{max}$, where C is a constant within the same vesicle preparation. An inhibition of the pump activity at high H^+ concentration, which is reflected as reduced fluorescence in *Figure 42*, could be explained by the competitive binding of protons, which are shown to be weak congeners of the transported K^+. At low H^+ concentrations (pH > 7.4) also a reduction of the pump activity was detected (*Figure 42*). This may be explained by a release of protons from allosteric binding sites with a pK of 7.5 (for detailed discussion see text below). The pump current was found to be maximal in the pH range of 7.3-7.4. These findings confirm the previously mentioned mixed inhibition between K^+ and H^+ (*Figure 34*), and the proposal that the presence of protons is necessary for the reaction cycle of KdpFABC, although they are not being transported. The results obtained in experiments with KdpFABC-containing vesicles in the absence of K^+, suggest that the KdpFABC complex is able to transport protons in opposite direction from the K^+ translocation, although with low efficiency (*Figure 43*). The existence of this unphysiological transport mode is in good agreement with the results of the H^+-induced enzyme activity in the absence of K^+ (*Figure 27B*, dashed line).

Pump activity was investigated with respect to different substrates present in the cytoplasmic medium that could affect the K^+ transport of the KdpFABC complex. To study these effects the initial slope of the fluorescence decrease was analyzed. This approach provides a measure of the pump current at zero transmembrane voltage (Eq. 11). According to the analysis of the initial pump activity as a function of extravesicular K^+ concentration (*Figure 44*), an inhibitory effect of K^+ ions was observed with a corresponding K_i of 23 mM. Under physiological conditions this would indicate that cytoplasmic K^+ concentration has an inhibitory effect on import of K^+ ions, and that the pump never reaches a maximal turnover rate. According to *Figure 44* the pump rate at a physiologic K^+ concentration of 140 mM would be only 25 % of the maximal value. A similar effect of extravesicular K^+ was reported also for the Na^+,K^+-ATPase (*177*). Magnesium ions are required for enzyme phosphorylation by ATP, and in case of the KdpFABC the half-saturating Mg^{2+} concentration was found to be 1.73 mM (*Figure 45*). In the absence of Mg^{2+} no pump activity was detected (*Figure 43B*). On the other hand, it has been shown that Mg^{2+} produces a shift of an apparently lower K^+ binding affinity because of a Gouy-Chapman

effect. With respect to the cytoplasmic side of KdpFABC this effect will reduce the local K^+ concentration at the exit channel for the K^+ ions. An estimate of the actual K^+ concentration at 5 mM Mg^{2+} would be, according to *Figure 36*, about half of the bulk concentration which would in turn increase the pump rate.

In case of the Na^+,K^+-ATPase both products of ATP hydrolysis, ADP and inorganic phosphate, have an inhibitory effect on the pumping rate (*178*). For ADP a strong non-competitive inhibitory effect was demonstrated, and the inhibitory constant K_i of ~0.1 mM was independent of ATP concentration. Considering the Post-Albers reaction scheme, a mechanism of ADP inhibition is the reversal of the phosphorylation reaction. On the other hand, only a weak effect of inorganic phosphate on the pump activity was detected, with a half-maximal inhibition constant of ~14 mM. The effect of both ADP and inorganic phosphate was investigated also for the KdpFABC, and a similar behavior was observed (*Figures 46* and *47*). The determined inhibition constants were found to be 0.13 mM and 0.27 mM for ADP and P_i, respectively. The obtained result for ADP inhibition is in the same range as one found in case of the Na^+,K^+-ATPase, and it is also in the range of physiological ADP concentrations (*185*). This finding suggest that mechanism of ADP inhibition should be similar for both the Na^+,K^+-ATPase and KdpFABC complex. The weak inhibition by inorganic phosphate for the Na^+,K^+-ATPase is, however, in contrast to the much stronger effect observed for the KdpFABC complex with a ~50 times lower inhibition constant. This indicates that the inhibition mechanism by inorganic phosphate must be different for both enzymes. For the Na^+,K^+-ATPase a non-competitive inhibition of inorganic phosphate with respect to ATP was proposed. The presence of inorganic phosphate shifts the dephosphorylation reaction in the Post-Albers cycle, $P\text{-}E_2(K_2) \leftrightarrow E_2(K_2)$ to the left side, thus slowing down the turnover rate. Additional experiments regarding the inhibition mechanism by inorganic phosphate are necessary to explain the significantly stronger inhibition observed in case of the KdpFABC than that revealed for the Na^+,K^+-ATPase.

The P-type ATPase inhibitor *o*-vanadate is known to bind to E_2 state (*186*), thereby inhibiting the transition reaction $E_2 \rightarrow E_1$, as schematically shown in *Figure 48*. Inhibition by *o*-vanadate was investigated with both detergent-solubilized and reconstituted KdpFABC. The first set of experiments was carried out with detergent-solubilized KdpFABC and yielded an *o*-vanadate inhibition constant, K_i, of ~1 µM, which is in agreement with previously reported concentration (*54*). The inhibition kinetics of *o*-vanadate with respect to ATP hydrolysis revealed a complex inhibition mechanism (*Figure 49*). At

ATP concentrations higher than 200 µM, a double-reciprocal plot revealed "partial" uncompetitive inhibition kinetics. This means that *o*-vanadate is able to bind to both KdpFABC and KdpFABC·ATP complex with the same affinity. Since the linear regression lines are not perfectly parallel, a true uncompetitive kinetics cannot be proposed. At ATP concentrations lower than 200 µM, the interception of linear regression lines suggests a competitive inhibition kinetics, which means that *o*-vanadate and ATP compete for the same binding sites. At lower ATP concentrations, ATP is known to predominantly bind to high-affinity binding site in the E_1 state, with a half-binding concentration of 60-80 µM. This indicates that *o*-vanadate most likely binds competitively to the low-affinity ATP binding sites accessible in the E_2 state. The second set of *o*-vanadate inhibition experiments was performed with KdpFABC-containing vesicles and provided an inhibition constant of ~60 µM for the ATPase activity, while the double-reciprocal plot indicated true uncompetitive inhibition kinetics over the whole range of tested ATP concentrations (*Figure 50A* and *B*). The inhibition constant of ~40µM was determined from the fluorescence measurements (*Figure 50C*). The explanation for higher inhibition constant and the absence of the biphasic behavior (as observed in case of the detergent-solubilized KdpFABC complex) for the reconstituted KdpFABC at the moment cannot be given, and additional measurements are certainly required.

The investigation of the energetics revealed that the activation energy of the β-DDM-solubilized KdpFABC was ~55 kJ/mol determined in ATP hydrolysis experiments (*Figure 51*). The activation energy of K^+ transport by reconstituted KdpFABC, determined with the $DiSC_3(V)$ fluorescence measurements, was found to be ~111 kJ/mol (*Figure 52*). The activation energy of KdpFABC under turnover conditions is controlled by the rate-limiting conformational change, and the observed difference by a factor of 2 between both values may be assigned to the effect of the different hydrophobic environments surrounding the KdpFABC complex in the solubilized form and after reconstitution.

Time-resolved experiments with detergent-solubilized KdpFABC

Additional kinetics properties of the KdpFABC reaction cycle were obtained from the time-resolved experiments. At saturating ATP concentration the rate-determining step is supposed to be located in the conformation transition E_1-P → P-E_2. The fluorescence decrease observed upon photorelease of ATP is a result of binding of a positive charge to a

membrane domain of KdpFABC (*Figure 23*). This confirms that the ATP-induced phosphorylation step and the conformation transition have to occur before the ion-binding step. Furthermore, it was found that the time constant of the conformation transition is independent of the potassium concentration (*Figure 53*), with the average value of ~600 ms.

The rate constant derived from the enzyme activity is k_1=2.2 s^{-1} at T_1=37 °C (considering the molar mass of the enzyme of 150 000 g/mol and the maximal activity of 0.86 µmol P_i mg^{-1} min^{-1} (*Table 2*)). On the other hand, the estimated average time constant of the conformation transition was found to be 600 ms (*Figure 53*), corresponding to the rate constant k_2=1.67 s^{-1} at T_2=25 °C. Assuming the activation energy of E_a=55 kJ/mol (*Figure 51*) and using the Arrhenius equation $ln(k_1/k_2) = - E_a/R\ (1/T_1 - 1/T_2)$, the calculated ratio between two rate constants k_1/k_2 is 2.4. Multiplying k_1 with the derived ratio yields ~4 s^{-1}, which further compared to the estimated value of ~2.2 s^{-1} gives a possible stoichiometry of two K^+ transported per one ATP hydrolyzed molecule. The minor difference between the calculated values can be reconciled by fact that the k_1 reflects the rate constant under turnover conditions, whereas k_2 is derived from the partial reaction.

The finding that τ is independent on K^+ further implies that the time constant of the K^+-binding step has to be significantly smaller than that of the conformation transition and that the presence of K^+ ions is not required for the phosphorylation step and the conformation transition. The detected fluorescence decrease in the absence of K^+, which was by factor ~3 lower than one observed in the presence of saturating 100 µM K^+, indicates H^+ binding and confirms the previously mentioned conclusion that H^+ acts as a congener of K^+ and can be transported when no K^+ is present. The ratio of the amplitude of fluorescence decrease and time constant, A/τ, reflects the initial slope of the fluorescence signal and, as derived above, the fraction of the pumps activated by the ATP release. This fraction increased with the increasing K^+ concentrations. The half-saturating concentration was found to be ~5 µM (*Figure 54*), and it is in good agreement with $K_{1/2}$ values obtained with other techniques shown above. This indicates that in the absence of K^+ the major fraction of the pump is trapped in the E_2 conformation and not readily available for enzyme phosphorylation upon the photorelease of ATP. At saturating K^+ concentrations the distribution between both conformations, E_1 and E_2, is shifted towards E_1 and a threefold higher number of pumps contribute to the phosphorylation reaction. The Hill coefficient of 2.3 supports the proposed stoichiometry of 2 K^+ transported per pump cycle.

The effect of H^+ on the rate constant, $1 / \tau$, in the absence and presence of saturating K^+, revealed a complex behavior, and the observed pH dependence suggest that H^+ plays a significant role in the ATP-driven half cycle.

In the presence of saturating 100 µM K^+, the rate constant increased from ~1.6 s^{-1} at pH >7.5 about threefold at pH 6.2. This observation indicates on the one hand that under physiological conditions at a pH > 7 the pump seems to work off its optimized conditions. On the other hand, binding of protons in the E_1 conformation accelerates the rate-limiting ATP-induced phosphorylation rate. Binding of H^+ to the E_1 conformation can occur to an allosteric site or a transport site. The experiments on equilibrium proton binding (*Figure 31*) showed that the binding sites are inside the membrane domain and mostly different from K^+-binding sites. Assuming binding from the cytoplasmic side in E_1, binding to a site that allows transport is rather unlikely since the study of H^+ transport from the cytoplasmic side plays only a minor role and could be detected only in the absence of K^+ (*Figure 43A*).

In the absence of K^+ (*Figure 55*, black data and line), a biphasic behavior was observed. Below pH 6.5 and above 7.8 low rate constants were observed, comparable to those in the presence of K^+ at high pH. Between pH 6.8 and 7.8 higher rate constants were found with a maximum at pH 7.2 – 7.3. The highest rate constant was found at pH 7.2 – 7.3 with values similar to that of maximal pump activity discussed at pH 6.2 in the presence of K^+. The high Hill coefficients (> 4) suggest that the cooperative action of several protons is involved in the observed process. The decrease of the observed rate constant with increasing H^+ concentration indicates that protons may bind from the cytoplasmic side to sites that prevent enzyme phosphorylation. One possibility would be the protonation of negatively charged amino-acid side chains, *e.g.* those within the K^+-binding sites that kinetically inhibit reaching the state in the pump cycle that is phosphorylated by ATP.

At non-saturating ATP concentrations, ATP-binding become rate-limiting step, and the observed time constant determined from the fluorescence decrease is controlled by the ATP concentration. An apparent ATP-binding concentration was found to be ~60 µM (*Figure 56*), and it is in good agreement with obtained values with both ATPase activity and fluorescence experiments, discussed above. It has to be mentioned, however, that the Hill coefficient of the fitted concentration dependence is only 0.66 ± 0.05, and this low value indicates that the effect of the conformation transition and ATP binding are intermingled even at the lowest ATP concentration used in the experiment.

Mechanistic implications and proposed Post-Albers reaction cycles

According to the results presented in this work, three different Post-Albers cycles may be proposed as shown in *Figure 57* that allow us to analyze the underlying reaction mechanism of the KdpFABC. In its general form (*Figure 57A*) it describes the Ping-Pong mechanism that has been accepted for all type II P-type ATPases. It includes the translocation of two different ion species contrariwise across the membrane (*92*). According to this model, the entire ion-transport process can be divided into two half cycles. The ATP-induced partial reaction starts with ion binding from the cytoplasm, followed by enzyme phosphorylation, accompanied by ion occlusion, the conformational transition, $E_1 \rightarrow E_2$, and subsequent deocclusion of the ion-binding sites on the opposite side of the membrane, followed by ion release to the extracellular side. The KdpFABC pump, a member of type Ia P-type ATPase, translocates K^+ ions into the cytoplasm and no counter transport of a second ion species has been detected so far. Two different scenarios, taking this information into account, could be applied to represent this behavior. Firstly, inward transport of K^+ takes place during the dephosphorylation half cycle, whereas in the ATP-driven half cycle no ions are transported (*Figure 57B*). This would correspond to the pump cycle of the type II P-type ATPases, such as the Na^+,K^+-ATPase and H^+,K^+-ATPase, and has already been suggested many years ago (*79;99*). An alternative proposal to this would be K^+ transport in the ATP-hydrolyzing half cycle, while no ions are translocated in the dephosphorylation half cycle (*Figure 57C*). This implies, however, that the ion-transport direction in the ATP-induced half cycle is reversed with respect to the pump mode of type II P-type ATPases. This proposal has been introduced by Bramkamp and Altendorf (*98*), and a detailed description is given in the theoretical introduction. Such a fundamental modification of the generally accepted Post-Albers model can be accepted because in the KdpFABC complex enzyme activity and ion transport are located on two different protein subunits which are coupled to perform the ATP-driven ion transport. This division of function provides an additional degree of freedom in comparison to other type II P-type ATPases, in which enzyme and transport function are located in the same subunit. Neither of these models, however, accounts for the role of protons in the reaction cycle of the KdpFABC, which has been revealed by the results presented in this work.

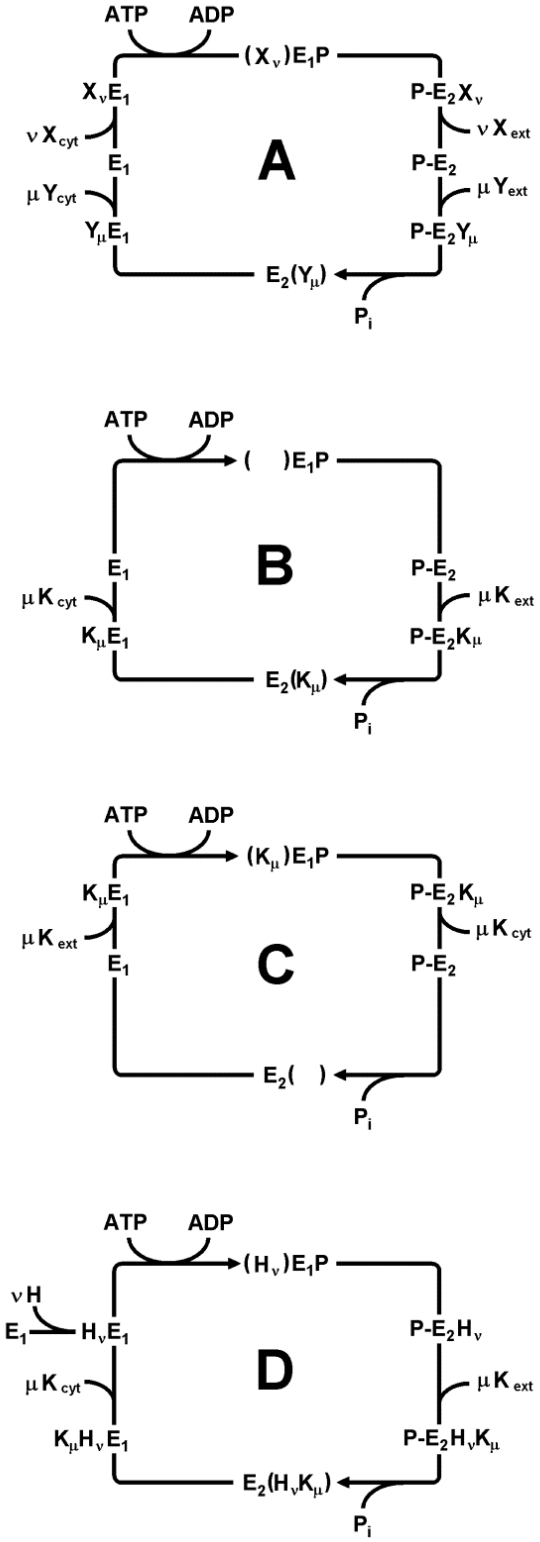

Figure 57. Post-Albers pump cycles of P-type ATPases and proposals of modifications for the KdpFABC pump. **A:** General scheme of the pump cycle, valid for type II P-type ATPases such as Na^+,K^+-ATPase, SR Ca^{2+}-ATPase, H^+,K^+-ATPase (*50*), and a general template for the function of type I pumps. **B – D:** Proposed models for the KdpFABC pump. For discussion see text.

As already discussed, protons perform at least two different functions. The first one is the action as a congener of K^+ which can be transported to the cytoplasm with low efficiency in the absence of K^+, as has been reported before for Rb^+, Na^+, and Li^+ (*84;89;90*). In this transport mode the ions are bound from the extracellular side to the "transporting" binding sites, where competition occurs when K^+ is also present. At low pH on the cytoplasmic side proton may bind to these sites after the release of K^+. This "back-binding" of protons kinetically blocks the pump from continuing through the pump cycle which requires empty or deprotonated binding sites. This would explain the observed reduced enzyme activity at low pH in the presence of saturating K^+ concentration (*Figure 27B*), the reduced K^+ transport (*Figure 42*) and the reduced rate constant (*Figure 55*) at decreasing pH. In the absence of K^+, however, a low transport capacity of H^+ into the vesicles was observed (*Figure 43A*). This finding may be interpreted as a low-rate counter transport with respect to the physiological relevant K^+ transport. So far it is not clear whether this mode only occurs in the absence of K^+ or whether it is a kind of undesired effect that cannot be prevented completely by the pump.

The second function of H^+ is the non-competitive or allosteric binding. It was found that H^+ binding is an electrogenic process (*Figure 31*) and that the K^+-transport activity decreased above pH 7.5, with a Hill coefficient > 2 (*Figure 42*). The electrogenicity indicates that H^+ bind to binding sites localized within the membrane domain. One proposal to include this role of H^+ in the pump cycle is shown in *Figure 57D*. The Post-Albers cycle represents the modified version of the more classical type (*Figure 57B*), in which K^+ is translocated during the dephosphorylation half cycle. In addition, protons bind to sites that have to be occupied to enable enzyme phosphorylation without being transported across the membrane. The protons remain "occluded" in their sites throughout the whole cycle, and their presence inside the membrane domain is a prerequisite for the ATP-driven half cycle.

On the basis of the quasi-steady state experiments, however, it cannot be discriminated between two different possibilities to allocate the allosteric H^+ binding. The first is that the binding sites are located in the KdpA subunit, where the H^+ would play the role of a precursor of the ions that are translocated in the ATP-driven half cycle in type II P-type ATPases. In this case the occlusion of protons may not be perfect, at least in the absence of K^+, since in experiments with reconstituted vesicles a small but significant H^+ transport has been observed. This current is directed from the cytoplasmic to the extracellular side of the KdpFABC complex and is assigned to the ATP-driven half cycle. Thus, H^+ may be lost in

the phosphorylated state, P-E_2, inadvertently to the extracellular side. Such a mechanism was reported in case of the H^+-ATPase from *Enterococcus hirae*, where the diffusion of a proton out of an occluded binding site was mediated by hydrogen bond without the need of a specific access channel (*187*). The displacement of protons from their binding site may cause a delayed transition to the dephosphorylation step and return to the E_1 conformation in which the binding sites are accessible to the cytoplasmic side again. The alternative possibility is that the H^+ binding site(s) are located in the KdpB subunit, where the protons have an allosteric effect in a process of the energy transfer from KdpB to KdpA. A supportive argument for this model would be the observed pH dependence of enzyme activity, which exhibited no decrease at pH higher than 7.5 (*Figure 27B*). This behavior can be explained by a less strict coupling of KdpA and KdpB subunits, allowing a dissipative ATP hydrolysis. Such a behavior would be a rather unfavorable condition for the cell. Opposing this proposal are the results obtained from the pH-dependent rate constant of the conformational transition (*Figure 55*). If protons would have an effect on the coupling between enzyme and transport activity, the rate constant should decrease at low pH independently of presence of K^+. This is not the case. Although the expected decrease was observed in the absence of K^+, the rate constant increased with increasing H^+ in the presence 100 µM K^+.

Further arguments supporting the model D in which the K^+ binding and transport occur in the dephosphorylation half cycle are the results obtained in time-resolved experiments (*Figures 53* and *54*). The ATP-induced half cycle (according to the *Figure 57D)* can be divided into three reaction steps:

1. $H_vE_1 \cdot ATP \rightarrow H_vE_1 - P$	phosphorylation step
2. $H_vE_1 - P \rightarrow P - E_2H_v$	conformation transition
3. $P - E_2H_v \rightarrow P - E_2H_vK_\mu$	K^+ binding step

Only the third reaction step is electrogenic and detectable by the RH421 dye. The fluorescence signal decreased upon photorelease of ATP, indicating that binding of positive charge occurs after the enzyme phosphorylation and conformation transition. The time constant was independent on K^+ concentration, leading to a conclusion that K^+ binding is not the rate-determining step of the ATP-induced partial reaction. This observation confirms that the rate-determining step is the conformation transition, $H_vE_1 - P \rightarrow P - E_2H_v$, and also

that only protons are required. If K^+ would be already bound to the pump before the ATP-induced phosphorylation step, no electrogenic response would occur at saturating K^+ concentrations. At low pH the conformational transition is inhibited, caused by back-binding of H^+, as mentioned above. This reaction would be represented as $H_\nu E_1 + \mu\ H^+ \rightarrow H_\mu H_\nu E_1$ according to the *Figure 57D*. In contrast, at high pH the rate of the forward reaction, $E_1 + \nu H^+ \rightarrow H_\nu E_1$, is decreased due to the lack of protons. In the presence of saturating K^+, however, no decrease in the rate constant was found, which could be explained by binding of K^+ in the P-E_2H_ν state, and a fast proceeding of the enzyme to the P-$E_2H_\nu K_\mu$ state. At this state, the effect of pH on the previous reaction steps is diminished, therefore, no inhibition can be observed. This finding supports the functional role of H^+ as non-transported ion, and that they become even more tightly occluded in the presence of saturating K^+.

Stoichiometry of K^+ transport

The analysis of the fluorescence decrease in the RH421 experiments obtained upon binding of K^+ and H^+ at more or less saturating concentrations (*Figures 31-33*) allows an estimation of the maximum amount of charge bound to the binding sites. The maximum fluorescence decrease obtained in the unphosphorylated state upon K^+ binding is in the order of ~0.4, whereas upon H^+ binding is ~0.6. So far, in case of the KdpFABC there is no absolute measure of the maximal number of ions bound. Since charge is quantized, the normalized fluorescence changes of 0.4 and 0.6 could account for 2 K^+ and 3 H^+ in the binding sites. While K^+ ions have to be bound in sites in which they are coordinated by oxygen atoms from amino-acid side chains, H^+ may bind directly to single charged amino-acid side chains. According to Becker et al. Arg493 located in the KdpA may play here a key role (*175*). A stoichiometry of 2 K^+ transported per one ATP hydrolyzed is feasible according to a simple estimate. Assuming a membrane potential in *E. coli* of -140 mV (*188*) and a cytoplasmic K^+ concentration of 180 mM (*189*), a Gibbs free enthalpy of -50 kJ/mol for the ATP hydrolysis, and a low extracellular K^+ concentration of 2 µM (a condition under which KdpFABC will be expressed and active), the electrochemical potential gradient for K^+ is 14.9 kJ/mol. Compared to the energy provided by ATP hydrolysis, up to 3 K^+ could be transferred across the membrane under physiological conditions. Protons, however, are considered in this calculation of the transmembrane electrochemical potential gradient since they are assumed to remain occluded and not transported.

Finally, taking into account the results and estimates presented in this project, it is justified to propose that the pump mechanism of the KdpFABC complex can be represented by the model D of the Post-Albers pump cycles shown in *Figure 57*, with the stoichiometric factors $v = 3$ and $\mu = 2$:

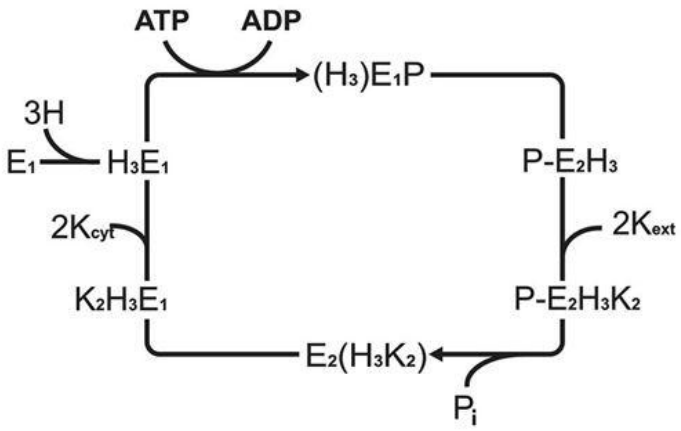

5. REFERENCES

1. Jackson, J. M. (2006) *Molecular and Cellular Biophysics* Cambridge University Press.
2. Bolsover, S. R. H. S. J. S. A. E. W. A. H. W. G. C. (2004) *Cell Biology: A Short Course, 2nd Edition* Wiley.
3. Ahmed, A. H. (2004) *Principles and Reactions of Protein Extraction, Purification, and Characterization* CRC PRESS Boca Raton London New York Washington, D.C..
4. Schultz, G. S. (1980) *Basic principle of membrane transport* Cambridge University Press, NY, USA.
5. Läuger, P. (1991) *Electrogenic Ion Pumps* Sinauer Assoc, Sunderland, MA.
6. Murray, K. R., Granner, D. K., Mayes, A. P., and Rodwell, W. V. (2003) *Harpers Illustrated Biochemistry* Mcgraw-Hill Professional.
7. Dunbar, L. A. and Caplan, M. J. (2000) The cell biology of ion pumps: sorting and regulation, *Eur. J. Cell Biol. 79*, 557-563.
8. Heinz, E. (1981) *Electrical Potentials in Biological Membrane Transport* Springer-Verlag.
9. Bot, C. T. and Prodan, C. (2010) Quantifying the membrane potential during *E. coli* growth stages, *Biophys. Chem. 146*, 133-137.
10. Gadsby, C. D. (2009) Ion channels versus ion pumps:the pricipal difference, in principle, *Nature Reviews Molecular Cell Biology 10*.
11. Läuger, P. (1979) A channel mechanism for electrogenic ion pumps, *Biochim. Biophys. Acta 552*, 143-161.
12. Gadsby, D. C., Vergani, P., and Csanady, L. (2006) The ABC protein turned chloride channel whose failure causes cystic fibrosis, *Nature 440*, 477-483.
13. Vergani, P., Lockless, S. W., Nairn, A. C., and Gadsby, D. C. (2005) CFTR channel opening by ATP-driven tight dimerization of its nucleotide-binding domains, *Nature 433*, 876-880.
14. Habermann, E. (1989) Palytoxin acts through Na^+,K^+-ATPase, *Toxicon 27*, 1171-1187.
15. Scheiner-Bobis, G., Meyer zu, H. D., Christ, M., and Habermann, E. (1994) Palytoxin induces K+ efflux from yeast cells expressing the mammalian sodium pump, *Mol. Pharmacol. 45*, 1132-1136.
16. Gadsby, D. C., Takeuchi, A., Artigas, P., and Reyes, N. (2009) Review. Peering into an ATPase ion pump with single-channel recordings, *Philos. Trans. R. Soc. Lond B Biol. Sci. 364*, 229-238.
17. Riordan, J. R., Rommens, J. M., Kerem, B., Alon, N., Rozmahel, R., Grzelczak, Z., Zielenski, J., Lok, S., Plavsic, N., Chou, J. L., and . (1989) Identification of the cystic fibrosis gene: cloning and characterization of complementary DNA, *Science 245*, 1066-1073.
18. Jordan, I. K., Kota, K. C., Cui, G., Thompson, C. H., and McCarty, N. A. (2008) Evolutionary and functional divergence between the cystic fibrosis transmembrane conductance regulator and related ATP-binding cassette transporters, *Proc. Natl. Acad. Sci. U. S. A 105*, 18865-18870.
19. Greie, J. C. and Altendorf, K. (2007) The K+-translocating KdpFABC complex from Escherichia coli: a P-type ATPase with unique features, *J. Bioenerg. Biomembr. 39*, 397-402.
20. Pedersen, P. L. (2005) Transport ATPases: structure, motors, mechanism and medicine: a brief overview, *J. Bioenerg. Biomembr. 37*, 349-357.

21. Wilkens, S., Zhang, Z., and Zheng, Y. (2005) A structural model of the vacuolar ATPase from transmission electron microscopy, *Micron. 36*, 109-126.
22. Imamura, H., Takeda, M., Funamoto, S., Shimabukuro, K., Yoshida, M., and Yokoyama, K. (2005) Rotation scheme of V1-motor is different from that of F1-motor, *Proc. Natl. Acad. Sci. U. S. A 102*, 17929-17933.
23. Imamura, H., Nakano, M., Noji, H., Muneyuki, E., Ohkuma, S., Yoshida, M., and Yokoyama, K. (2003) Evidence for rotation of V1-ATPase, *Proc. Natl. Acad. Sci. U. S. A 100*, 2312-2315.
24. Boyer, P. D. (1997) The ATP synthase--a splendid molecular machine, *Annu. Rev. Biochem. 66*, 717-749.
25. Stock, D., Gibbons, C., Arechaga, I., Leslie, A. G., and Walker, J. E. (2000) The rotary mechanism of ATP synthase, *Curr. Opin. Struct. Biol. 10*, 672-679.
26. Sweadner, K. J. and Donnet, C. (2001) Structural similarities of Na,K-ATPase and SERCA, the Ca^{2+}-ATPase of the sarcoplasmic reticulum, *Biochem. J. 356*, 685-704.
27. Skou, J. C. (1957) The influence of some cations on an adenosine triphosphatase from peripheral nerves, *Biochim. Biophys. Acta 23*, 394-401.
28. Pedersen, P. L. and Carafoli, E. (1987) Ion motive ATPase. I. Ubiquity, properties, and significance to cell function, *TIBS 12*, 146-150.
29. Pedersen, P. L. and Carafoli, E. (1987) Ion motive ATPases. II. Energy coupling and work output, *TIBS 12*, 186-189.
30. Pedersen, P. L. (2007) Transport ATPases into the year 2008: a brief overview related to types, structures, functions and roles in health and disease, *J. Bioenerg. Biomembr. 39*, 349-355.
31. Jones, P. M., O'Mara, M. L., and George, A. M. (2009) ABC transporters: a riddle wrapped in a mystery inside an enigma, *Trends Biochem. Sci. 34*, 520-531.
32. Lodish, H. B. A. Z. S. L. e. al. (2000) Active Transport by ATP-Powered Pumps, in *Molecular Cell Biology* 4th ed., New York: W.H. Freeman.
33. Kühlbrandt, W. (2004) Biology, structure and mechanism of P-type ATPases, *Nat. Rev. Mol. Cell Biol. 5*, 282-295.
34. Palmgren, M. G. and Axelsen, K. B. (1998) Evolution of P-type ATPases, *Biochim. Biophys. Acta 1365*, 37-45.
35. Palmgren, M. G. and Nissen, P. (2011) P-type ATPases, *Annu. Rev. Biophys. 40*, 243-266.
36. Toyoshima, C., Nakasako, M., Nomura, H., and Ogawa, H. (2000) Crystal structure of the calcium pump of sarcoplasmatic reticulum at 2.6 Å resolution, *Nature 405*, 647-655.
37. Stokes, D. L. and Green, N. M. (2003) Structure and function of the calcium pump, *Annu. Rev. Biophys. Biomol. Struct. 32*, 445-468.
38. Suzuki, T. and Wang, J. H. (1986) Stimulation of bovine cardiac sarcoplasmic reticulum Ca2+ pump and blocking of phospholamban phosphorylation and dephosphorylation by a phospholamban monoclonal antibody, *J. Biol. Chem. 261*, 7018-7023.
39. Yazawa, M., Vorherr, T., James, P., Carafoli, E., and Yagi, K. (1992) Binding of calcium by calmodulin: influence of the calmodulin binding domain of the plasma membrane calcium pump, *Biochem. 31*, 3171-3176.
40. Jorgensen, P. L., Hakansson, K. O., and Karlish, S. J. (2003) Structure and mechanism of Na,K-ATPase: functional sites and their interactions, *Annu. Rev. Physiol 65*, 817-849.
41. Geering, K. (2006) FXYD proteins: new regulators of Na-K-ATPase, *Am. J. Physiol Renal Physiol 290*, F241-F250.
42. Scarborough, G. A. (2000) The plasma membrane proton-translocating ATPase, *Cell Mol. Life Sci. 57*, 871-883.

43. Daleke, D. L. (2003) Regulation of transbilayer plasma membrane phospholipid asymmetry, *J. Lipid Res. 44*, 233-242.
44. Axelsen, K. B. and Palmgren, M. G. (1998) Evolution of substrate specificities in the P-type ATPase superfamily, *J. Mol. Evol. 46*, 84-101.
45. Toyoshima, C. and Nomura, H. (2002) Structural changes in the calcium pump accompanying the dissociation of calcium, *Nature 418*, 605-611.
46. Xu, C., Rice, W. J., He, W., and Stokes, D. L. (2002) A structural model for the catalytic cycle of Ca^{2+}-ATPase, *J. Mol. Biol. 316*, 201-211.
47. Jencks, W. P. (1989) Utilization of binding energy and coupling rules for active transport and other coupled vectorial processes, *Methods Enzymol. 171*, 145-164.
48. Post, R. L., Hegyvary, C., and Kume, S. (1972) Activation by adenosine triphosphate in the phosphorylation kinetics of sodium and potassium ion transport adenosine triphosphatase, *J. Biol. Chem. 247*, 6530-6540.
49. Albers, R. W. (1967) Biochemical aspects of active transport, *Ann. Rev. Biochem. 36*, 727-756.
50. Apell, H. J. (2004) How do P-type ATPases transport ions?, *Bioelectrochemistry. 63*, 149-156.
51. Harold, F. M. and Altendorf, K. (1974) Cation transport in bacteria: K, Na and H, *Curr. Top. Membr. Transp. 5*, 1-50.
52. Suelter, C. H. (1970) Enzymes activated by monovalent cations, *Science 168*, 789-795.
53. Booth, I. R. (1985) Regulation of cytoplasmic pH in bacteria, *Microbiol. Rev. 49*, 359-378.
54. Rhoads, D. B. and Epstein, W. (1978) Cation transport in Escherichia coli. IX. Regulation of K transport, *J. Gen. Physiol 72*, 283-295.
55. McLaggan, D., Naprstek, J., Buurman, E. T., and Epstein, W. (1994) Interdependence of K+ and glutamate accumulation during osmotic adaptation of Escherichia coli, *J. Biol. Chem. 269*, 1911-1917.
56. Galinski, E. A., Pfeiffer, H. P., and Truper, H. G. (1985) 1,4,5,6-Tetrahydro-2-methyl-4-pyrimidinecarboxylic acid. A novel cyclic amino acid from halophilic phototrophic bacteria of the genus Ectothiorhodospira, *Eur. J. Biochem. 149*, 135-139.
57. Dinnbier, U., Limpinsel, E., Schmid, R., and Bakker, E. P. (1988) Transient accumulation of potassium glutamate and its replacement by trehalose during adaptation of growing cells of Escherichia coli K-12 to elevated sodium chloride concentrations, *Arch. Microbiol. 150*, 348-357.
58. Schleyer, M., Schmid, R., and Bakker, E. P. (1993) Transient, specific and extremely rapid release of osmolytes from growing cells of Escherichia coli K-12 exposed to hypoosmotic shock, *Arch. Microbiol. 160*, 424-431.
59. Heitkamp, T. (2009) Structure and functional dynamics of the KdpFABC P-type ATPase from Escherichia coli.
60. Ferguson, G. P., Nikolaev, Y., McLaggan, D., Maclean, M., and Booth, I. R. (1997) Survival during exposure to the electrophilic reagent N-ethylmaleimide in Escherichia coli: role of KefB and KefC potassium channels, *J. Bacteriol. 179*, 1007-1012.
61. Verkhovskaya, M. L., Verkhovsky, M. I., and Wikstrom, M. (1995) A novel antiporter activity catalyzing sodium and potassium transport from right-side-out vesicles of E. coli, *FEBS Lett. 363*, 46-48.
62. Berrier, C., Besnard, M., Ajouz, B., Coulombe, A., and Ghazi, A. (1996) Multiple mechanosensitive ion channels from Escherichia coli, activated at different thresholds of applied pressure, *J. Membr. Biol. 151*, 175-187.
63. Bakker, E. P. (1993) Low-affinity K uptake systems, in *Alkali cation transport systems in prokaryotes* pp 253-276, CRC Press, Boca Raton, Florida.

64. Bossemeyer, D., Schlosser, A., and Bakker, E. P. (1989) Specific cesium transport via the Escherichia coli Kup (TrkD) K+ uptake system, *J. Bacteriol. 171*, 2219-2221.
65. Laimins, L. A., Rhoads, D. B., Altendorf, K., and Epstein, W. (1978) Identification of the structural proteins of an ATP-driven potassium transport system in Escherichia coli, *Proc. Natl. Acad. Sci. U. S. A 75*, 3216-3219.
66. Epstein, W., Walderhaug, M. O., Polarek, J. W., Hesse, J. E., Dorus, E., and Daniel, J. M. (1990) The bacterial Kdp K^+-ATPase and its relation to other transport ATPases, such as the Na^+/K^+- and Ca^{2+}-ATPases in higher organisms, *Philos. Trans. R. Soc. Lond B Biol. Sci. 326*, 479-486.
67. Rhoads, D. B., Waters, F. B., and Epstein, W. (1976) Cation transport in Escherichia coli. VIII. Potassium transport mutants, *J. Gen. Physiol 67*, 325-341.
68. Hesse, J. E., Wieczorek, L., Altendorf, K., Reicin, A. S., Dorus, E., and Epstein, W. (1984) Sequence homology between two membrane transport ATPases, the Kdp-ATPase of Escherichia coli and the Ca2+-ATPase of sarcoplasmic reticulum, *Proc. Natl. Acad. Sci. U. S. A 81*, 4746-4750.
69. Siebers, A. and Altendorf, K. (1996) K-translocating Kdp-ATPases and ither bacterial P-type ATPases, in *Alkali cation transport systems in prokaryotes* pp 225-252, CRC Press, Boca Raton, Florida.
70. Walderhaug, M. O., Polarek, J. W., Voelkner, P., Daniel, J. M., Hesse, J. E., Altendorf, K., and Epstein, W. (1992) KdpD and KdpE, proteins that control expression of the kdpABC operon, are members of the two-component sensor-effector class of regulators, *J. Bacteriol. 174*, 2152-2159.
71. Polarek, J. W., Williams, G., and Epstein, W. (1992) The products of the kdpDE operon are required for expression of the Kdp ATPase of Escherichia coli, *J. Bacteriol. 174*, 2145-2151.
72. Altendorf, K., Voelkner, P., and Puppe, W. (1994) The sensor kinase KdpD and the response regulator KdpE control expression of the kdpFABC operon in Escherichia coli, *Res. Microbiol. 145*, 374-381.
73. Zimmann, P., Puppe, W., and Altendorf, K. (1995) Membrane topology analysis of the sensor kinase KdpD of Escherichia coli, *J. Biol. Chem. 270*, 28282-28288.
74. Voelkner, P., Puppe, W., and Altendorf, K. (1993) Characterization of the KdpD protein, the sensor kinase of the K(+)-translocating Kdp system of Escherichia coli, *Eur. J. Biochem. 217*, 1019-1026.
75. Heermann, R., Altendorf, K., and Jung, K. (1998) The turgor sensor KdpD of Escherichia coli is a homodimer, *Biochim. Biophys. Acta 1415*, 114-124.
76. Jung, K., Tjaden, B., and Altendorf, K. (1997) Purification, reconstitution, and characterization of KdpD, the turgor sensor of Escherichia coli, *J. Biol. Chem. 272*, 10847-10852.
77. Rhoads, D. B. and Epstein, W. (1977) Energy coupling to net K+ transport in Escherichia coli K-12, *J. Biol. Chem. 252*, 1394-1401.
78. Siebers, A. and Altendorf, K. (1988) The K+-translocating Kdp-ATPase from Escherichia coli. Purification, enzymatic properties and production of complex- and subunit-specific antisera, *Eur. J. Biochem. 178*, 131-140.
79. Siebers, A. and Altendorf, K. (1989) Characterization of the phosphorylated intermediate of the K+-translocating Kdp-ATPase from Escherichia coli, *J. Biol. Chem. 264*, 5831-5838.
80. Laimins, L. A., Rhoads, D. B., and Epstein, W. (1981) Osmotic control of kdp operon expression in Escherichia coli, *Proc. Natl. Acad. Sci. U. S. A 78*, 464-468.
81. Møller, J. V., Juul, B., and le Maire, M. (1996) Structural organization, ion transport, and energy transduction of P-type ATPases, *Biochim. Biophys. Acta 1286*, 1-51.

82. Durell, S. R., Bakker, E. P., and Guy, H. R. (2000) Does the KdpA subunit from the high affinity K(+)-translocating P-type KDP-ATPase have a structure similar to that of K(+) channels?, *Biophys. J. 78*, 188-199.
83. Durell, S. R. and Guy, H. R. (1999) Structural models of the KtrB, TrkH, and Trk1,2 symporters based on the structure of the KcsA K(+) channel, *Biophys. J. 77*, 789-807.
84. Buurman, E. T., Kim, K. T., and Epstein, W. (1995) Genetic evidence for two sequentially occupied K+ binding sites in the Kdp transport ATPase, *J. Biol. Chem. 270*, 6678-6685.
85. Dorus, S., Mimura, H., and Epstein, W. (2001) Substrate-binding clusters of the K+-transporting Kdp ATPase of Escherichia coli investigated by amber suppression scanning mutagenesis, *J. Biol. Chem. 276*, 9590-9598.
86. van der, L. M., Gassel, M., and Altendorf, K. (2002) Characterization of amino acid substitutions in KdpA, the K+-binding and -translocating subunit of the KdpFABC complex of Escherichia coli, *J. Bacteriol. 184*, 5491-5494.
87. Bertrand, J., Altendorf, K., and Bramkamp, M. (2004) Amino acid substitutions in putative selectivity filter regions III and IV in KdpA alter ion selectivity of the KdpFABC complex from Escherichia coli, *J. Bacteriol. 186*, 5519-5522.
88. Durell, S. R., Hao, Y., Nakamura, T., Bakker, E. P., and Guy, H. R. (1999) Evolutionary relationship between K(+) channels and symporters, *Biophys. J. 77*, 775-788.
89. Bertrand, J., Altendorf, K., and Bramkamp, M. (2004) Amino acid substitutions in putative selectivity filter regions III and IV in KdpA alter ion selectivity of the KdpFABC complex from Escherichia coli, *J. Bacteriol. 186*, 5519-5522.
90. Schrader, M., Fendler, K., Bamberg, E., Gassel, M., Epstein, W., Altendorf, K., and Drose, S. (2000) Replacement of glycine 232 by aspartic acid in the KdpA subunit broadens the ion specificity of the K(+)-translocating KdpFABC complex, *Biophys. J. 79*, 802-813.
91. Doyle, D. A., Morais, C. J., Pfuetzner, R. A., Kuo, A., Gulbis, J. M., Cohen, S. L., Chait, B. T., and MacKinnon, R. (1998) The structure of the potassium channel: molecular basis of K+ conduction and selectivity, *Science 280*, 69-77.
92. Bramkamp, M., Altendorf, K., and Greie, J. C. (2007) Common patterns and unique features of P-type ATPases: a comparative view on the KdpFABC complex from Escherichia coli (Review), *Mol. Membr. Biol. 24*, 375-386.
93. Bramkamp, M. and Altendorf, K. (2004) Functional modules of KdpB, the catalytic subunit of the Kdp-ATPase from Escherichia coli, *Biochemistry 43*, 12289-12296.
94. Serrano, R. (1988) Structure and function of proton translocating ATPase in plasma membranes of plants and fungi, *Biochim. Biophys. Acta 947*, 1-28.
95. Haupt, M., Bramkamp, M., Coles, M., Kessler, H., and Altendorf, K. (2005) Prokaryotic Kdp-ATPase: recent insights into the structure and function of KdpB, *J. Mol. Microbiol. Biotechnol. 10*, 120-131.
96. Bramkamp, M., Gassel, M., and Altendorf, K. (2004) FITC binding site and p-nitrophenyl phosphatase activity of the Kdp-ATPase of Escherichia coli, *Biochemistry 43*, 4559-4567.
97. Bramkamp, M. and Altendorf, K. (2003) Mutational analysis of charged residues in the putative KdpB-TM5 domain of the Kdp-ATPase of Escherichia coli, *Ann. N. Y. Acad. Sci. 986*, 351-353.
98. Bramkamp, M. and Altendorf, K. (2005) Single amino acid substitution in the putative transmembrane helix V in KdpB of the KdpFABC complex of Escherichia coli uncouples ATPase activity and ion transport, *Biochemistry 44*, 8260-8266.
99. Fendler, K., Drose, S., Altendorf, K., and Bamberg, E. (1996) Electrogenic K+ transport by the Kdp-ATPase of Escherichia coli, *Biochemistry 35*, 8009-8017.

100. Fendler, K., Drose, S., Epstein, W., Bamberg, E., and Altendorf, K. (1999) The Kdp-ATPase of Escherichia coli mediates an ATP-dependent, K+-independent electrogenic partial reaction, *Biochemistry 38*, 1850-1856.
101. Anthonisen, A. N., Clausen, J. D., and Andersen, J. P. (2006) Mutational analysis of the conserved TGES loop of sarcoplasmic reticulum Ca2+-ATPase, *J. Biol. Chem. 281*, 31572-31582.
102. Aravind, L., Galperin, M. Y., and Koonin, E. V. (1998) The catalytic domain of the P-type ATPase has the haloacid dehalogenase fold, *Trends Biochem. Sci. 23*, 127-129.
103. Sazinsky, M. H., Mandal, A. K., Arguello, J. M., and Rosenzweig, A. C. (2006) Structure of the ATP binding domain from the Archaeoglobus fulgidus Cu+-ATPase, *J. Biol. Chem. 281*, 11161-11166.
104. Toyoshima, C. and Mizutani, T. (2004) Crystal structure of the calcium pump with a bound ATP analogue, *Nature 430*, 529-535.
105. Morth, J. P., Pedersen, B. P., Toustrup-Jensen, M. S., Sorensen, T. L., Petersen, J., Andersen, J. P., Vilsen, B., and Nissen, P. (2007) Crystal structure of the sodium-potassium pump, *Nature 450*, 1043-1049.
106. Olesen, C., Picard, M., Winther, A. M., Gyrup, C., Morth, J. P., Oxvig, C., Moller, J. V., and Nissen, P. (2007) The structural basis of calcium transport by the calcium pump, *Nature 450*, 1036-1042.
107. Rice, W. J., Young, H. S., Martin, D. W., Sachs, J. R., and Stokes, D. L. (2001) Structure of Na+,K+-ATPase at 11-A resolution: comparison with Ca2+- ATPase in E1 and E2 states, *Biophys. J. 80*, 2187-2197.
108. Haupt, M., Bramkamp, M., Heller, M., Coles, M., ckers-Hebestreit, G., Herkenhoff-Hesselmann, B., Altendorf, K., and Kessler, H. (2006) The holo-form of the nucleotide binding domain of the KdpFABC complex from Escherichia coli reveals a new binding mode, *J. Biol. Chem. 281*, 9641-9649.
109. Haupt, M., Bramkamp, M., Coles, M., Altendorf, K., and Kessler, H. (2004) Inter-domain motions of the N-domain of the KdpFABC complex, a P-type ATPase, are not driven by ATP-induced conformational changes, *J. Mol. Biol. 342*, 1547-1558.
110. Kubala, M. (2006) ATP-binding to P-type ATPases as revealed by biochemical, spectroscopic, and crystallographic experiments, *Proteins 64*, 1-12.
111. Dmitriev, O. Y., Tsivkovskii, R., Abildgaard, F., and Lutsenko, S. (2006) NMR assignment of the Wilson disease associated protein N-domain, *J. Biomol. NMR 36 Suppl 1*, 61.
112. Abu-Abed, M., Mal, T. K., Kainosho, M., MacLennan, D. H., and Ikura, M. (2002) Characterization of the ATP-binding domain of the sarco(endo)plasmic reticulum Ca^{2+}-ATPase: probing nucleotide binding by multidimensional NMR, *Biochemistry 41*, 1156-1164.
113. Gassel, M. and Altendorf, K. (2001) Analysis of KdpC of the K(+)-transporting KdpFABC complex of Escherichia coli, *Eur. J. Biochem. 268*, 1772-1781.
114. Epstein, W. and Davies, M. (1970) Potassium-dependant mutants of Escherichia coli K-12, *J. Bacteriol. 101*, 836-843.
115. Gassel, M., Siebers, A., Epstein, W., and Altendorf, K. (1998) Assembly of the Kdp complex, the multi-subunit K+-transport ATPase of Escherichia coli, *Biochim. Biophys. Acta 1415*, 77-84.
116. Ahnert, F., Schmid, R., Altendorf, K., and Greie, J. C. (2006) ATP binding properties of the soluble part of the KdpC subunit from the Escherichia coli K(+)-transporting KdpFABC P-type ATPase, *Biochemistry 45*, 11038-11046.

117. Irzik, K., Pfrotzschner, J., Goss, T., Ahnert, F., Haupt, M., and Greie, J. C. (2011) The KdpC subunit of the Escherichia coli K+-transporting KdpB P-type ATPase acts as a catalytic chaperone, *FEBS J. 278*, 3041-3053.
118. Smith, P. C., Karpowich, N., Millen, L., Moody, J. E., Rosen, J., Thomas, P. J., and Hunt, J. F. (2002) ATP binding to the motor domain from an ABC transporter drives formation of a nucleotide sandwich dimer, *Mol. Cell 10*, 139-149.
119. Gassel, M., Mollenkamp, T., Puppe, W., and Altendorf, K. (1999) The KdpF subunit is part of the K(+)-translocating Kdp complex of Escherichia coli and is responsible for stabilization of the complex in vitro, *J. Biol. Chem. 274*, 37901-37907.
120. Heitkamp, T., Kalinowski, R., Bottcher, B., Borsch, M., Altendorf, K., and Greie, J. C. (2008) K+-translocating KdpFABC P-type ATPase from Escherichia coli acts as a functional and structural dimer, *Biochemistry 47*, 3564-3575.
121. Heitkamp, T., Bottcher, B., and Greie, J. C. (2009) Solution structure of the KdpFABC P-type ATPase from Escherichia coli by electron microscopic single particle analysis, *J. Struct. Biol. 166*, 295-302.
122. Taniguchi, K., Kaya, S., Abe, K., and Mardh, S. (2001) The oligomeric nature of Na/K-transport ATPase, *J. Biochem. (Tokyo) 129*, 335-342.
123. Shin, J. M., Grundler, G., Senn-Bilfinger, J., Simon, W. A., and Sachs, G. (2005) Functional consequences of the oligomeric form of the membrane-bound gastric H,K-ATPase, *Biochemistry 44*, 16321-16332.
124. Hilge, M., Siegal, G., Vuister, G. W., Guntert, P., Gloor, S. M., and Abrahams, J. P. (2003) ATP-induced conformational changes of the nucleotide-binding domain of Na,K-ATPase, *Nat. Struct. Biol. 10*, 468-474.
125. Bakker, E. P. and Mangerich, W. E. (1981) Interconversion of components of the bacterial proton motive force by electrogenic potassium transport, *J. Bacteriol. 147*, 820-826.
126. Kollmann, R. and Altendorf, K. (1993) ATP-driven potassium transport in right-side-out membrane vesicles via the Kdp system of Escherichia coli, *Biochim. Biophys. Acta 1143*, 62-66.
127. Price-Whelan, A., Poon, C. K., Benson, M. A., Eidem, T. T., Roux, C. M., Boyd, J. M., Dunman, P. M., Torres, V. J., and Krulwich, T. A. (2013) Transcriptional profiling of Staphylococcus aureus during growth in 2 M NaCl leads to clarification of physiological roles for Kdp and Ktr K+ uptake systems, *MBio. 4*.
128. Smith, P. K., Krohn, R. I., Hermanson, G. T., Mallia, A. K., Gartner, F. H., Provenzano, M. D., Fujimoto, E. K., Goeke, N. M., Olson, B. J., and Klenk, D. C. (1985) Measurement of protein using bicinchoninic acid, *Anal. Biochem. 150*, 76-85.
129. LOWRY, O. H., ROSEBROUGH, N. J., FARR, A. L., and RANDALL, R. J. (1951) Protein measurement with the Folin phenol reagent, *J. Biol. Chem. 193*, 265-275.
130. Laemmli, U. K. (1970) Cleavage of structural proteins during the assembly of the head of bacteriophage T4, *Nature 227*, 680-685.
131. Vagin, O., Denevich, S., Munson, K., and Sachs, G. (2002) SCH28080, a K^+-competitive inhibitor of the gastric H,K-ATPase, binds near the M5-6 luminal loop, preventing K^+ access to the ion binding domain, *Biochemistry 41*, 12755-12762.
132. Apell, H. J. and Bersch, B. (1987) Oxonol VI as an optical indicator for membrane potentials in lipid vesicles, *Biochim. Biophys. Acta 903*, 480-494.
133. Ollivon, M., Lesieur, S., Grabielle-Madelmont, C., and Paternostre, M. (2000) Vesicle reconstitution from lipid-detergent mixed micelles, *Biochim. Biophys. Acta 1508*, 34-50.
134. Szoka, F., Jr. and Papahadjopoulos, D. (1980) Comparative properties and methods of preparation of lipid vesicles (liposomes), *Annu. Rev. Biophys. Bioeng. 9*, 467-508.

135. Seddon, A. M., Curnow, P., and Booth, P. J. (2004) Membrane proteins, lipids and detergents: not just a soap opera, *Biochim. Biophys. Acta 1666*, 105-117.
136. Lasic, D. D. (1988) The mechanism of vesicle formation, *Biochem. J. 256*, 1-11.
137. White, G. F., Racher, K. I., Lipski, A., Hallett, F. R., and Wood, J. M. (2000) Physical properties of liposomes and proteoliposomes prepared from Escherichia coli polar lipids, *Biochim. Biophys. Acta 1468*, 175-186.
138. Lambert, O., Levy, D., Ranck, J. L., Leblanc, G., and Rigaud, J. L. (1998) A new "gel-like" phase in dodecyl maltoside-lipid mixtures: implications in solubilization and reconstitution studies, *Biophys. J. 74*, 918-930.
139. Apell, H. J. (1989) Electrogenic properties of the Na,K pump, *J. Membr. Biol. 110*, 103-114.
140. Holmgren, M., Wagg, J., Bezanilla, F., Rakowski, R. F., de Weer, P., and Gadsby, D. C. (2000) Three distinct and sequential steps in the release of sodium ions by the Na^+/K^+-ATPase, *Nature 403*, 898-901.
141. Wuddel, I. and Apell, H. J. (1995) Electrogenicity of the sodium transport pathway in the Na,K-ATPase probed by charge-pulse experiments, *Biophys. J. 69*, 909-921.
142. Fedosova, N. U., Cornelius, F., and Klodos, I. (1995) Fluorescent styryl dyes as probes for Na,K-ATPase reaction mechanism: significance of the charge of the hydrophilic moiety of RH dyes, *Biochemistry 34*, 16806-16814.
143. Clarke, R. J., Kane, D. J., Apell, H. J., Roudna, M., and Bamberg, E. (1998) Kinetics of Na(+)-dependent conformational changes of rabbit kidney Na+,K(+)-ATPase, *Biophys. J. 75*, 1340-1353.
144. Butscher, C., Roudna, M., and Apell, H. (1999) Electrogenic partial reactions of the SR-Ca-ATPase investigated by a fluorescence method, *J. Membr. Biol. 168*, 169-181.
145. Peinelt, C. and Apell, H. J. (2002) Kinetics of the Ca(2+), H(+), and Mg(2+) interaction with the ion-binding sites of the SR Ca-ATPase, *Biophys. J. 82*, 170-181.
146. Diller, A., Vagin, O., Sachs, G., and Apell, H. J. (2005) Electrogenic partial reactions of the gastric H,K-ATPase, *Biophys. J. 88*, 3348-3359.
147. Witzke, A., Lindner, K., Munson, K., and Apell, H. J. (2010) Inhibition of the gastric H,K-ATPase by clotrimazole, *Biochemistry 49*, 4524-4532.
148. Apell, H. J. and Karlish, S. J. (2001) Functional properties of Na,K-ATPase, and their structural implications, as detected with biophysical techniques, *J. Membr. Biol. 180*, 1-9.
149. Lakowicz, J. R. (2006) *Principles of Fluorescence* Springer.
150. Karlish, S. J. (1988) Use of formycin nucleotides, intrinsic protein fluorescence, and fluorescein isothiocyanate-labeled enzymes for measurement of conformational states of Na^+,K^+-ATPase, *Methods Enzymol. 156*, 271-277.
151. Rephaeli, A., Richards, D. E., and Karlish, S. J. (1986) Electrical potential accelerates the E1P(Na)----E2P conformational transition of (Na,K)-ATPase in reconstituted vesicles, *J. Biol. Chem. 261*, 12437-12440.
152. Loew, L. M., Scully, S., Simpson, L., and Waggoner, A. S. (1979) Evidence for a charge-shift electrochromic mechanism in a probe of membrane potential, *Nature 281*, 497-499.
153. Loew, L. M. and Simpson, L. L. (1981) Charge-shift probes of membrane potential: a probable electrochromic mechanism for p-aminostyrylpyridinium probes on a hemispherical lipid bilayer, *Biophys. J. 34*, 353-365.
154. Buhler, R., Sturmer, W., Apell, H. J., and Lauger, P. (1991) Charge translocation by the Na,K-pump: I. Kinetics of local field changes studied by time-resolved fluorescence measurements, *J. Membr. Biol. 121*, 141-161.

155. Sturmer, W., Buhler, R., Apell, H. J., and Lauger, P. (1991) Charge translocation by the Na,K-pump: II. Ion binding and release at the extracellular face, *J. Membr. Biol. 121*, 163-176.
156. Pedersen, M., Roudna, M., Beutner, S., Birmes, M., Reifers, B., Martin, H. D., and Apell, H. J. (2002) Detection of charge movements in ion pumps by a family of styryl dyes, *J. Membr. Biol. 185*, 221-236.
157. Habeck, M., Cirri, E., Katz, A., Karlish, S. J., and Apell, H. J. (2009) Investigation of electrogenic partial reactions in detergent-solubilized Na,K-ATPase, *Biochemistry 48*, 9147-9155.
158. Andersen, J. P. and Vilsen, B. (1996) Primary ion pumps., in *Cell chemistry and physiology* (Bittar, E. E. and Bittar, N., Eds.) pp 1-66, JAI Press Inc., Greenwich, CT.
159. McCray, J. A., Herbette, L., Kihara, T., and Trentham, D. R. (1980) A new approach to time-resolved studies of ATP-requiring biological systems; laser flash photolysis of caged ATP, *Proc. Natl. Acad. Sci. U. S. A 77*, 7237-7241.
160. Kaplan, J. H. and Hollis, R. J. (1980) External Na dependence of ouabain-sensitive ATP:ADP exchange initiated by photolysis of intracellular caged-ATP in human red cell ghosts, *Nature 288*, 587-589.
161. Apell, H.-J., Roudna, M., Corrie, J. E., and Trentham, D. R. (1996) Kinetics of the phosphorylation of Na,K-ATPase by inorganic phosphate detected by a fluorescence method, *Biochemistry 35*, 10922-10930.
162. Peinelt, C. and Apell, H. J. (2005) Kinetics of Ca^{2+} binding to the SR Ca-ATPase in the E_1 state, *Biophys. J. 89*, 2427-2433.
163. Deluca, M. and McElroy, M. D. (1978) Purification and properties of firefly luciferase, *Meth. Enzymol. 57*, 3-15.
164. Waggoner, A. S. (1979) Dye indicators of membrane potential, *Annu. Rev. Biophys. Bioeng. 8*, 47-68.
165. Hoffman, J. F. and Laris, P. C. (1974) Determination of membrane potentials in human and Amphiuma red blood cells by means of fluorescent probe, *J. Physiol 239*, 519-552.
166. Waggoner, A. (1976) Optical probes of membrane potential, *J. Membr. Biol. 27*, 317-334.
167. Plasek, J. and Hrouda, V. (1991) Assessment of membrane potential changes using the carbocyanine dye, diS-C3-(5): synchronous excitation spectroscopy studies, *Eur. Biophys. J. 19*, 183-188.
168. Tsien, R. Y. and Hladky, S. B. (1978) A quantitative resolution of the spectra of a membrane potential indicator, diS-C3-(5), bound to cell components and to red blood cells, *J. Membr. Biol. 38*, 73-97.
169. Bashford, C. L. (1981) The measurement of membrane potential using optical indicators, *Biosci. Rep. 1*, 183-196.
170. Cirri, E., Kirchner, C., Becker, S., Katz, A., Karlish, S. J., and Apell, H. J. (2013) Surface Charges of the Membrane Crucially Affect Regulation of Na,K-ATPase by Phospholemman (FXYD1), *J. Membr. Biol.*
171. Hovers, J., Potschies, M., Polidori, A., Pucci, B., Raynal, S., Bonnete, F., Serrano-Vega, M. J., Tate, C. G., Picot, D., Pierre, Y., Popot, J. L., Nehme, R., Bidet, M., Mus-Veteau, I., Busskamp, H., Jung, K. H., Marx, A., Timmins, P. A., and Welte, W. (2011) A class of mild surfactants that keep integral membrane proteins water-soluble for functional studies and crystallization, *Mol. Membr. Biol. 28*, 171-181.
172. Haviv, H., Habeck, M., Kanai, R., Toyoshima, C., and Karlish, S. J. (2013) Neutral phospholipids stimulate Na,K-ATPase activity: a specific lipid-protein interaction, *J. Biol. Chem. 288*, 10073-10081.

173. Schneeberger, A. and Apell, H. J. (1999) Ion selectivity of the cytoplasmic binding sites of the Na,K-ATPase: I. Sodium binding is associated with a conformational rearrangement, *J. Membr. Biol. 168*, 221-228.
174. Nakamura, H., Kobayashi, J., Nakamura, Y., Ohizumi, Y., Kondo, T., and Hirata, Y. (1986) Theonellamine B, a novel peptidal Na,K-ATPase inhibitor from an okinawan marie sponge of the genus theonella, *Tetrahedron Letts. 27*, 4319-4322.
175. Becker, D., Fendler, K., Altendorf, K., and Greie, J. C. (2007) The conserved dipole in transmembrane helix 5 of KdpB in the Escherichia coli KdpFABC P-type ATPase is crucial for coupling and the electrogenic K+-translocation step, *Biochemistry 46*, 13920-13928.
176. Terada, H. (1975) Some biochemical and physiochemical properties of the potent uncoupler SF 6847 (3,5-di-tert-butyl-4-hydroxybenzylidenemalononitrile), *Biochim. Biophys. Acta 387*, 519-532.
177. Apell, H.-J. and Marcus, M. M. (1986) (Na^+ + K^+)-ATPase in artificial lipid vesicles: influence of the concentration of mono- and divalent cations on the pumping rate, *Biochim. Biophys. Acta 862*, 254-264.
178. Apell, H. J., Nelson, M. T., Marcus, M. M., and Lauger, P. (1986) Effects of the ATP, ADP and inorganic phosphate on the transport rate of the Na+,K+-pump, *Biochim. Biophys. Acta 857*, 105-115.
179. Cantley, L. C., Josephson, L., Warner, R., Yanagisawa, M., Lechene, C., and Guidotti, G. (1977) Vanadate is a potent (Na,K)-ATPase inhibitor found in ATP derived from muscle, *J. Biol. Chem. 252*, 7421-7423.
180. Stankiewicz, P. J., Tracey, A. S., and Crans, D. C. (1995) Inhibition of phosphate-metabolizing enzymes by oxovanadium(V) complexes, *Met. Ions. Biol. Syst. 31*, 287-324.
181. Borlinghaus, R. T., Apell, H. J., and Lauger, P. (1988) Fast charge translocations associated with partial reactions of Na,K-ATPase induced by ATP concentration-jump, *Prog. Clin. Biol. Res. 268A*, 477-484.
182. McCray, J. A. and Trentham, D. R. (1989) Properties and uses of photoreactive caged compounds, *Annu. Rev. Biophys. Biophys. Chem. 18*, 239-270.
183. Sturmer, W., Apell, H. J., Wuddel, I., and Lauger, P. (1989) Conformational transitions and change translocation by the Na,K pump: comparison of optical and electrical transients elicited by ATP-concentration jumps, *J. Membr. Biol. 110*, 67-86.
184. Niggli, V. and Sigel, E. (2008) Anticipating antiport in P-type ATPases, *Trends Biochem. Sci. 33*, 156-160.
185. Veech, R. L., Lawson, J. W., Cornell, N. W., and Krebs, H. A. (1979) Cytosolic phosphorylation potential, *J. Biol. Chem. 254*, 6538-6547.
186. Fedosova, N. U., Cornelius, F., and Klodos, I. (1998) E2P phosphoforms of Na,K-ATPase. I. Comparison of phosphointermediates formed from ATP and Pi by their reactivity toward hydroxylamine and vanadate, *Biochemistry 37*, 13634-13642.
187. Apell, H. J. and Solioz, M. (1990) Electrogenic transport by the Enterococcus hirae ATPase, *Biochim. Biophys. Acta 1017*, 221-228.
188. Bot, C. T. and Prodan, C. (2010) Quantifying the membrane potential during *E. coli* growth stages, *Biophys. Chem. 146*, 133-137.
189. Shabala, L., Bowman, J., Brown, J., Ross, T., McMeekin, T., and Shabala, S. (2009) Ion transport and osmotic adjustment in Escherichia coli in response to ionic and non-ionic osmotica, *Environ. Microbiol. 11*, 137-148.